



Special Edition Submission: 3D Printing for Medicine: Biomaterials, Processes and Techniques

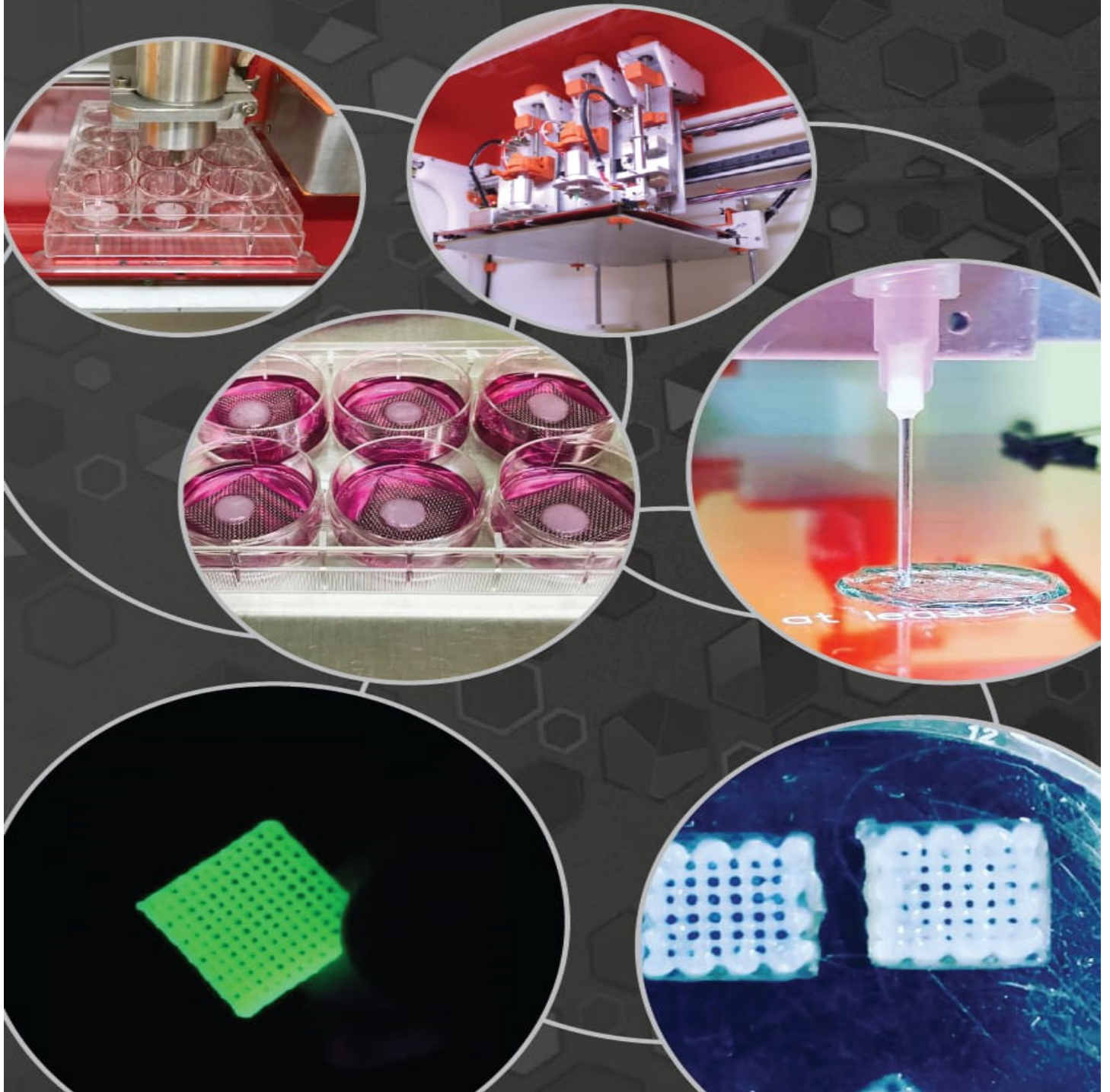


Figure credit: Cover art was created by Otávio Henrique Junqueira Amorim, assignment of authors' images: Ana Luísa Millás, Pedro Massaguer, Marcos Antonio Sabino and Silvyta Stucchi Maria-Engler.



I am very proud and honoured for the opportunity to organize this special edition named “3D Printing for Medicine: Biomaterials, Processes and Techniques” inside the International Journal of Advances in Medical Biotechnology (IJAMB), whose theme is a rapidly growing field in health deserving spotlight by its new scientific and technological developments oriented for society.

In this IJAMB special edition readers will find a collection with 8 interesting papers visiting topics comprehending bio-fabrication of skin development by 3D bioprinters; cartilage types and most recent studies towards possibilities of tissue regeneration including bioprinting use; the development of smart biomaterials usable as intelligent gels for biomedical aspects; the electrospinning technique for building micro- and nanofibers in order to fabricate scaffolds for tissue engineering; bio-inks created for extrusion-based 3D printing of scaffolds for regenerative medicine; computational simulation of fluid flow and cells growth in scaffolds to be used as human auricular cartilage for microtia repparing; the concept of robocasting, an additive manufacturing technique, to extrude colloidal systems to be used as bioceramic scaffolds in tissue engineering; and finally a very fresh survey concerning the current brazilian innovation system on tissue engineering and bioprinting and its perspectives taking into account entrepreneurship and innovative issues. I hope readers enjoy this selection of papers !

Lastly, I may not end my work without express my sincere and enthusiastic thanks to the editorial members of IJAMB besides Dr. Hernane Barud for this kind invitation and the choice to bring high level researchers and their results and the current state-of-the-art of each topic presented to enrich IJAMB and this special edition. It is highlightable the work of all reviewers for those work and the direct and indirect people involved in this project.

Welcome to the International Journal of Advances in Medical Biotechnology !



Prof. Rodrigo Alvarenga Rezende, Ph.D.
Researcher of Renato Archer Information Technology Center (CTI), Campinas, SP, Brazil.
Professor at the Post-Graduate Program in Biotechnology at the University of Araraquara, Araraquara, SP, Brazil.

Approaches to the development of 3D bioprinted skin models: the case of natura cosmetics

Ana Millás^{1-3*}, Juliana Lago¹, Luciana Vasquez-Pinto¹, Pedro Massaguer², Silvy Stuchi Maria-Engler³

*Corresponding author: E-mail address: analuizamillas@gmail.com

Abstract: We are close to achieving the production of a biomimetic functional skin and this advance is mainly due to the demand that is not limited to the field of regenerative medicine, the need for transplantation of this organ due to the aging of the population, but for ethical reasons related to the tests of safety and efficacy of new formulas in animal models by the cosmetic and pharmaceutical industries. The limitations involved in traditional 2D cell culture approaches and manual techniques for biomimetic generation have driven the use of innovative technologies such as 3D bioprinting. One of the main advantages of the bioprinted skin is the authenticity, scalability and reproducibility of tissues compared to conventional constructs, via precise positioning of multiple cell types and the inclusion of appendages. The models of bioprinted skins will serve as a platform for the development of new formulations, molecule testing, disease simulation, as well as an alternative to chronic wound biocuratives and clinical transplants. This paper reviews the state-of-the-art approaches available for skin model bioprinting, discusses the context of the drug-cosmetic industry in the adoption of these models and presents the characteristics of the project under development at Natura Cosmetics.

Keywords: 3D bioprinting; biofabrication; alternative methods; Natura Cosmetics; in vitro skin.

Introduction

Curiosity catches the eye when it comes to guessing what will be the first bioprinted functional organ to hit the market^{1,2}. The skin is among the first in this list due to a demand that is not only limited to regenerative medicine and the need for transplantation of this organ, but due to ethical issues related to animal testing³. Animal use has already been banned in many countries and the demand for equivalent skin models in the cosmetics and pharmaceutical industries is a worldwide trend⁴⁻⁷. Players like Natura, L'Oréal and Procter & Gamble are investing in bioprinting technology for the development of organotypic skin models.

As of 2019, the Normative Resolution of the National Council for Animal Experimentation Control (RN 18/2014, CONCEA) entered into force. This requirement obliges cosmetics manufacturers and pharmaceutical laboratories to adopt alternative methods avoiding the use of animals for product testing. Along this line, the European Union has banned imports of animal-tested products since 2013 (Amendment 2003/15 / EC of Directive 76/768 EEC). Besides the high cost and import-related issues of these equivalent models, they are limited as they are sold as kits that can be used only in specific assays, as an accompaniment to morphological and molecular changes^{8,9}.

An example in the Brazilian cosmetic industry, Natura Cosmetics has not conducted animal safety and efficacy tests since 2006, nor does it purchase resources or ingredients that have been tested on animals. In 2018 the company was certified by Cruelty Free International, the first in Latin America to have this certification.

Regarding the field of regenerative medicine, Brazil today has 20.6 million elderly people, a number that represents 10.8% of the population. By 2060, the country is expected to have 58.4 million elderly (Bra-

zilian Institute of Geography and Statistics-IBGE)¹⁰. With rising rates of obesity, diabetes, and aging populations, the repair of damaged or lost tissue is a worldwide concern and the demand for in vitro recreated artificial skin has grown.

Chronic lesions are followed by severe, often fatal, disorders with difficult extracellular matrix remodeling and that usually require transplantation and urgent intervention to restore tissue integrity. One possibility is the transplantation of allogeneic grafts with a high cure rate, but these are a complex process whose demand exceeds availability.

Burns, in turn, are also a major public health problem. In Brazil there are around 1,000,000 burn accidents per year, of these, 100,000 patients seek hospital care and about 2,500 die^{11,12}, it is the second leading cause of death in children not only in the United States and, in Brazil as well¹³. According to US statistics, about 10% of patients awaiting life-saving transplants die before they can receive donor organs¹⁴.

Given the regulatory challenges and obstacles of agencies such as ANVISA in Brazil and the FDA in the United States, regulating products that will contact a patient's body is substantially more costly and complex than approving an in vitro skin model, which will only be used on the lab bench for simulations and testing of drugs and cosmetics. Nevertheless, the fact that there are already commercially available skin replacements for the treatment of chronic wounds such as Apligraf® and INTEGRA®, the accumulated prior knowledge and the paved roads for regulatory approval of this type of product are already established in some countries.

From a market perspective, the global size of 3D cell culture was estimated at USD 558.0 million in 2016, displaying a CAGR of 14.8% over the forecast period. The BCC Research report¹⁶ predicts that the bioprinting market will reach \$ 1.8 billion by 2021. This growth is estimated at a compound annual growth rate of 43.9% from 2016 to 2021. Another report from the consulting firm Grand View Research (2018)¹⁷ estimated the global bioprinting market at \$ 682 million in 2016 with a forecast

¹Natura Cosméticos

²Startup 3D Biotechnology Solutions – 3DBS

³Faculdade de Ciências Farmacêuticas – Universidade de São Paulo

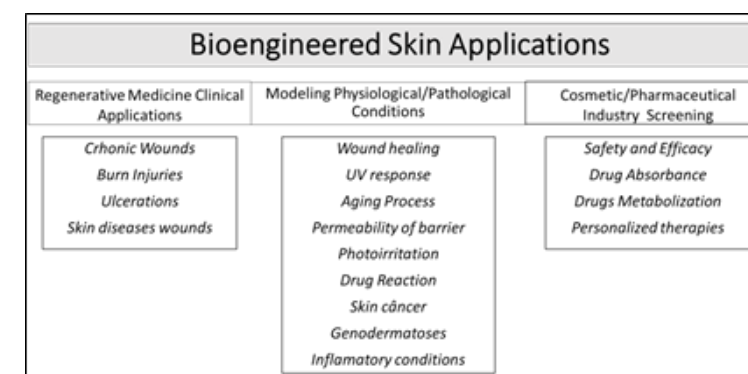


Figure 1 – Diagram of the different applications of bioengineered skin: reconstructive surgery, modeling of physiological and pathological skin conditions, pharmaceutical screening (Adapted Source¹⁵ Sarkiri *et al.* 2019).

that the market could reach \$ 2.6 billion by 2024.

Growth is expected to be driven by new printing technologies as well as expansion of new applications in the medical field, such as blood vessels and other applications.

With regard to bioprinted skin models, there is a notable progress that has been made, especially in the last decade. Although we are close to achieving a biomimetic functional skin, dialogue and joint efforts are needed for products to leave the benches and reach patients and industry, since it is an essentially interdisciplinary area^{18,19}.

Brazil is the fourth largest global market for beauty products, surpassed by the United States, China and Japan. About 2.5 thousand companies in the segment had revenues of R\$ 42.6 billion in 2015, according to the Brazilian Association of the Personal Hygiene, Perfumery and Cosmetics Industry (ABIHPEC)¹⁶ (Bergin, 2016). Cosmetic products must be safe for the user and effective for the declared activity. Often, the cosmetic industry launches new products with diverse purpose appeals. Thus, testings that prove the marketing appeal and safety of these products are expected to be conducted. In a report by FAPESP Magazine: "As of 2019, any new beauty product must undergo dermatological tests on reconstructed human skin, in Brazil or abroad"^{20,21}.

This paper provides a review of the state-of-the-art 3D bioprinting technology for human skin reconstruction, presenting aspects and challenges of the project (preprocessing), printing (processing), and tissue maturation (post-processing) phases for applications in the cosmetic industry. Finally, the case of the company Natura Cosmetics is presented.

Skin structure and functions

The skin is the largest organ in the human body, representing up to 16% of body weight²². It is the boundary between an organism and the environment, acting as a defense organ protecting against the penetration of pathogens and external toxins, controlling the damage caused by the UV rays and preventing desiccation²³. The skin consists of three main compartments: the epidermis, the dermis and the hypodermis²⁴.

The epidermis, the superficial and thinner layer, consists mainly of keratinocytes and melanocytes, and because it has high cell density, acts as a vital barrier, preventing the entry of exogenous aggressors, chemical, physical or biological, and acting on water balance which avoids excessive transepidermal loss of water and protein to the environment²⁵. Melanin, which is a substance produced and accumulated in the epidermis, protects against ultraviolet rays, which are in turn important in the fixation of vitamin D3. The dermis located just below the epidermis is known as the core of the skin, composed mainly of collagen, elastin, glycosaminoglycans (GAGs) and fibroblasts, besides being important in the biomechanical protection of the skin. It performs sensory and immunological functions through the lymphocytes that protect against antigens and allergens that come in contact with the epidermis. The sweat glands, also present in the dermis, help in the excretion of some substances. The hypodermis is located just below the dermis and is a very vascularized layer, consisting

mainly of adipose tissue, which contributes to thermal regulation and also to mechanical protection^{22,26} (Figure 2).

Some authors do not consider hypodermis as part of the skin; however, the hypodermic layer plays an important role in paracrine signaling of the skin, with functions related to skin protection and maintenance of homeostasis. It includes activities that help to protect bacterial infections, control of hair growth cycles, thermogenesis and plays an important role in wound healing, therefore increasing the relevance of the skin model²⁷. Thus, studies show that when adipocytes are co-cultured in a monolayer with keratinocytes they stimulate their proliferation and differentiation²⁸, whereas adipocytes in co-culture with fibroblasts and keratinocytes demonstrate the same proliferative effect in addition to the recruitment of fibroblasts, which play an important role in wound healing²⁹.

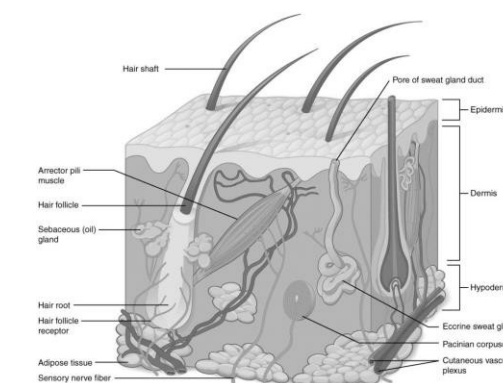


Figure 2– Skin structure model. Source: <https://courses.lumenlearning.com/wmopen-biology2/chapter/structure-and-function-of-skin/> (09/09/2019).

Commercial Reconstructed Skin Models

Some reconstructed skin models are commercially available. However, the high importation cost and very long delivery times make the process unfeasible^{8,30,31}. The development of new models of reconstructed skin translates to autonomy for many countries and companies.

In this context, the OECD encourages the production of new reconstructed skin models by providing detailed guidance in its OECD Guide No. 439 on the quality and performance control parameters that the model should present. Such parameters include standardized criteria for cell viability, barrier function, morphology and reproducibility⁴. Different approaches have been developed to achieve this goal, such as the development of reconstructed skin models, for example, reconstructed human epidermis models and full thickness skin models³².

The first skin substitute from epidermal cells was described in 1974 by Rheinwald and Howard Green of Harvard Medical University, who cultivated a small fragment of healthy skin over a wound. The success of the graft depended on the presence of dermal elements remaining or transported

to the wound, which motivated further research and triggered the development of the first commercialized product, Epicel, from the American company Genzyme (Figure 3). An epidermal substitute obtained from isolating autologous keratinocytes and co-culturing of these cells over a layer of rat mesenchymal cells, which are expanded numerous times over weeks. It is extremely fragile and is rarely used. This product has been classified by the FDA as a xenograft (derived from other non-human animal species) as it uses a rat mesenchymal cell layer as a supplement for in vitro cultivation^{33,34}.

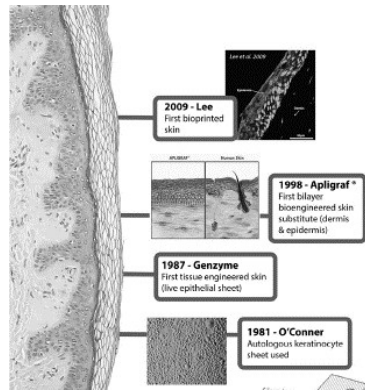


Figure 3 – Timeline of skin substitutes used in medicine³⁵ (Adapted from Tarassoli et al., 2017).

Another product developed by Americans from 1979–80, Integra, was not approved by the FDA for commercialization until 2002. Integra is a synthetic “acellular artificial skin” that acts as a two-layer dermal analogue, an internal matrix of Type I bovine collagen crosslinked via a controlled freeze-drying process with chondroitin-6-sulfate, glycosaminoglycan (GAG) (1-ethyl-3-(3-dimethylaminopropyl) and carbodiimide EDC, and an outer silicone layer that simulates the epidermis. Each layer performs a function, the inner layer is bioresorbable and simulates a dermal matrix, allowing the invasion of fibroblasts and capillaries (angiogenesis) from the receptor bed, enabling the repair of an equivalent dermal structure and promoting cell growth and the synthesis of a new collagen matrix. Gradually, the collagen is degraded, and over a period of 3 to 6 weeks a new matrix forms. After healing, the external silicone layer with an anti-infection

and mechanical barrier function, that controls fluid loss (homeostasis) can be withdrawn^{36–38}.

Another group from the Massachusetts Institute of Technology (MIT) (Jim Bell, 1981) developed Apligraf® (Organogenesis Inc., USA), also marketed and approved by the FDA, since 2001. A bilaminar structure consisting of a dermal layer of human neonatal fibroblasts on a Type I bovine (calf) collagen gel, and an epidermal layer of keratinocytes from allogeneic culture³⁹. The resistance and insolubility of collagen are obtained by shrinkage of the gel by the fibroblasts, resulting in the dermal equivalent⁴⁰. Orcel® is a cellular skin substitute consisting of a bilayer cell matrix. With human donor fibroblasts grown inside a Type I bovine collagen matrix, and keratinocytes from the same donor grown outside the collagen matrix. Orcel® serves as a bioresorbable matrix, which provides a favorable environment for host cell migration due to cytokines and growth factors secreted by allogeneic fibroblasts. According to the manufacturer, after 2–3 weeks of application, no traces of allogeneic DNA are found in the wound⁴¹.

Biobrane® is a synthetic acellular skin substitute consisting of a bilaminated membrane formed by a nylon mesh filled with porcine collagen type I (dermal analogue) and covered with a thin layer of silicone (epidermal analogue). It has small pores that allow the drainage of the transudate, being considered a semipermeable substitute. It enables fibroblasts and capillaries to invade the wound and repair the dermal defect. Reepithelization occurs from the presence of keratinocytes at the wound edge⁴².

Dermagraft® (Organogenesis) is the product that most closely resembles the product that this thesis proposes to develop. It is a dermal substitute with a layer of allogeneic fibroblasts grown on a layer of Vicryl polyglycolic acid polymer. The product is cryopreserved but becomes viable and metabolically active when placed on the wound bed. For the major skin models marketed today, see Figure 4.

The Laboratoire Organogénèse Expérimental (LOEX) in Quebec City, Canada, has developed a skin reconstructed from the self-assembly technique, a new approach to tissue engineering. This technique is based on the intrinsic property of cells self-organizing to form three-dimensional tissue under appropriate conditions. For example, skin fibroblasts secrete their own extracellular matrix in the presence of ascorbic acid, allowing the production of supportive dermal leaflets on which keratinocytes can be seeded⁴⁴.

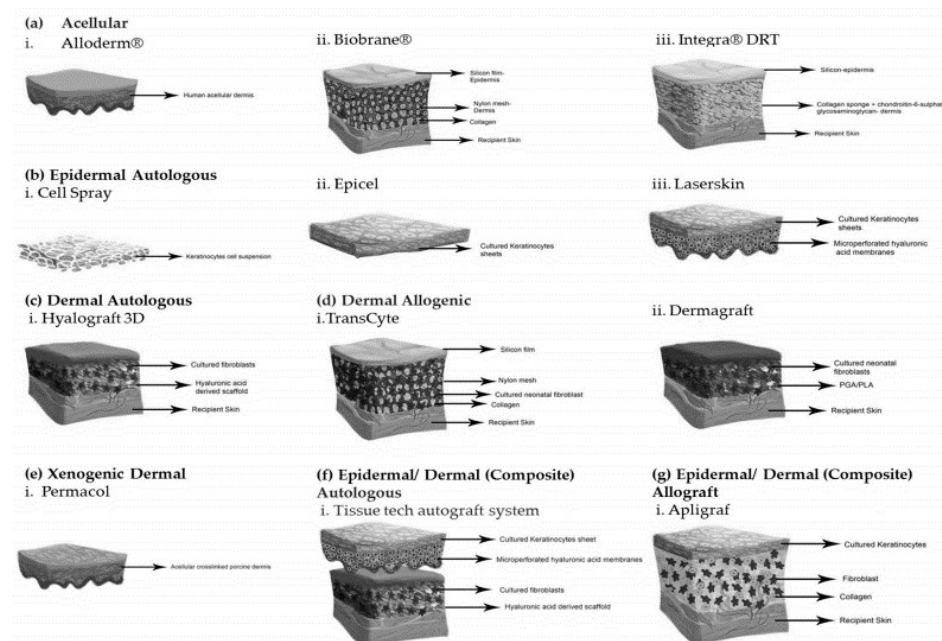


Figure 4 – Tissue engineered skin substitutes. (a) Acellular: i. Karoderm ii. Biobrane iii. Integra (b) Epidermal Autologous: i. Cell Spray ii. Epicel iii. Laserskin (c) Dermal Autologous: i. Hyalograft 3D (d) Dermal Allogenic: i. TransCyte ii. Dermagraft (e) Dermal Xenogenic: i. Permacol (f) Epidermal/Dermal (Composite) Autologous i. Tissue tech Autograft system (g) Epidermal/Dermal (Composite) Allograft i. Apligraf. (Source with permission for use: Vig et al., 2017).

3D Bioprinting: The Additive Manufacturing

Before we start the discussion on the state of the art of bioprinted skin models, it is important to situate and define some key terms for this area. Automated skin reconstruction is part of a large area called biofabrication. The term biofabrication is defined as “the automated generation of functional biological products with structural organization of living cells, bioactive molecules, biomaterials, cell aggregates (such as micro-tissues, or hybrid cell-material structures) through bioprinting or bioassembly, followed by a tissue maturation process”^{45,46}. In either case, additive manufacturing may be used in some of the fabrication stages of these structures.

Additive manufacturing, or more commonly known as 3D printing, is a process of controlled deposition of materials layer-by-layer to generate a three-dimensional structure (ISO – INTERNATIONAL ORGANIZATION FOR STANDARDIZATION, 2017). These technologies bring with them unique capabilities of rapid prototyping, repeatability and high accuracy^{47,48}. Bioprinting is a subarea of additive manufacturing and an emerging and revolutionizing field of technology that is part of the wider field of tissue engineering and regenerative medicine⁴⁹.

Bioprinting is used to fabricate three-dimensional structures of biological materials, generally cells and biomolecules, through layer-

by-layer precise positioning^{50,51}. The printing process is controlled by a computer instruction, usually a computer-aided design (CAD) file of the respective tissues structures⁵¹. The advantage of this technology is the ability to manufacture biomimetic tissues to meet specific needs related to in vitro models or patients, the so-called personalized medicine.

The set of bioprinting techniques that allow living cell deposition includes: inkjet printing, which is subdivided into two types, continuous inkjet (CIJ)^{52,53} and drop-on-demand (DoD)^{54,55}, direct ink writing (DIW), which can be controlled by mechanic pistons or pneumatic control^{56–58} and laser printing or stereolithography (Stereolithography–SLA) or laser-induced forward transfer (LIFT)^{59–62} (Figure 5).

Today, microextrusion and inkjet techniques are the most used^{48,58}. Microextrusion bio printers are one of the conventional 3D printheads that use high temperature fused polymeric filament reels (FDM Fused Deposition Modeling mechanism). The micro-extrusion mechanism is the most widespread in literature and the most used worldwide as it offers greater flexibility in the rheological conditions of bioinks. It also allows working with high densities and cell types in the same construction and allows the deposit of pre-differentiated cells in three-dimensional spherical (spheroids) structures. These advantages are of paramount importance for the production of complex structures since it is necessary to manipulate several types and large cell densities to simulate the

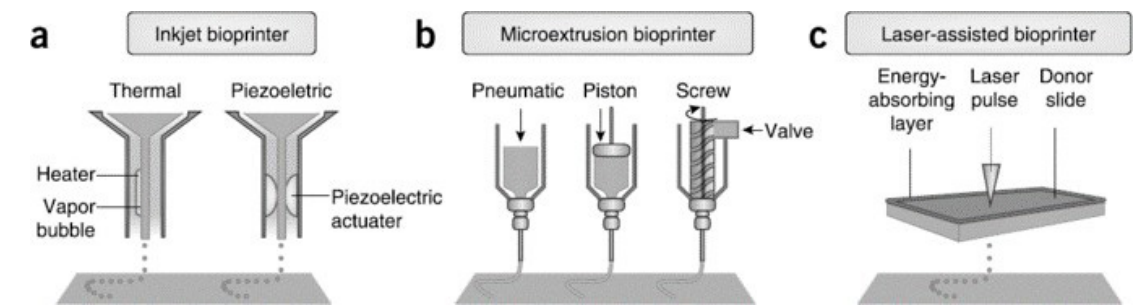


Figure 5 – Bioprinting mechanisms of inkjet, microextrusion, and laser-assisted. A) Inkjet printers, the print head is electrically heated to produce air-pressure pulses that force droplets from the nozzle, while acoustic printers use pulses formed by piezoelectric or ultrasound pressure. B) Microextrusion printers use pneumatic or mechanical dispensing pistons systems to extrude continuous beads of material and/or cells. C) Laser-assisted printers use lasers focused on an absorbing substrate to generate pressures that propel cell-containing materials onto a collector substrate⁵⁰. Reprinted by permission from: Murphy and Atala, 2014.

heterogeneous environment of complex tissues⁵⁰.

The Challenges Associated with Skin Bioprinting

Challenges for tissue, and more specifically, skin bioprinting, are primarily associated with the selection of bioinks, which are the primary input for bioprinters.

Bioinks, defined as biomaterials that carry cells during the bioprinting process^{63–65}. Therefore, cells are a mandatory component in the formulation of bioinks, which may or may not also carry biomolecules; otherwise, these inks are called hydrogels or biomaterial ink. Biomaterial inks produce cell-free scaffolds that can be seeded with the cells of interest or combined in bioink hybrid systems to produce more complex tissues. Another example of biomaterial inks is the case of sacrificial materials which when interspersed with bioinks are subsequently washed away leaving clear spaces such as channels (ex.: the synthetic Pluronic F127, gelatin), as illustrated in Figure 6.

Therefore, the bioinks to be printed must meet certain requirements taking into account rheological (physicochemical) and biocompatibility properties, such as: printability, biocompatibility, degradation and byproduct kinetics, structural and mechanical properties, and material biomimicry⁶⁰. Moreover, the rheological properties of gelation and preservation of the three-dimensional post-impression structures must be in synergy with the biocompatibility properties, also allowing the growth, differentiation and cellular preservation of the dermis-epidermis layers in air-liquid interface (Figure 7).

Some important characteristics for a bioink are summarized in Table 1. Note that the requirements for obtaining a printable material are associated with the characteristics that it must have before and after printing.

Smart hydrogels and bioinks are emerging materials that act in response to external stimulus, such as temperature, pressure or pH, and have been developed to accompany the so-called 4D Bioprinting, where the Time variable is also considered. While bio-printing of functional organs is still a Herculean task to be achieved, the good news is that this is happening faster than we ever imagined. We already have scientific reports of orga-

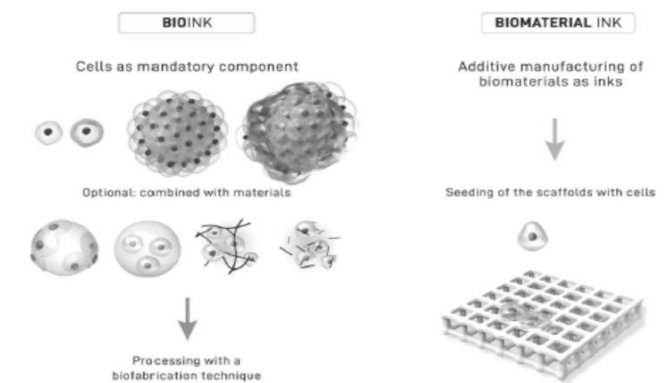


Figure 6 – Distinction between a bioink (left side), where cells are a mandatory component of the bioink formulation, loaded with individual cells, cell aggregates (spheroids), one or more cell types, and biomaterial ink (right side), where a biomaterial is used for printing and the cells may or may not be seeded after manufacture⁶⁶ (Source: Groll et al., 2018).

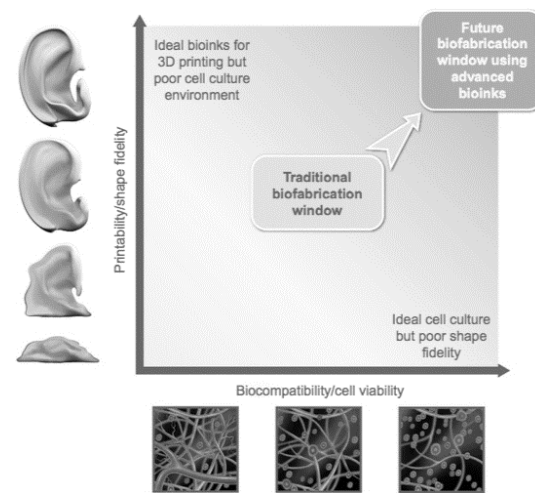


Figure 7 – The challenge for the development of new bioinks aimed at tissue reconstruction. Bioinks must have dual functionality: *rheological properties* that maintain the printed structure and *biocompatibility* that promote cell viability 66 (Source: Kyle et al., 2018).

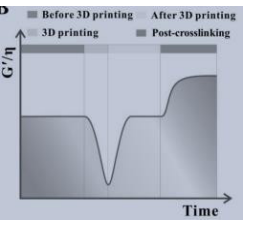
Bioink requirements	Goal	Desired Value or Condition	References
Biocompatibility	Must support cell viability	Cellular viability superior to 70%	(50,67,68)
Viscoelasticity (Fiber shape fidelity)	reproduce shear stress during the printing process, as increasing the shear rate reduces the viscosity by up to an order of magnitude	30 when over $6 \cdot 10^7$ mPa.s; 764 mPa.s for Nivea Cream, considered adequate for purpose	(50,64,67,68)
Shear-thinning behavior (printability)	reproduce shear stress during the printing process, as increasing the shear rate reduces the viscosity by up to an order of magnitude	$K = 26,1 \text{ e } n = 0,552$ for Nivea Cream	(50,64,67,68)
Storage Modulus (Temporary structure fidelity)	Increases the stability of the structure. It can be physical, chemical or a combination of both.		(50,64,68)
Gelation/crosslinking (Permanent structure fidelity)	Must be of the same order of magnitude as native skin.	Physical Crosslink (ionic) due to mild conditions	(50,64).
Crosslinking process	Increases the stability of the structure. It can be physical, chemical or a combination of both.	Thermal or chemical crosslinking, thrombin and calcium chloride	(69)
Biocompatibility	Must be Biocompatible	Cellular viability superior to 70%	(50)

Table 1 – Requirements of useful bioinks formulations for application in tissue engineering in bioprinting processes.

noids such as liver, heart, bladder, skin and bioprinted cartilage tissues⁷⁰.

Bioprinted Skin Models

The role of biomimetics is crucial for tissue engineering. Unraveling the secrets of nature and trying to mimic them, starting from the observation and understanding of their forms and biogenesis is the main challenge in this field⁷¹. Despite the traditional approach of simplifying highly complex structures, in nature, structures are complex and nano- and micro-metrically designed. Both industry and academia are driving the development of new approaches to human skin engineering and in vitro skin models for research, not just compartmentalizing it in the dermis and epidermis, using only two cell types, keratinocytes and fibroblasts, and 3D bioprinting technology is supporting this evolution.

Didactically, skin bioprinting can be divided into three major stages, preprocessing, processing and post-processing. These three steps are subdivided into five activity centers: 1) project image acquisition and 3D generation and modeling of a digital (.gcode) file, 2) bioink selection, 3) cell selection, 4) selection of the bioprinting technique to be used and, 5) maturation of this tissue in the time variable (Figure 8).

1) 3D modeling: Image preprocessing for bioprinting purposes is the phase in which the capture of the biomaging and the representation of this image in 3D occurs, using CAD-compatible software (eg InVesalius, BioCAD software)⁷². If the intended application of the bioprinted skin is for wound healing and transplantation in humans or animals, it is necessary

to know the type, size and depth of the wound. Capturing characteristics such as skin color and texture are often important. For cosmetic testing, this approach to complex designs is not required as a basic organotypic pattern for testing is more interesting. However, a database of various skin types (normal, dry, oily, mixed or sensitive), texture, age and color is relevant for skin models focused on product efficacy testing^{73,74}.

2) Bioink: Next is the stage of materials and bioinks selection, natural polymers, synthetic polymers or decellularized cell matrices. Natural polymers such as collagen gelatin, fibrin and chitosan resemble the native extracellular matrix and are more cell compatible, while synthetic polymers have better mechanical properties and help promote structural integrity.

3) Cell: Concomitant with the materials, we have the stage of cell selection, primary, from an immortalized lineage, autologous, heterologous or xenographic, this will depend on the application. To make a multilayer skin mimetic, it is necessary to use more than one cell type (fibroblasts, keratinocytes, melanocytes, mesenchymal cells)⁷³.

4) Printing: After the preprocessing steps are completed, we reach the processing step, when one of the three possibilities (ex.: micro-extrusion, inkjet or laser-based) of bioprinting is selected to achieve the best resolution, precision and required scalability.

5) Post-processing: Post-processing of the bioprinted construct involves maturation of the tissue in the time variable (currently known as the 4D dimension), in a greenhouse or bioreactor. Finally, the biomimetic skin is transplanted to a patient or used for drug or and cosmetic testing.

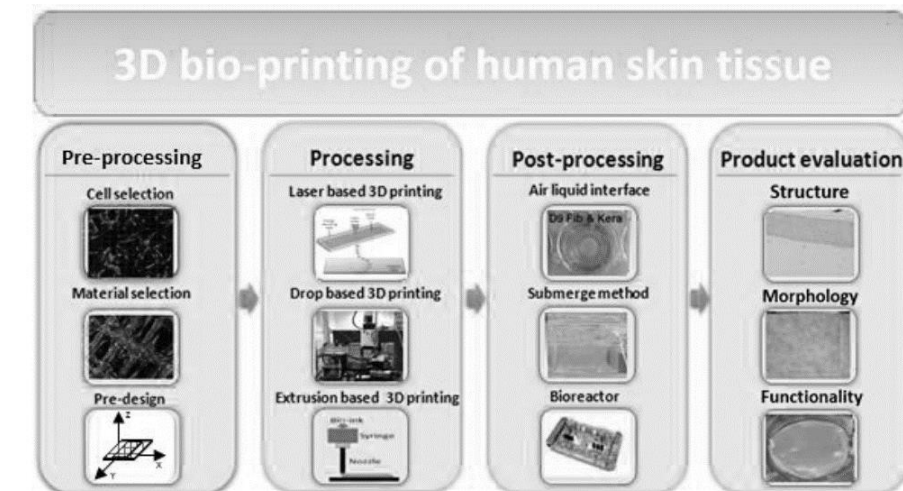


Figure 8 – Schematic of the overall 3D bioprinting process for human skin tissue. Preprocessing, processing and post-processing, which is divided into five main activities: 1) project image acquisition and 3D generation and modeling of a digital (.gcode) file, 2) bioink selection, 3) cell selection, 4) selection of the bioprinting technique to be used and, 5) maturation of this tissue in the time variable¹⁹. Source adapted from Wei-Cheng, 2018.

Bioprinted Skin Mimetics: State of the Art

About the state of the art of bioprinted biomimetic skin, mouse fibroblast (NIH3T3) and human immortalized keratinocyte (HaCat), well-established cell lines have been widely combined in studies to print 3D skin constructs^{75,76}. In these researches were confirmed high viability of printed cells in hydrogel, secretion of collagen by the fibroblasts, and cytokeratin (CK14) expression of keratinocytes⁷⁷. Collagen type I (from rat tail), the main extracellular matrix (ECM) protein in skin, was used as a bioink, embedding cells to print skin structures and approximating native skin as far as possible^{78,79}. Koch and collaborators generate dermis-epidermis structure with 20 layers of keratinocytes embedded in collagen printed by a Laser-assisted bioprinter on a sheet of Matrigel[®] (decellularized dermal matrix)⁶², to generate dermis-epidermis structure. The researchers labeled the fibroblasts and keratinocytes using fluorescent cell membrane markers. In another study, dermal/epidermal-like distinctive layers were successfully printed by an extrusion printer with primary adult human dermal fibroblasts and primary adult human epidermal keratinocytes in a 3D hydrogel scaffold. Ten layers of type I collagen precursor (rat tail origin) were printed. These constructs were able to generate dermis

and epidermis structures; however, the construct did not show tissue generation or the establishment of intercellular junction⁷⁸.

Abaci and collaborators built a 3D bioprinted vascular perfusion network from the generation of channels embedded in an alginate layer simulating the dermis⁸⁰. Endothelial primary cells and induced pluripotent stem cells (IPS) were employed to obtain a permeable endothelial barrier. This model enables the study and systemic administration of medications, as well as being a developing platform for drug screening. Michael et al. (2013)⁷⁵, printed a laser bilayer skin and implanted the substitute in the skin fold of rats. In addition to dermis and epidermis formation, a small amount of neovascularization was observed at the site of the wound 11 days after implantation. Similarly, Cube and collaborators (2016)⁸¹ used microextrusion bioprinting and implanted it in mice. They demonstrated that equivalent skin is similar to native skin in structural and functional terms.

However, despite these progresses in skin bioprinting, a scaffold-free model bioprinted with human primary skin cells is still not available.

Natura Skin Model Case

The company Natura Cosmetics in 2018 signed a research collaboration agreement with the Faculty of Pharmaceutical Sciences of the State University of São Paulo and since then it has been developing its own skin models using 3D bioprinting technology⁷⁴. The company has not used animal models for efficacy and safety tests since 2006 and had been importing reconstructed models and mostly using the skin model developed by University of São Paulo at the laboratory of Prof. Silvy Maria-Engler (USP / Sao Paulo).

To conduct this research, Natura is using the 3D bioprinting platform. The goal is to translate the technology used by USP of manually fabricated full thickness skin models to an automated model and biofabricated via 3D bioprinting^{82,85}. The research uses a bioink composed of collagen Type I^{6,9} alginate^{86,87} gelatin⁸⁷ and fibrinogen^{89,88} developed in conjunction with optimal printing conditions and 3D printer functions. Two bioprinters are being used in the research, the Inkredible model, from the Swedish company Cellink and the GenesisII™ model from the Brazilian startup 3D Biotechnology Solutions – 3DBS. Both work as a microextrusion-based mechanism with two printheads, with the exception that Inkredible uses air pressure extrusion and Genesis uses mechanical pistons. They are an open source machine developed to fully comply with laboratory safety standards (Figure 9).

The bioink formulation has three purposes: (i) maintaining an appropriate gel rheology during the extrusion process, (ii) enabling the consolidation of the printed object during the post-processing step, and (iii) allowing the adequate development of the 3D cell network leading to a correct organization and function of the matured tissue. These three

functions are supported by the following biomaterials. Type I collagen, the main component of the dermal layer, is soluble in acidic pH. Gelatin, a collagen-based polymer, with a phase transition temperature at 35°C, is used as a rheological component giving the bioink its strength once printed on a cooled substrate but still being soluble and then eliminated in the subsequent steps of the process. Alginate, a carbohydrate-based polymer, with the ability to form hydrogel in the presence of calcium, is used as a structural component giving the printed bioink mechanical stability once the gelatin solubilized⁸⁹. Fibrinogen, a glycoprotein with the ability to form hydrogel was used both as a structural and a maturation component thanks to its cellular adhesion RGD pattern⁸⁹.

For the generation of a dermo-epidermal equivalent, the bioinks are loaded with primary cell lines, fibroblasts and keratinocytes and melanocytes, in the case of pigmented skin models. Once we have obtained the three-dimensional structure, the stratum corneum should meet the requirements of OECD Guide 439⁹⁰ (Figure 10).

Initially, the ability to extrude the material is rheologically evaluated by evaluating its pseudoplasticity. Next, the printed structure should be stabilized immediately after printing using a material that does not collapse after deposition. This stability can also be assessed by material rheology, through viscosity and yield stress⁶⁷. The crosslinking after printing is done due to the need to manipulate the printed structure without losing its geometry and to impart some mechanical resistance to the printed scaffold. Among the possible types of crosslinking, ionic is used because it has milder conditions during the process^{46,50}.

The study is focused on the demonstration of the capability of both 3D printers to produce full thickness skin equivalents in an effective way

and with a cellular architecture of the mature tissue highly similar to the *in vivo* skin composition and organization. The final aim of the developed technique is of course, the production of highly complex skin models.

Conclusions

Despite the advances, there are still challenges in the reconstruction of this organ, such as the inclusion of appendages, hair follicles, hypodermic layer, microvessels and immune cells. Recently, researchers at Rensselaer Polytechnic Institute/USA have developed a full thickness 3D print skin with microvessels⁹¹, also, a group of scientists from Japan developed a 3D skin with hair follicles and sebaceous glands⁹², a major leap in the Bioprinting field. Even so, more effort is needed to create functional skin with sufficient vascularity, innervation, and functions such as sensation of touch and perception. Reproducing the color and texture of native skin is another major challenge. Ex vivo skin is a valuable model for skin penetration studies but due to logistical and viability limitations the development of *in vitro* alternatives is required⁹³.

Now the challenge is to produce dry, oily skin with different texture, pigmented with different shades of European white, moderate Asian and dark African tones⁹³. Scalability and accessibility are still two other obstacles to overcome. There are some ethical, social and legal challenges that need attention before the technology and product can be successful.

On a timescale, the bioprinted skin mimetics will follow logic of market regulation and maturation:

- Cosmetics Industry: Cosmetic companies would first test their products on skin models as an alternative to animal testing;
- Pharmaceutical / Chemical Industry: Pharmaceutical industries will test their medicines and chemical products using these *in vitro* skin models (microfluidic systems);
- Organ Transplantation: treatment of burns and injuries using bioprinted skins; cells taken from the patient himself (autologus) will be used in this bioprinting process;
- In vitro* 3D tumor models: Tumor models with tumor microenvironment designed to study the *modus operandi* of cancer proliferation, metastasis and response to drugs; and
- Precision Medicine: With the 3D skin / tumor model, the effectiveness of the medicine can be studied for each patient and thus help in personalized medicine.

References

1. Kang, Hyun-Wook, et al. "A 3D bioprinting system to produce human-scale tissue constructs with structural integrity." *Nature biotechnology* 34.3 (2016): 312.
2. Vijayavenkataraman, S. "3D bioprinted skin: the first 'to-be'successful printed organ?." (2017): 143–144.
3. Vijayavenkataraman, S., W. F. Lu, and J. Y. H. Fuh. "3D bioprinting of skin: A state-of-the-art review on modelling, materials, and processes." *Biofabrication* 8.3 (2016): 032001.
4. Jung, K.-M.M., Lee, S.-H.H., Jang, W.-H.H., Jung, H.-S.S., Heo, Y., Park, Y.-H.H., Bae, S., Lim, K.-M.M., Seok, S.H., 2014. KeraSkin™-VM: a novel reconstructed human epidermis model for skin irritation tests. *Toxicol. in Vitro* 28, 742–750. <http://dx.doi.org/10.1016/j.tiv.2014.02.014>.
5. Lemper, M., De Paepe, K., Rogiers, V., 2014. Practical problems encountered during the cultivation of an open-source reconstructed human epidermis model on a polycarbonate membrane and protein quantification. *Skin Pharmacol. Physiol.* 27, 106–112. <http://dx.doi.org/10.1159/000351814>.
6. Catarino, C.C., T. do Nascimento Pedrosa, P.C. Pennacchi, S.R. de Assis, F. Gimenes, M.E.L. Consolaro, S.B. de Moraes Barros, S.S. Maria-Engler, Skin corrosion test: comparison between reconstructed human epidermis and full thickness skin models, *European Journal of Pharmaceutics and Biopharmaceutics* (2018), doi: <https://doi.org/10.1016/j.ejpb.2018.01.002>.
7. Girardeau-Hubert, Sarah, Céline Deneuve, Hervé Pigeon, Kahna Abed, Charlotte Tacheau, Nükhet Cavusoglu, Mark Donovan, Dominique Bernard & Daniel Asselineau. Reconstructed Skin Models Revealed Unexpected Differences in Epidermal African and Caucasian Skin. *Scientific Reports* | (2019) 9:7456 | <https://doi.org/10.1038/s41598-019-43128-3> Nature.
8. MARIA-ENGLER, S.S. et al. Artificial skin as an alternative to animal testing. *Ciência Veterinária nos Trópicos*, v. 13, n. Supl. 1, p. 118–125, 2010.
9. Pedrosa, Tatiana do nascimento ; Catarino, Carolina motter ; Pennacchi, Paula Comune ; Assis, Sílvia Romano de ; Gimenes, Fabricia ; Consolaro, Márcia Edilaine Lopes ; Barros, Sílvia Berlanga de Moraes ; Maria-Engler, Silvy. Stuchi . A New Reconstructed Human Epidermis For In Vitro Skin Irritation Testing. *TOXICOLOGY IN VITRO*, V. 42, P. 31–37, 2017.
10. IBGE – INSTITUTO BRASILEIRO DE GEOGRAFIA E ESTATÍSTICA. *SINOPSE DO CENSO DEMOGRÁFICO*. Rio de Janeiro; 2015.
11. CURADO ALCF. *Redução da dor em pacientes queimados através da acupuntura [Monografia]*. Goiânia: Universidade Estadual de Goiás; 2006.
12. CRUZ, B.F.; CORDOVIL, P.; BATISTA, K. N. M.. Epidemiological profile of patients who suffered burns in Brazil: literature review. Perfil epidemiológico de pacientes que sofreram queimaduras no Brasil: revisão de literatura. *Rev Bras Queimaduras*. 11(4):246– 50. 2012.
13. Mock C, Peck M, Peden M, Krug E. *A Who Plan For Burn Prevention And Care*. Geneva: World Health Organization; 2008.
14. Mchale, M.k.; Bergmann, N.m.; And West, J.I. *Histogenesis in Three-dimensional Scaffolds. Handbook of Stem Cells. Adult and Fetal Stem Cells. Volume II*. 2013.
15. Sarkiri, Maria, Stephan C. Fox 2 , Lidy E. Fratila-Apachitei 1,* and Amir A. Zadpoor. (2019). Review: Bioengineered Skin Intended for Skin Disease Modeling. *Int. J. Mol. Sci.* 2019, 20, 1407; doi:10.3390/ijms20061407.
16. Bergin, J. 2016: *Bioprinting: Technologies and Global markets*, BCC Research, USA.
17. 3D Bioprinting Market Size, share and trends analysis report by technology (Magnetic levitation , inkjet based, syringe based, laser based), by application , and segment forecast, 2018–2024, 2018. Available from: www.grandviewresearch.com/industry-analysis/3Dioprinting-market.
18. Augustine, Robin. (2018) REVIEW PAPER. Skin bioprinting: a novel approach for creating artificial skin from synthetic and natural building blocks. *Progress in Biomaterials* (2018) 7:77–92. <https://doi.org/10.1007/s40204-018-0087-0>
19. Wei-Cheng, Yan; Pooya Davoodi, S. Vijayavenkataraman, Yuan Tian, Wei Cheng Ng, Jerry Y.H. Fuh, Kim Samirah Robinson, Chi-Hwa Wang. 2018. 3D bioprinting of skin tissue: From pre-processing to final product evaluation. *Adr* (2018), doi:10.1016/j.addr.2018.07.016

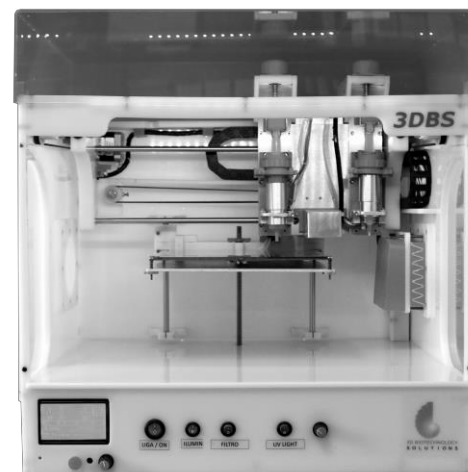
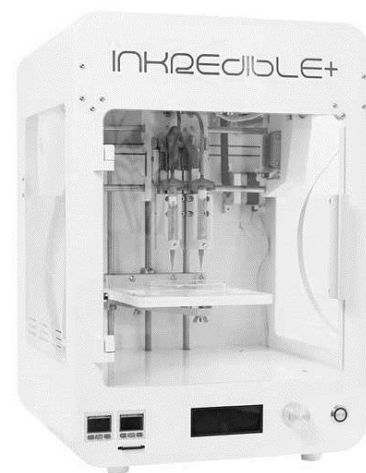


Figure 9 – The two bioprinters used under the project to develop skin models to meet the cosmetic industry. A) Cellink, Inkredible model (Natura Cosmetics). Source: Cellink / EU. B) 3DBS, Genesis II model (Faculty of Pharmaceutical Sciences / USP). Source: 3DBS site/BR.

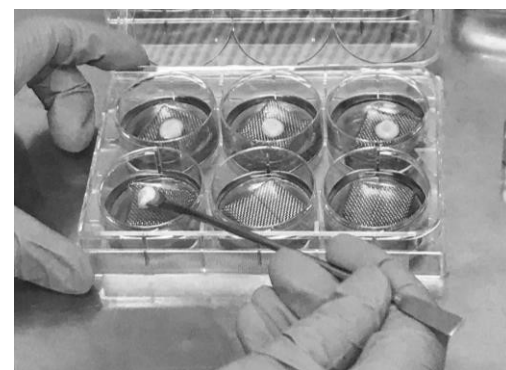


Figure 10 – a) Dermal-epidermal skin model printed prior to the passage to air-liquid surface (Source: Natura Cosmetics / 2019), b) Full thickness skin on an air-liquid surface (Lab. Prof. Silvy Maria-Engler Stucchi / USP).

20. Vasconcelos, Yuri. Pele de Laboratório. (2016). RevistaFAPESP. Pesquisa Maria-Engler, Silvy Stucchi. Universidade Estadual de São Paulo/Usf. Junho/2016.
21. Maria-Engler, Silvyastuchi. Assessing The Effects Of Advanced Glycation End Products In The Skin. *British Journal Of Dermatology*, V. 176, N. 1, P. 12–13, 2017.
22. Junqueira & Carneiro. Basic Histology. 11th Ed. Mcgraw-Hill. 2005.
23. Qiu, J., Zhong, L., Zhou, M. Et Al (2016). Establishment And Characterization Of A Reconstructed Chinese Human Epidermis Model. *International Journal Of Cosmetic Science* **38**, 60–67. Doi:10.1111/ics.12249.
24. Kamel Ra, Ong Jf, Eriksson E, Junker Jp, Caterson Ej. Tissue Engineering Of Skin. *Journal Of American College Of Surgeons*. 2013;**217**(3):533–555.
25. Ponc, M., Gibbs, S., Pilgram, G. Et al. (2001). Barrier Function In Reconstructed Epidermis And Its Resemblance To Native Human Skin. *Skin Pharmacology And Applied Skin Physiology* **14**, 63–71. Doi:10.1159/000056392.
26. Caliar Sr, Ramirez Ma, Harley Bac. The Development Of Collagen-Gag Scaffold-Membrane Composites For Tendon Tissue Engineering. *Biomaterials*. **32**:8990–8998. 2011.
27. Nicu, Carina Et al. A Guide To Studying Human Dermal Adipocytes In Situ. *Experimental Dermatology*, V.27, N. 6, P. 589–602, 2018.
28. Moon, Kyoung Mi Et al. The Effect Of Secretory Factors Of Adipose-Derived Stem Cells On Human Keratinocytes. *International Journal Of Molecular Sciences*, V. 13, N. 1, P. 1239–1257, 2012.
29. Schmidt Ba, Horsley V.(2013) Intradermal Adipocytes Mediate Fibroblast Recruitment During Skin Wound Healing. *Development*;140(7):1517–27. Doi: 10.1242/Dev.087593.
30. Powmay, Y. Et al., 2004. A Simple Reconstructed Human Epidermis: Preparation Of The Culture Model And Utilization In In Vitro Studies. *Archives Of Dermatological Reserarch*, V. 296, N.5, P. 203–211.
31. De Vuyst Et al., 2014. Reconstruction Of Normal And Pathological Human Epidermis On Polycarbonate Filter. *Methods In Molecular Biology*, V. 1195, P. 191–201.
32. Zhang Z, Michniak-Kohn Bb. 2012. Tissue Engineered Human Skin Equivalents. *Pharmaceutics*. 2012 Jan 6;4(1):26–41. Doi: 10.3390/Pharmaceutics4010026.
33. Shevchenko Rv, James Sl, James Se (2010) A Review Of Tissue-Engineered Skin Bioconstructs Available For Skin Reconstruction. *J R Soc Interface* **7**:229–258. <https://doi.org/10.1098/rsif.2009.0403>
34. Berthiaume, F.; Maguire, T.j. and Yarmush, M.I. tissue Engineering And Regenerative Medicine: History, Progress, And Challenges. *Annu. Rev. Chem. Biomol. Eng.* **2**:403–30. 2011.
35. Tarassoli, Sam.p., Zita M. Jessop, Ayesha Al-Sabah, Neng Gao, Sairan Whitaker, Shareen Doak, Iain S. Whitaker. Review. Skin Tissue Engineering Using 3d Bioprinting: An Evolving Research Field. 1748–6815/© 2017 Published By Elsevier Ltd On Behalf Of British Association Of Plastic, Reconstructive And Aesthetic Surgeons. <https://doi.org/10.1016/j.bjps.2017.12.006>
36. Yannas Iv, Burke Jf, Orgill Dp, Skrabut Em. Wound Tissue Can Utilize A Polymeric Template To Synthesize A Functional Extension Of Skin. *Science*. **215**:174–76. 1982.
37. Groos N, Guillot M, Zilliox R, Braye F. Use Of An Artificial Dermis (Integra) For The Reconstruction Of Extensive Burn Scars In Children. About 22 Grafts. *Eur J Pediatr Surg*. 2005;15(3):187–92.
38. Candido, Luiz Claudio. Livro Do Feridologo. Tratamento Clinico-Cirurgico De Feridas Cutaneas Agudas E Cronicas. Isbn 85–906486–0–5. 2006.
39. Bell E, Ehrlich Hp, Buttle Dj, Nakatsuji T. Living Tissue Formed In Vitro And Accepted As Skin Equivalent Tissue Of Full Thickness. *Science*. 211:1052–54. 1981.
40. Falanga V & Sabolinski M. (1999) A Bilayered Living Skin Construct (Apligraf) Accelerates Complete Closure Of Hard-To-Heal Venous Ulcers. *Wound Repair Regen*. **7**(4):201–7.
41. Shores Jt, Gabriel A, Gupta S. Skin Substitutes And Alternatives: A Review. *Adv Skin Wound Care*.20(9 Pt 1):493–508. 2007.
42. Cassidy, C. Et al. Biobrane Versus Duoderm For The Treatment Of Intermediate Thickness Burns In Children: A Prospective, Randomized Trial. (2005) *Burns* [S. L.], V. 31, N. 7, P. 890–893. Disponível Em: <<https://www.ncbi.nlm.nih.gov/pubmed/16023298>>.
43. Vig Komal, Atul Chaudhari, Shweta Tripathi, Saurabh Dixit, Rajnish Sahu, Shreekumar Pillai, Vida A. Dennis And Shree R. Singh .Review Advances In Skin Regeneration Using Tissue Engineering Int. J. Mol. Sci. 2017, 18, 789; Doi:10.3390/ijms18040789
44. Jean J, Garcia-Pérez Me, Pouliot R. Bioengineered Skin: The Self-Assembly Approach. *J Tissue Sci Eng* S5:001. 2011. Doi: 10.4172/2157-7552.S5-001.
45. Groll, J.; Boland, T.; Blunk, T.; Burdick, J. A.; Cho, D.-W.; Dalton, P. D.; Derby, B.; Forgacs, G.; Li, Q.; Mironov, V. A.; Moroni, L.; Nakamura, M.; Shu, W.; Takeuchi, S.; Vozzi, G.; Woodfield, T. B. F.; Xu, T.; Yoo, J. J.; Malda, J. Biofabrication: Reappraising The Definition Of An Evolving Field. *Biofabrication*, V. 8, N. 1, P. 13001, 2016.
46. Moroni, L.; Boland, T.; Burdick, J. A.; De Maria, C.; Derby, B.; Forgacs, G.; Groll, J.; Li, Q.; Malda, J.; Mironov, V. A.; Mota, C.; Nakamura, M.; Shu, W.; Takeuchi, S.; Woodfield, T. B. F.; Xu, T.; Yoo, J. J.; Vozzi, G. Biofabrication: A Guide To Technology And Terminology. *Trends In Biotechnology*, V. 36, N. 4, P. 384–402, 2018.
47. Watanabe, J. & Ishihara, Phosphorylcholine And Poly(D,L-Lactic Acid) Containing Copolymers As Substrates For Cell Adhesion, *Artif. Organs* **27**; 242 – 248. 2003.
48. Ozbolat, I. T.; Moncal, Kazim K.; Gudapati, Hemanth. Evaluation Of Bioprinter Technologies. *Additive Manufacturing*. Volume 13, Pages 179–200. 2017. <https://doi.org/10.1016/j.addma.2016.10.003>
49. JASPER, L. Tran, To Bioprint Or Not To Bioprint, 17 (1) N.c. J.I. & Tech., 123, 132 (2015), Refers To Bioprinting As “The Stepchild Of 3d Printing And Synthetic Biology”.
50. Murphy, S. V.; Atala, A. (2014) 3d Bioprinting Of Tissues And Organs. *Nature Biotechnology*, V. 32, N. 8, P. 773.
51. Chua, Chee And Wai Yee Yeong, Bioprinting : Principles And Applications, 53 World Scientific Publishing Company (2015); Mathew Varkey And Anthony Atala, Organ Bioprinting: A Closer Look At Ethics And Policies, *5 Wake Forest Journal Of Law & Policy* **275**, 277 (2015).
52. Boland, V. T Mironov, A. Gutowska, E.a. Roth, R.r. Markwald, Cell And Organ Printing 2: Fusion Of Cell Aggregates In Three-Dimensional Gels, *Anat. Rec. A Discov. Mol. Cell Evol. Biol.* **272** (2003) 497–502.
53. Burg, T.c.; C. A P. Cass, R. Groff, M. E. Pepper, K. J. L. Burg, Building Off-The-Shelf Tissue-Engineered Composites, *Philos. T. R. Soc A* **368**, 1839–1862 (2010).
54. Moon S.j. Et al., Layer By Layer Three-Dimensional Tissue Epitaxy By Cell-Laden Hydrogel Droplets, *Tissue Eng. Pt-C. Meth.* **16**, 157–166 (2010).
55. Xu F. Et al., A Droplet-Based Building Block Approach For Bladder Smooth Muscle Cell (Smc) Proliferation, *Biofabrication* **2**, 014105 (2010).
56. Mironov, V.; R.p. Visconti, V. Kasyanov, G. Forgacs, C.j. Drake, R.r. Markwald, Organ Printing: Tissue Spheroids As Building Blocks, *Biomaterials* **30** (2009) 2164–74.
57. Gaetani, P. Doevendans, C.h.g. Metz, J. Alblas, E. Messina, A. Giacomello, Et al., Cardiac Tissue Engineering Using Tissue Printing Technology And Human Cardiac Progenitor Cells, *Biomaterials* **33** (2012) 1782e1790, <http://dx.doi.org/10.1016/j.biomaterials.2011.11.003>
58. Ozbolat, I. T., And Hospodiuk, M. Current Advances And Future Perspectives In Extrusion-Based Bioprinting. *Biomaterials* **76**, 321–343.2016. Doi:10.1016/j.biomaterials.2015.10.076
59. Schiele N.r. Et al., Laser-Based Direct-Write Techniques For Cell Printing, *Biofabrication* **2**, 032001 (2010).
60. Gruene M. Et al., Laser Printing Of Stem Cells For Biofabrication Of Scaffold-Free Autologous Grafts, *Tissue Eng. Pt-C. Meth.* **17**, 79–87 (2011).
61. Barron, J.a.; D. B. Krizman, B. R. Ringeisen, Laser Printing Of Single Cells: Statistical Analysis, Cell Viability, And Stress, *Ann. Biomed. Eng.* **33**, 121–130 (2005).
62. KOCH, L.; DEIWICK A, SCHLIE S, MICHAEL S, GRUENE M, COGER V, Et al. Skin Tissue Generation By Laser Cell Printing. *Biotechnol Bioeng.* 2012;109(7): 1855–63.
63. Levato R, Webbwr, Otto I A, Mensinga A, Zhang Y, Van Rijen M, Van Weeren R, Khan Imand Malda J 2017 The Bio In The Ink: Cartilage Regeneration With Bioprintable Hydrogels And Articular Cartilage-Derived Progenitor Cells *Acta Biomater.* **61** 41–53
64. Malda, J., Visser, J., Melchels, F.p., Jüngst, T., Hennink, W.e., Dhert, W.j., Groll, J., & Huttmacher, D.w. (2013). 25th Anniversary Article: Engineering Hydrogels For Biofabrication. *Advanced Materials*, **25** **36**, 5011–28 .
65. Groll, J.; Burdick, J. A.; Cho, D.-W.; Derby, B.; Gelinsky, M.; Heilshorn, S. C.; Jüngst, T.; Malda, J.; Mironov, V. A.; Nakayama, K.; Ovsianikov, A.; Sun, W.; Takeuchi, S.; Yoo, J. J.; Woodfield, T. B. F. A Definition Of Bioinks And Their Distinction From Biomaterial Inks. *Biofabrication*, V. 11, N. 1, P. 13001, 2018.
66. Kyle, S., Jessop, S.p. tarassoli@al-sabah@i.s.whitaker. 9 – Assessing Printability Of Bioinks.2018. Bioprinting For Reconstructive Surgery. Techniques And Applications. Pages 173–189. <https://doi.org/10.1016/B978-0-08-101103-4.00027-2>.
67. Paxton, N.; Smolan, W.; Böck, T.; Melchels, F.; Groll, J.; Jungst, T. Proposal To Assess Printability Of Bioinks For Extrusion-Based Bioprinting And Evaluation Of Rheological Properties Governing Bioprintability. *Biofabrication*, V. 9, N. 4, P. 44107, 2017.
68. Gao, C. Ruan And W. Li. (2019). High-Strength Hydrogel-Based Bioinks. *Mater. Chem. Front.* Doi: 10.1039/C9qm00373h.
69. Pourchet, L., Amélie Thepot, Marion Albouy, Edwin J. Courtial, Aurélie Boher, Loïc J. Blum, And Christophe A. Marquette. (2017). Human Skin 3d Bioprinting Using Scaffold-Free Approach. *Adv. Healthcare Mater.* 2017, 6, 1601101. 2016 Wiley-Vch Verlag Gmbh & Co. Kga, Weinheim
70. Zhang, Yu Shrike, Et al. “3d Bioprinting For Tissue And Organ Fabrication.” *Annals Of Biomedical Engineering* **45.1** (2017): 148–163.
71. Benyus, J.m. Biomimética Inovação Inspirada Pela Natureza. Editora: Cultrix. 2005.
72. Sun Y, Wang Q. In-Silico Analysis On 3d Biofabrication Using Kinetic Monte Carlo Simulations. *Adv Tissue Eng Regen Med Open Access*. 2017;2(5):256–259. Doi: 10.15406/atroa.2017.02.00045
73. Wei Long, Ng, Et al. “Proof-Of-Concept: 3d Bioprinting Of Pigmented Human Skin Constructs.” *Biofabrication* **10.2** (2018): 025005.
74. Planz, V., Lehr, C.-M. And Windbergs, M. (2016). In Vitro Models For Evaluating Safety And Efficacy Of Novel Technologies For Skin Drug Delivery. *Journal Of Controlled Release* **242**, 89–104. Doi:10.1016/j.jconrel.2016.09.002.
75. Michael, S, Sorg H, Peck Ct, Koch L, Deiwick A, Chichkov B, Et al. Tissue Engineered Skin Substitutes Created By Laser-Assisted Bioprinting Form Skin-Like Structures In The Dorsal Skin Fold Chamber In Mice. *Plos One*. 2013;8(3):E57741.
76. He, Peng, Junning Zhao4, Jiumeng Zhang2,3, Bo Li2,3, Zhiyuan Gou2,3, Maling Gou2,3 And Xiaolu Li1,4. Bioprinting Of Skin Constructs For Wound Healing. *He Et al. Burns & Trauma* (2018) **6**:5 Doi 10.1186/S41038-017-0104-X
77. Admane, Prasad Abhishak C. Gupta, Prashanth Jois, Subhadeep Roy, Chittur Chandrasekharan Lakshmanan, Gurpreet Kalsi, Balaji Bandyopadhyay, Sourabh Ghosh. (2019) Direct 3d Bioprinted Full-Thickness Skin Constructs Recapitulate Regulatory Signaling Pathways And Physiology Of Human Skin. *Bioprinting* **15**. E00051.
78. Lee W, Debasitis Jc, Lee Vk, Lee Jh, Fischer K, Edminster K, Et al. Multilayered Culture Of Human Skin Fibroblasts And Keratinocytes Through Threedimensional Freeform Fabrication. *Biomaterials*. 2009;**30**(8):1587–95.
79. Lee, Vivian, Gurtej Singh, John P. Trasatti, Chris Bjornsson, Xiawei Xu, Thanh Nga Tran, Seung-Schik Yoo, Guohao Dai And Pankaj Karande. Design And Fabrication Of Human Skin By Three-Dimensional Bioprinting. *Tissue Engineering: Part C*. Volume 20, Number 6, 2014. Mary Ann Liebert, Inc. Doi: 10.1089/Ten.tec.2013.0335
80. Abaci, H.e., Z. Guo, A. Coffman, B. Gillette, W.h. Lee, S.k. Sia, Et Al. human Skin Constructs With Spatially Controlled Vasculature Using Primary And Ipsc-Derived Endothelial Cells. *Adv Healthc Mater*, **5** (14) (2016), Pp. 1800–1807.
81. Cubo, Nieves, Et al. “3d Bioprinting Of Functional Human Skin: Production And In Vivo Analysis.” *Biofabrication* **9.1** (2016): 015006.

82. Maria–Engler, S. S. Harnessing Skin Reconstruction For Testing Topical Agents In A Healthy And Diseased Skin. *Toxicology Letters*, N. 259, P. S45, 2016.
83. Pedrosa, T. Do N., Catarino, C. M., Pennacchi, P. C. *Et al.* (2017). A New Reconstructed Human Epidermis For In Vitro Skin Irritation Testing. *Toxicology In Vitro : An International Journal Published In Association With Bibra* **42**, 31–37. Doi:10.1016/J.tiv.2017.03.010.
84. Pennacchi, P.c., De Almeida, M. E. S., Gomes, O. L. A. *Et al.* (2015). Glycated Reconstructed Human Skin As A Platform To Study The Pathogenesis Of Skin Aging. *Tissue Engineering. Part A* **21**, 2417–25. Doi:10.1089/Ten.tea.2015.0009.
85. Pennacchi, Paula Comune ; Almeida, Maíra Estanislau Soares De ; Gomes, Octávio Luís Alves ; Faião–Flores, Fernanda ; Crepaldi, Maria Clara De Araújo ; Dos Santos, Marilice Fagundes ; Barros, Silvia Berlanga De Moraes ; Maria–Engler, Silvy S. . Glycated Reconstructed Human Skin As A Platform To Study Pathogenesis Of Skin Aging. *Tissue Engineering. Part A*, V. 1, P. 150701104440009, 2015.
86. Jia, D., D. J. Richards, S. Pollard, Y. Tan, J. Rodriguez, R. P. Visconti, T. C. Trusk, M. J. Yost, H. Yao, R.R. Markwald, Y. Mei, *Acta Biomater.* 2014, **10**, 4323.
87. Yu, Z., Y. Rui, O. Liliang, D. Hongxu, Z. Ting, Z. Kaitai, C. Shujun, S. Wei, *Biofabrication* 2014, **6**, 035001.
88. Yang, Y.i., D. L. Seol, H. I. Kim, M. H. Cho, S. J. Lee, *Curr. Appl. Phys.* 2007, **7**, E103.
89. Bini, A., P. Haidaris, B. J. Kudryk, *Encyclopedic Reference Of Vascular Biology And Pathology*, Springer Verlag, New York 2000.
90. Oecd. In Vitro Skin Irritation: Reconstructed Human Epidermis Test Method. Oecd Guidelines For The Test Of Chemicals. Section 4. July, 2015. 1–21.
91. Takagi R, Ishimaru J, Sugawara A *Et Al.* Bioengineering A 3d Integumentary Organ System From Ips Cells Using An *In Vivo* Transplantation Model. *Sci. Adv.* 2(4), E1500887 (2016).
92. Rodrigues Neves C., Gibbs S. (2018) Progress On Reconstructed Human Skin Models For Allergy Research And Identifying Contact Sensitizers. In: . *Current Topics In Microbiology And Immunology*. Springer, Berlin, Heidelberg.
93. Li, Z., S. Huang, X. Fu. 3d Bioprinting Skin. General Hospital Of PLA, Beijing, China 3d Bioprinting For Reconstructive Surgery. <https://doi.org/10.1016/B978-0-08-101103-4.00017-X> © 2018 Elsevier Ltd. All Rights Reserved.



Tissue engineering of different cartilage types: a review of different approaches and recent advances

Karim Boumediene¹, Mira Hammad¹, Justin Dugué², Alexis Veysié³, Catherine Baugé¹

*Corresponding author: E-mail address: karim.boumediene@unicaen.fr

Abstract: Cartilage is a connective tissue that serves as a structural support for maintaining the shape for specific appendices (nose, ear) and also helps for shock absorption when present in joints. Different types of cartilage coexist in the body: hyaline, elastic and fibrocartilage. Due to their different embryologic origin, they produce distinct extracellular matrix and therefore have specific functions according to their location. Cartilage is frequently subjected to many different lesions. Those include traumatic, metabolic and congenital forms, concerning all regions where this tissue is present: joints, head and neck area, intervertebral disks, etc. Increasing number of cancers also affects cartilage; especially in ear, nose and trachea. Unfortunately, this tissue has a poor regeneration ability. Few therapeutic options exist for cartilaginous lesions and most of them concern articular cartilage. They include micro fracture, autologous chondrocytes implantation, mosaicplasty, allograft and prosthesis. Ear and trachea are also targeted for reconstruction with lesser extent. Therefore, cartilage engineering highly addresses increasing number of pathologies associated to this tissue. In the last two decades, several trials were investigated using both progenitor cells and scaffolds. Even bone marrow derived stem cells were widely used and served as gold standard. Many progenitors from different areas are investigated for their capacity of chondrogenesis. On the other hand, biomaterials, natural and synthetic, are used to induce a 3D environment that allows proper growth and differentiation toward cartilage formation. Their characteristics depend on the location of the expected graft where porosity, biodegradability, ability to support strength and large scale use are the key points. Favorable environments are also needed to achieve appropriate chondrogenesis, including biochemical or mechanical stimuli and low oxygen tension. Bioprinting showed also encouraging outcomes in cartilage reconstruction with the investigation of several scaffolds.

Keywords: Cartilage; Tissue engineering.

Introduction

Different cartilage types and functions

Cartilage is a connective tissue that serves as a structural support in several areas of the body. Its main function is maintaining the shape (ear, nose) and absorbing shocks (joints). Three different types of cartilage coexist in humans. Hyaline cartilage is the most abundant and is found mainly in joints and also in the trachea and nasal septum. With a blue aspect and a smooth surface, it is usually surrounded by a thin membrane called perichondrium. At biochemical level, the extracellular matrix contains type II collagen, aggrecan, keratan and chondroitin sulfate. Elastic cartilage is found in organs like ear, Eustachian tube, larynx, nostril opening and epiglottis. Its function is to allow both support and flexibility. These characteristics are provided by its high elastin and collagen content. The third type is called fibrocartilage is restricted to areas that need a high resistance to strength, like intervertebral discs, sacroiliac and costochondral joints, or pubis symphysis. In addition to type II collagen, fibrocartilage contains type I collagen as well.

Cartilage during development

Differences between cartilage composition and functions are explained by their distinct origin during embryologic development. Indeed, hyaline cartilage derives from the mesenchyme with key role of SOX transcription factors during its formation. Under the effect of paracrine factors and hormones, cartilage specific genes and mesenchymal stem

cells are activated and differentiated toward chondrocytes (Decker, 2017). The facial cartilage develops from neural crest (neuroectoderm) and mesenchyme. During development, cells migrate to specific locations where they differentiate under the control of *HOX* genes, leading to segmentary organization and different segments in buds of the face and pharyngeal arches (Suzuki and Osumi, 2015). The external ear derives from the first branchial cleft (Anthwal and Thompson, 2016). Tracheal cartilage in its turn, develops from endodermal origin. Beside *SOX* and *HOX* transcription factors, were described to play key roles in cartilage development. Knockdown experiments in *X. laevis* highlighted the role of *FOXP3* in the development of new cartilage. *RUNX3* and *SOX9B* are also involved through a regulation cascade via BMPs (Dalcq, et al., 2012). In addition, *MIR 140* was also described to be involved in cranial cartilage formation via *PDGFRa*, since it provokes cranio facial defects in both zebra fish and mouse.

Cartilage lesions

Depending on its location, cartilage is subject to several injuries and lesions. In joints, osteoarthritis (OA) and rheumatoid arthritis (RA) are degenerative diseases with multiple causes, including mechanical stresses, genetic factors and trauma. Concerning head and neck cartilage, main lesions are from traumatic, congenital and metabolic origin. Beside, a lot of congenital abnormalities of the ear (microtia, anotia) and the nose (Apert syndrome) lead to heavy and multiple interventions with

many prostheses or autologous transplantations which could provoke donor sites. The trachea is also subject to trachea bronchial tumors and congenital deformity. Tracheal stenosis is also an especially risk after an intubation. Unfortunately, only few options exist in regards to ear and nose reconstruction, with stents application and tracheotomy. In addition, the growing number of cancers in the area of head and neck affects cartilage and therefore increases the need of its reconstruction in several areas.

Specificity of cartilage biology

Cartilage is avascular and non-innervated tissue. During decades, it was described to harbor a single cell type, namely chondrocytes. However, it also contains progenitors which activate and participate in its repair (OA cartilage). However due to its hypoxic microenvironment with a gradient of oxygen comprised between 1 to 7% of oxygen, the regeneration potential is very limited. At biochemical level, the cartilaginous extra cellular matrix (ECM) is specific to the tissue and contains a complex macromolecular network of collagens, proteoglycans and several glycoproteins, and possibly elastin for some areas (ear). The cell-ECM interactions are established through integrins, CD44 and proteoglycans receptors (syndecans). The contents of ECM differs in both quality and quantity, depending on the function and type of cartilage.

Clinical approaches of cartilage reconstruction

Historically, OA is the main cartilage disease targeted by reconstruction at clinical level. Therefore, orthopedic surgeons used several techniques with more or less success: microfracture, mosaicplasty, autologous chondrocyte implantation and allograft. Auricular cartilage is also targeted by cartilage reconstruction. Its complex anatomic tridimensional structure is a challenge for reconstruction. Here again, multiple approaches were used between two- and four stage techniques using autologous costal cartilage which led to good results in terms of contour and framework definition. However, long term outcomes show several cons, including the need to carry out several operations, calcification of the construct, necrosis, contraction of the skin, as well as cartilage resorption (Whatson and Hecht, 2017). Moreover, even if the two-step techniques provides the best pros regarding long term outcomes, limits in its use concern the age of patient concerned (under age of 10) (Jessop et al, 2016). All in all, despite these approaches, it is still yet very difficult to reproduce native tissue with appropriate flexibility, strength and elasticity. Due to its complex anatomy and function, trachea reconstruction undergoes several challenges. It needs to build a safe and stable conduct to ensure breathing without assistance and avoid airways collapses. Therefore, multiple trials were done with insertion of small pieces of cartilage to strengthen the upper airways. The trachea is also more complex since it includes several cell types and tissues, i.e. chondrocytes, epithelial cells and neurons. Recently, assays were done with decellularized matrixes used with chondrocytes and bronchial epithelial cells. Synthetic scaffolds including nanocomposite polymers complexed with growth factors are also tried to optimize progenitor's recruitment in the trachea. The loss of voluminous cartilage substances in head and neck area remains to date without effective treatment in terms of safety, preservation of cartilage properties and aesthetic performance.

Cells for cartilage tissue engineering

Like lot of tissue, cartilage undergoes extensive research aiming at its ex vivo reconstruction. They involve the choice of primary cells or progenitors combined with scaffolds, natural or synthetic, as they are decellularized, which are then incubated in appropriate conditions chosen to favor chondrogenesis. Primary chondrocytes would be suitable for this purpose but their small number in biopsies requires extensive amplification. Unfortunately, chondrocytes undergo dedifferentiation during this step, which limits their use in cartilage engineering. In addition, the need of biopsies of cartilage from healthy area is likely to create donor sites. Instead, several progenitors are tested with a lot of advantages, such as the ease of obtaining, several types and tissue sources. The gold standard are mesenchymal stromal cells (MSCs) due to their proliferative rate

Approaches to the development of 3D bioprinted...

and multipotency (Baugé and Boumediene, 2015). Hundreds of studies, in vitro, in vivo or clinical trials, described their suitability to repair large cartilaginous and connective tissue defects. They derived mainly from bone marrow, but are also obtained from blood, umbilical cord, Wharton jelly, amniotic liquid, dental pulp, adipose tissue, synovial tissue and perichondrium (Mazor et al., 2014). Even their molecular signature is not completely defined, these cells are known to harbor several surface markers such as CD28, CD33, CD44, CD71, CD73, CD90, CD91, CD105, CD106, CD120a, CD124, CD131, CD166 and class I HLA. In addition, MSCs are negative to others markers, mainly hematopoietic ones, i.e. CD14, CD31, CD34, CD45, CD117. While many tissues contain MSCs, they are not equal for the construction of different types of cartilage. Indeed, specificities of some areas require the expression of peculiar ECM. For example, auricular cartilage which is elastin-rich is more likely obtained by using progenitors from amniotic liquid or from auricular perichondrium (Kunisaki, et al. 2007, Takebe, 2012). Therefore, the investigation of multiple sources of progenitors would bring more precise definition on the choice of which cells to use to target a specific cartilage.

Scaffolds

A lot of them are assayed for their biocompatibility. Requirements of scaffolds include also immunocompatibility, ability to mimics the host tissue shape. They should also allow cell adhesion, proliferation and differentiation in a tridimensional environment (Korkusuz et al., 2016). Regarding the great variety of tissues to be constructed, their characteristics depend on the location of the graft. Hence, porosity, ability to support strength and biodegradability, are needed for certain tissues. Among natural scaffolds used for cartilage are agarose, alginate, collagens and hyaluronic acid or chitosan (Agrawal and Pramanik, 2019). Beside, several combinations of synthetic biomaterials serve also to mimic the biomechanical properties of cartilage by hosting chondrocytes or differentiating progenitors. The fact that they should be biodegradable is yet a question open to debate. Polyhydroxyacids like PLLA, PCL, PGA and also polyurethane are then used, some of them tried for cartilage reconstruction (Pourbashir et al., 2019). Polyethylene glycol which is already FDA approved is also an option, where its analogs are investigated. Recently, new synthetic scaffolds gave good outcomes. For example, sericin, a silkworm protein that could be functionalized with methacryloyl, and RAD16-I, a self-assembling peptide into nanofiber network yielded promising results in vitro.

In vitro chondrogenesis environment

The achievement of chondrogenesis in vitro is a combination of multiple conditions (Ciuffreda, et al., 2016). Addition of growth factors such as *TGFβs*, *IGF*, or *Wnt* as biochemical stimuli are widely used. Indeed, chondrogenic media are used for chondrogenesis induction and phenotype sustaining. In addition, progenitor's differentiation toward chondrocyte may need mechanical tension and shear stress. CSM are mechanosensitive and then chondrogenesis can be triggered by compression forces which modulate protein synthesis to achieve their differentiation (Gaut and Sugaya, 2015; Glatt et al., 2019). Cartilage is a hypoxic tissue with low oxygen content (1-7%). Therefore, hypoxia is usually used to ensure a proper environment during cartilage engineering. At the molecular level, low oxygen tension activates peculiar transcription factors such as HIF-1 and HIF-2 (Duval et al., 2012), which in turn, modulate multiple target genes. Among them, specific cartilage markers like type II collagen and aggrecan are enhanced in hypoxia, while undesirable ones such as type I collagen are inhibited (Duval et al., 2016). Finally, in vitro chondrogenesis, should include culturing cells in bioreactors. These latter can ensure perfusion of cellularized matrixes, shaking with or without rolling and eventually compression for mechanical stimuli.

Cartilage bioprinting

Since cartilage is an avascular and non-innervated tissue, it is obvious that it was one of the first tissues targeted by bioprinting. Indeed, except few progenitors embedded inside, this tissue contains a single cell type, namely chondrocytes. Therefore, it appears simple to try its construction once 3D printing came to tissue engineering. Several trials were done with

¹Normandie Université, UNICAEN, EA7451, BioConnect, 14032, Caen, France; Fédération hospitalo universitaire SURFACE (Amiens, Caen, Rouen).

²Normandie Université, UNICAEN, EA7451, BioConnect, 14032, Caen, France; Fédération hospitalo universitaire SURFACE (Amiens, Caen, Rouen); Service ORL et chirurgie cervico-faciale, CHU, avenue de la Côte-de-Nacre, 14033 Caen cedex 9, France.

³Normandie Université, UNICAEN, EA7451, BioConnect, 14032, Caen, France; Fédération hospitalo universitaire SURFACE (Amiens, Caen, Rouen); Service de chirurgie maxillo faciale, CHU, avenue de la Côte-de-Nacre, 14033 Caen, cedex 9, France.

different scaffolds or combination of them as bioinks (hydrogels, alginate, gelatin, chondroitin sulfate, lutrol...). They were printed as specific shapes corresponding to particular organs (ear, nose, trachea) before seeding them with cells (Bae et al., 2018; Di Gesu et al., 2019). Therefore, this approach might make bioprinting very beneficial for tissular reconstruction for several reasons. Indeed, it permits to replicate the anatomical forms while reducing surgical techniques and outcomes, to avoid donor site morbidity. However, whatever the methods of biofabrication used, investigations are still ongoing to select the suitable scaffold material to ensure a good encapsulation and printing directly with living cells, knowing that they could be altered during printing and by biomechanical properties of bioinks. Moreover, a good bioink for cartilage should ensure adequate resistance to mechanical strength (Zamborsky et al., 2019).

Conclusion

Despite its apparent simple structure with a single cell type, cartilage remains complex to be reconstructed in vitro. Multiple organs that contain this tissue exhibit differences at the biochemical level, explained by divergent embryologic origins and then subsequent roles. These parameters should be taken into account during cartilage engineering by choosing appropriate progenitors that provide the right biochemistry of the desired tissue, and the appropriate scaffold that ensures a good environment for cell proliferation and chondrogenesis. The recent input of 3D printing technology brought encouraging outcomes and will probably help to improve this field by reducing surgical operating times and replicating complex anatomical forms.

References

- Agrawal P, Pramanik K. Enhanced chondrogenic differentiation of human mesenchymal stem cells in silk fibroin/chitosan/glycosaminoglycan scaffolds under dynamic culture condition. *Differentiation*. 2019 Sep 19;110:36–48
- Anthwal N, Thompson H. The development of the mammalian outer and middle ear. *J Anat*. 2016 Feb;228(2):217–32. doi: 10.1111/joa.12344. Epub 2015 Jul 30. Review.
- Bae SW, Lee KW, Park JH, Lee J, Jung CR, Yu J, Kim HY, Kim DH. 3D Bioprinted Artificial Trachea with Epithelial Cells and Chondrogenic-Differentiated Bone Marrow-Derived Mesenchymal Stem Cells. *Int J Mol Sci*. 2018 May 31;19(6). pii: E1624. doi: 10.3390/ijms19061624
- Baugé C, Boumediene K. Use of Adult Stem Cells for Cartilage Tissue Engineering: Current Status and Future Developments. *Stem Cells Int*. 2015;2015:438026. doi: 10.1155/2015/438026. Epub 2015 Jul 9. Review.
- Ciuffreda MC, Malpasso G, Musarò P, Turco V, Gnecci M. Protocols for in vitro Differentiation of Human Mesenchymal Stem Cells into Osteogenic, Chondrogenic and Adipogenic Lineages. *Methods Mol Biol*. (2016). *Methods Mol Biol*. 2016;1416:149–58. doi: 10.1007/978-1-4939-3584-0_8.
- Decker RS. Articular cartilage and joint development from embryogenesis to adulthood. *Semin Cell Dev Biol*. 2017 Feb;62:50–56. doi: 10.1016/j.semcdb.2016.10.005. Epub 2016 Oct 20. Review.
- Di Gesu R, Acharya AP, Jacobs I, Gottardi R. 3D printing for tissue engineering in otolaryngology. *Connect Tissue Res*. 2019
- Duval E, Baugé C, Andriamanalijaona R, Bénateau H, Leclercq S, Du-toit S, Poulain L, Galéra P, Boumediene K. Molecular mechanism of hypoxia-induced chondrogenesis and its application in in vivo cartilage tissue engineering. *Biomaterials*. 2012 Sep;33(26):6042–51. doi: 10.1016/j.biomaterials. 2012.04.061. Epub 2012 Jun 6.
- Duval E, Bouyoucef M, Leclercq S, Baugé C, Boumediene K. Hypoxia inducible factor 1 alpha down-regulates type I collagen through Sp3 transcription factor in human chondrocytes. *IUBMB Life*. 2016 Sep;68(9):756–63. doi: 10.1002/iub.1539. Epub 2016 Aug 13.4
- Gaut C, Sugaya K. Critical review on the physical and mechanical factors involved in tissue engineering of cartilage. *Regen Med*. 2015;10(5):665–79. Epub 2015 May 22. Review.
- Glatt V, Evans CH, Stoddart MJ. Regenerative rehabilitation: The role of mechanotransduction in orthopaedic regenerative medicine. *J Orthop Res*. 2019 Jun;37(6):1263–1269. doi: 10.1002/jor.24205. Epub 2019 Jan 16. Review.
- Jessop, ZM Javed M, Otto IA, Combelleck EJ, Morgan S, Breugem CC, Archer CW, Khan IM, Lineaweaver WC, Kon M, Malda J, Whittaker IS. Combining regenerative medicine strategies to provide durable reconstructive options: auricular cartilage tissue engineering Stem Cell research and therapy, 2016 Jan 28;7:19. doi: 10.1186/s13287-015-0273-0
- Korkusuz P, Kose S, Kopru CZ. Biomaterial and Stem Cell Interactions: Histological Biocompatibility. *Curr Stem Cell Res Ther*. 2016;11(6):475–486. Review.
- Kunisaki C, Makino H, Takagawa R, Yamamoto N, Nagano Y, Fujii S, Kosaka T, Ono HA, Otsuka Y, Akiyama H, Ichikawa Y, Shimada H. (2007,) Surgical outcomes in esophageal cancer patients with tumor recurrence after curative esophagectomy. *J Gastrointest Surg*. 2008 May;12(5):802–10. Epub 2007 Oct 20.
- Mazor M, Lespessailles E, Coursier R, Daniellou R, Best TM, Toumi H. Mesenchymal stem-cell potential in cartilage repair: an update. *J Cell Mol Med*. 2014 Dec;18(12):2340–50. doi: 10.1111/jcmm.12378. Epub 2014 Oct 29. Review
- Pourbashir S, Shahrousvand M, Ghaffari M. Preparation and characterization of semi-IPNs of polycaprolactone/poly (acrylic acid)/cellulosic nanowhisker as artificial articular cartilage. *Int J Biol Macromol*. 2019 Oct 5. pii: S0141-8130(19)33740-7.
- Suzuki J, Osumi N. Neural crest and placode contributions to olfactory development. *Curr Top Dev Biol*. 2015;111:351–74. doi: 10.1016/bs.ctdb.2014.11.010. Epub 2015 Jan 20. Review
- Takebe T, Kobayashi S, Kan H, Suzuki H, Yabuki Y, Mizuno M, Adegawa T, Yoshioka T, Tanaka J, Maegawa J, Taniguchi H. Human elastic cartilage engineering from cartilage progenitor cells using rotating wall vessel bioreactor. *Transplant Proc*. 2012 May;44(4):1158–61. doi: 10.1016/j.transproceed.2012.03.038
- Watson D, Hecht A. Repair of Auricular Defects. *Facial Plast Surg Clin North Am*. 2017.
- Zamborsky R, Kilian M, Jacko P, Bernadic M, Hudak R. Perspectives of 3D printing technology in orthopaedic surgery. *Bratisl Lek Listy*. 2019;120(7):498–504.



Intelligent Copolymers Based On Poly (N-Isopropilacrylamide). PART II: Grafts polysaccharide to obtain new biomaterials for biomedical and pharmacological applications

Marcos Antonio Sabino¹, Maria Gabriela Carrero¹, Carlos Julio Rodriguez¹

*Corresponding author: E-mail address: msabinog@gmail.com

Abstract: Biopolymers such as polysaccharides are compounds that have functional groups and they are very susceptible to be used in chemical modifications and also allows them to synthesizer of new copolymers (used as graft-like chains). Poly (N-Isopropylacrylamide) PNIPAm, is a thermosensitive synthetic polymer widely used in the preparation of intelligent gels for the biomedical field, but have some limitations in use as biodegradable matrix or scaffolds. In this research were the synthesis and characterization of copolymers their PNIPAm grafted with the polysaccharides: chitosan (CS) or hyaluronic acid (HA), were performed to obtain new biodegradable and biocompatible biomaterials that conserve the intelligent character (thermosensitivity). The PNIPAm was in first chemically modified with 3-butenic acid in order to generate carboxyl end groups on the graft-polymer chain (PNIPAm-co-COOH) which serve as anchor points and then covalently graft the polysaccharides. For the specific case of grafting with hyaluronic acid, it was necessary to perform a second modification using piperazine (PIP) and obtain the graft-polymers PNIPAm-co-COO-g-PIP. All this modification process was previously reported (Carrero et al, 2018). In this case, the polysaccharides used as grafts-like chains were: (1) chitosan oligomers obtained by acid degradation and (2) hyaluronic acid. The characterization of all copolymers obtained was follow by infrared spectroscopic (FT-IR); the differential scanning calorimetric (DSC) technique was used to determine the lower critical solution transition temperature (LCST), resulting in the range of 29–34 °C. Its morphology was studied using scanning electron microscopy (SEM), but previously was simulate an inject process, for the reversible gel character presented by these novel copolymers; resulting a high porosity and interconnection between pores (scaffold-like micrometric structures). Hemocompatibility assays were performed on agar/blood systems, showing non cytotoxicity. All these results give these graft-copolymers a high potentiality of use as scaffolds in tissue engineering and also for pharmacological applications.

Keywords: Poly (N-Isopropylacrylamide); Chitosan; Hyaluronic acid; Intelligent graft copolymer; LCST temperature; Scaffolds.

Introduction

The science and technology of biomaterials has develop enormously in recent decades. Examples of this development are the intelligent materials that respond reversibly to a change in their environment, such as those exhibited by intelligent hydrogels^{1,2}. Materials sensitive to stimuli that are capable of modifying their conformation and properties in response to changes in different physiological variables, receive more attention for the manufacture and design of therapeutic devices for biomedical applications^{3,4}. Especially, materials sensitive to temperature and pH are the most studied because these parameters change naturally and can be easily controlled², also because pH and temperature are physiological parameters that controlled several organics route in regenerative process.

Thanks to the intelligent thermosensitive character, Poly (N-Isopropylacrylamide) (PNIPAm) has become one of the most studied synthetic polymers in the reported scientific literature^{5,6}. Particularly through copolymers synthesis and grafting reactions, because it is possible to obtain a macromolecular chain with one or more monomers attached in the form of blocks, or even side chains or ramifications^{7,8}. In this last type of copolymerization, different monomers are covalently bound to the main backbone of the polymer. Depending on the degree of bonding and the incorporated side chain length, the physical/chemistry, morphological and mechanical properties of the grafted copolymer will be defined⁹. This is one of the reason why graft copolymers have attracted increasing attention for applications from materials science to biology⁸, medicine^{10,11} and pharmacology^{12,13}. For example, the design of polysaccharides grafted

with a thermosensitive synthetic polymer has been reported^{14–17}, where the polysaccharide can provide biodegradability character and non-toxicity, while the synthetic polymer provides thermal sensitivity²⁰.

In the case of PNIPAm, although N-isopropylacrylamide monomer (NIPAm) is cytotoxic, the polymer does not show toxicity^{6,18,19}. This led the design of various biomaterials based on this polymer, such as: sensors²¹, devices for controlled drug release^{22,23}, artificial muscles and injectable scaffolds^{24,25}, between others. However, synthetic biomaterials, in most cases, do not provide biological signals in their molecular chains to facilitate cell-material interaction. Therefore, the modification of synthetic polymers with biopolymers could facilitate the response of the biomaterial with biological systems and improve their biocompatibility. It has been reported in the literature that the incorporation of natural products allows to improve the biocompatibility of synthetic polymers^{26,27}.

Consider all this aspect, the aim of this work is to obtain an intelligent copolymer based on Poly (N-Isopropylacrylamide) as the bone chain and grafting by side chain incorporation of chitosan oligomers or hyaluronic acid as ramifications. A preliminary evaluation was made on the minimum molar ratio between the main polymer chain and the branch to be grafted. So if a high concentration of the polymer to be grafted is placed it could cause steric impediments, as shown in the proposed model of Figure 1, and is related to the previously reported by Carrero et al (Part I, 2018). This study including the exhaustive characterization, and propose the potential application in these copolymers for biomedical and pharmacological area.

Materials and methods

¹Grupo B5IDA, Departamento de Química, Universidad Simón Bolívar, Caracas, Venezuela, AP 89000.

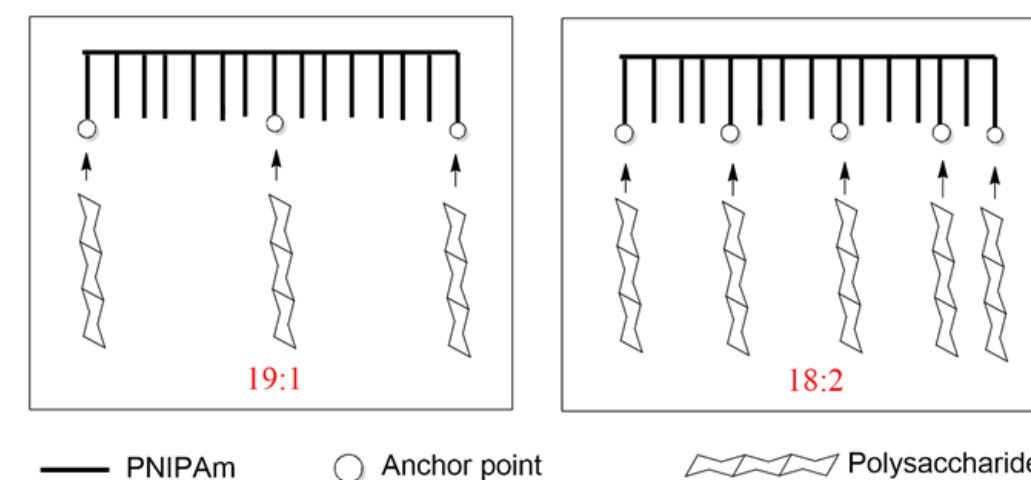


Figure 1– Representative model for the modification of the functionalized PNIPAm chain, which presents anchoring points for grafting reactions with polysaccharides.

Materials

N-Isopropylacrylamide (NIPAm), 3-butenic acid, piperazine (PIP), 1-ethyl- (3-3-dimethylaminopropyl) carbodiimide (EDC), N-hydroxy-succinimide (NHS) and high molecular weight chitosan (CS) were provided by Sigma-Aldrich. Potassium peroxydisulfate (KPS) Riedel de Haën. Hyaluronic acid (HA), commercial drug of Suprahyl (Laboratory NOLVER). All other chemicals used were analytical grade.

The viscosimetric molecular weights (M_v) of grafting polysaccharides were determined using a capillary viscometer, resulting: for HA a $M_v = 2,0 \times 10^6$; and CS oligomers a $M_v = 2,9 \times 10^4$ consider their preparation as oligomers using the acid degradation process reported by Vieira et al²⁵.

Methods

Synthesis of the precursors PNIPAm-co-COOH y PNIPAm-co-COOH-g-PIP

The precursors were synthesized according to previously described methods reported by Carrero et al²⁸. However, in this case the NIPAm monomer was polymerized with 3-butenic acid at molar ratios of 19: 1 and 18: 2 respectively, thus obtaining the PNIPAm-co-COOH. For the incorporation of HA side chains, the PNIPAm-co-COOH was modified by grafting piperazine (PNIPAm-co-COOH-g-PIP). Figure 1 shows a structural model proposed in this work. In which it reflected how the chemical modification is given with the 3-butenic acid and/or piperazine, on PNIPAm main chain, and after the incorporation of ramifications of CS(oligomers) or HA.

Synthesis of the graft copolymer PNIPAm-g-CS y PNIPAm-g-HA

A condensation process was carried out for the copolymerization. The carboxylic acid group is coming from PNIPAm-co-COOH, and the amine group is coming from CS, for the synthesis of PNIPAm-g-CS. The process follow with constant stirring for 12 hours, at room temperature. The molar ratio use was PNIPAm-co-COOH: CS 10:1 respectively. During the reaction, EDC was used as the activating agent of the carbonyl groups and NHS as a condensing agent in aqueous medium (EDC/NHS ratio 1:2). Under these conditions the grafting reaction with the amino groups of the chitosan is favored, and proposed in figure 2.

The PNIPAm-g-HA graft is obtained from previously PNIPAm-co-COOH functionalized with piperazine (PNIPAm-co-COOH-g-PIP), which has amino groups available for the reaction with activated carbonyls of HA; due to the presence of the EDC/NHS in the medium, as shown in figure 3. The process follow with constant stirring for 24 h, at room temperature, and consider a PNIPAm-co-COOH-g-PIP:HA ratio 10:0,7.

Obtained each graft copolymer separately, the gels were dialyzed for 48 h, after were freeze-dry by lyophilized, and subsequent characterized.

Characterization

FTIR-ATR spectroscopy of graft copolymers

Samples were analyzed by Fourier Transform infrared spectroscopy FT-IR (coupled to an ATR with ZnSe attenuated total reflectance crystal) Thermo Scientific brand, model Nicolet IS5, performing 32 scans at 4 cm^{-1} resolution, in a range of 4000 and 400 cm^{-1} .

Determination of the LCST of the graft copolymers by using DSC

After lyophilizing the copolymers, each sample was placed in aluminum capsules. The sample weight was approximately 5.00 mg, and 5 μL of distilled water was add, and after capsules were sealed with pressurized hermetic. The tests were perform on a Differential Scanning Calorimetry (DSC) equipment, Perkin-Elmer Model DSC 7. The DSC calorimeter was calibrate with indium (In) in inert nitrogen atmosphere to obtain the corresponding baseline. Only one way of heating was carry out at 20°C/min, in a temperature range from 25 to 50°C for each sample.

Morphological study of graft copolymers

Because the gel-like character and thermo sensitive response of the copolymers obtained, the process of injectability was simulated according procedure described by Coronado et al²⁹, Vieira et al²⁵ and Carrero et al²⁸. In this way, the morphology of the copolymers could be closer of the morphology that they can developed in the biomedical applications. The samples studied were those obtained after freeze-drying (xerogel) which were cryogenically fractured in $\text{N}_2(\text{liquid})$ to ensure the morphological observation of the inside of each sample. Then, they were coated with a thin layer of gold in a Balzers-SCD 030 sputter coater, and a JEOL JSM6390 scanning electron microscope was used for the morphological analysis of sample porosity. The voltage of the SEM equipment was set to 20–25 kV.

Cytotoxicity test by cell hemolysis on blood agar

Blood compatibility was evaluated with hemolysis assay according procedure described by Coronado et al²⁹, Vieira et al²⁵ and Carrero et al²⁸. The blood was mixed with agar in a totally sterile medium and was gelled for 2 h in an oven at 37 °C. Each lyophilized sample was subjected to 1h of UV irradiation for sterilization. Once the gels were sterile, they were brought into contact with blood/agar system and were transferred in the oven for cell culture at 37 °C and a 5% CO_2 flow. The protocol was perform according to ISO-10993-4 (2002) test assay. The surface around each gel or copolymer sample was observed and photograph several time for a total time of 48 h.

Results and Discussion

Characterization of graft copolymers

After the grafting reaction, the characteristic signals of the precursors PNIPAm-co-COOH and PNIPAm-co-COOH-g-PIP are conserved in the FTIR spectrum. However, the stretch band produced by the presence of hydroxyl groups (-OH) is more pronounced in the FTIR spectrum of the

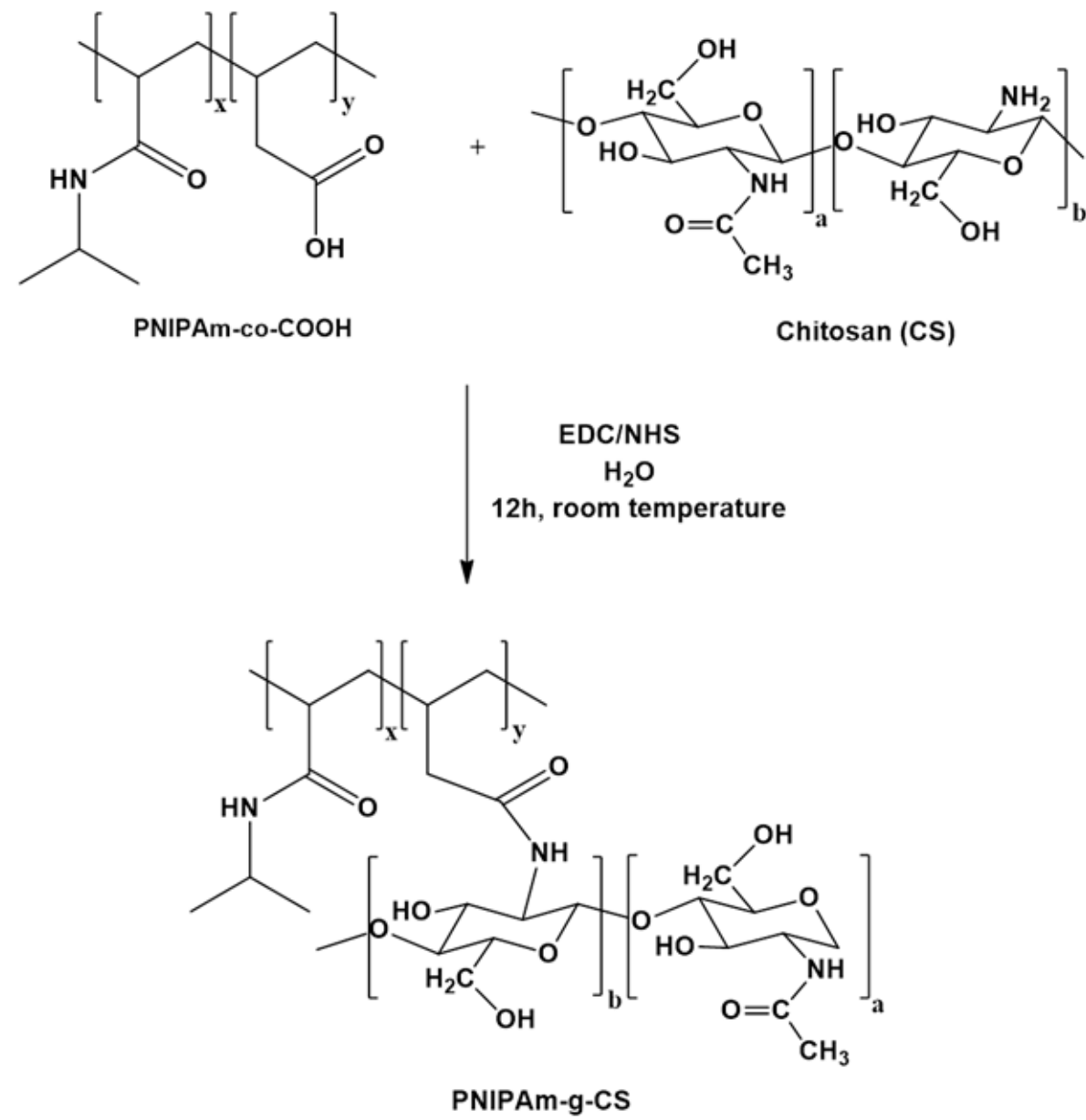


Figure 2 – Copolymerization reaction to obtain the PNIPAm-co-COOH grafts and the chitosan oligos (PNIPAm-g-CS).

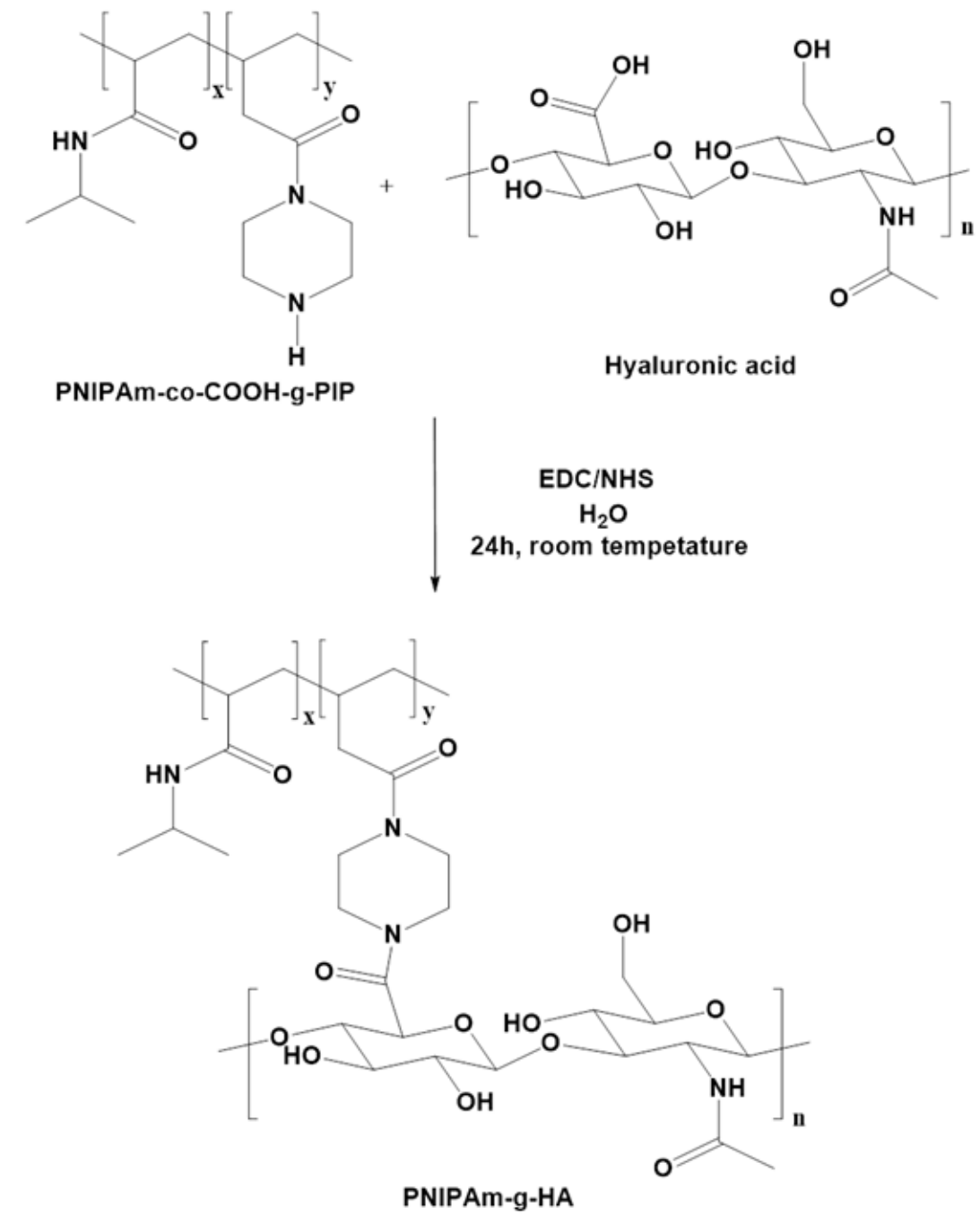


Figure 3 – Copolymerization reaction to obtain the grafts of PNIPAm-co-COOH-g-PIP and hyaluronic acid (PNIPAm-g-HA).

graft copolymers, due to the abundance of these groups in the structure of the incorporated polysaccharide. This signal is present above 3000 cm^{-1} , and can be distinguished in both cases of study (see figure 4A and 5A). In the FTIR figures, the spectrum of the precursors (PNIPAm-co-COOH, and PNIPAm-co-COOH-g-PIP) were present as a control. When CS or HA is incorporated into the copolymer, the structural change is clear and show the characteristic signals of polysaccharides, which have been widely studied and reported in the literature³⁰⁻³⁶. All these structural changes are according to the reactions shown in figures 2 and 3.

In general, it is possible to observe with intensity the band in 1044 cm^{-1} attributed to the stretching C-O-C, as well as the stretching signal of carbonyl group C=O around 1600 cm^{-1} and the deformation band of -NH between $1350-1450\text{ cm}^{-1}$; and the signal in 3000 cm^{-1} is due to stretching -CH.

The amine signal present in the precursor PNIPAm-co-COOH-g-PIP, around 1215 cm^{-1} , disappears due to the formation of an amide bond with hyaluronic acid. A more pronounced signal appeared at 1250 cm^{-1} product of the C-N tension of the new bond between piperazine and HA

(see Figure 5B). Similarly, for the PNIPAm-g-CS graft it is possible to observe the appearance of a band in 1250 cm^{-1} , as shown in Figure 4B, which can be attributed to the formation of the amide bond between the precursor PNIPAm-co-COOH and the CS oligomers.

For the copolymer PNIPAm-g-CS, it was verify that the carbonyl band returns to 1624 cm^{-1} indicating the formation of a new amide bond between the PNIPAm-co-COOH and the chitosan oligomers (see Figure 4B).

Additionally, in figure 5B, the signals between 1500 and 1700 cm^{-1} are better defined in the grafts, than in the precursor and HA. The amide mode-I signal, product of the vibration tension of the carbonyl group, is intensified above 1600 cm^{-1} , as is the amide mode-II signal due to the flexion vibration of the N-H bond and vibration tension of the C-N links is around to 1550 cm^{-1} , confirming the formation of the covalent amide bond between the chain of PNIPAm-co-COOH-g-PIP and HA³⁷. This behavior is seen for both PNIPAm-g-HA grafts (ratio 19:1 and 18:2).

Determination of the LCST of the graft copolymers

In Figure 6, it can be observed as all synthesized graft copolymers

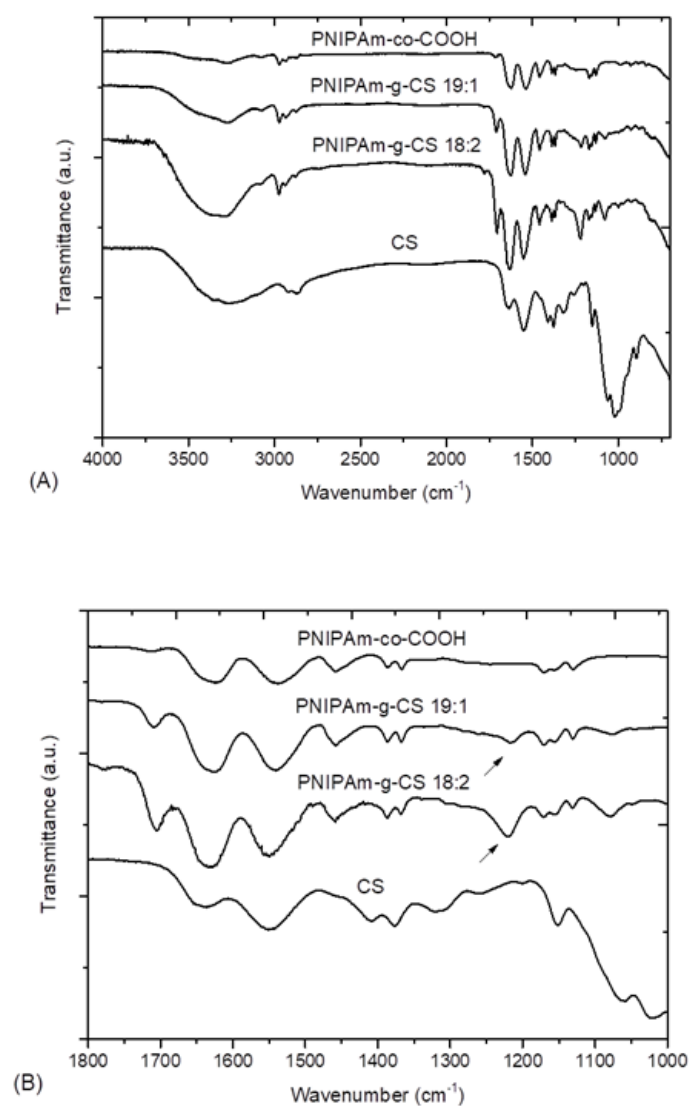


Figure 4 – FTIR spectrum of the precursor PNIPAm-co-COOH, CS and PNIPAm-g-CS grafts in formulations 19:1 and 18:2 in the region (A) $4000-500\text{ cm}^{-1}$ and (B) $1800-1000\text{ cm}^{-1}$.

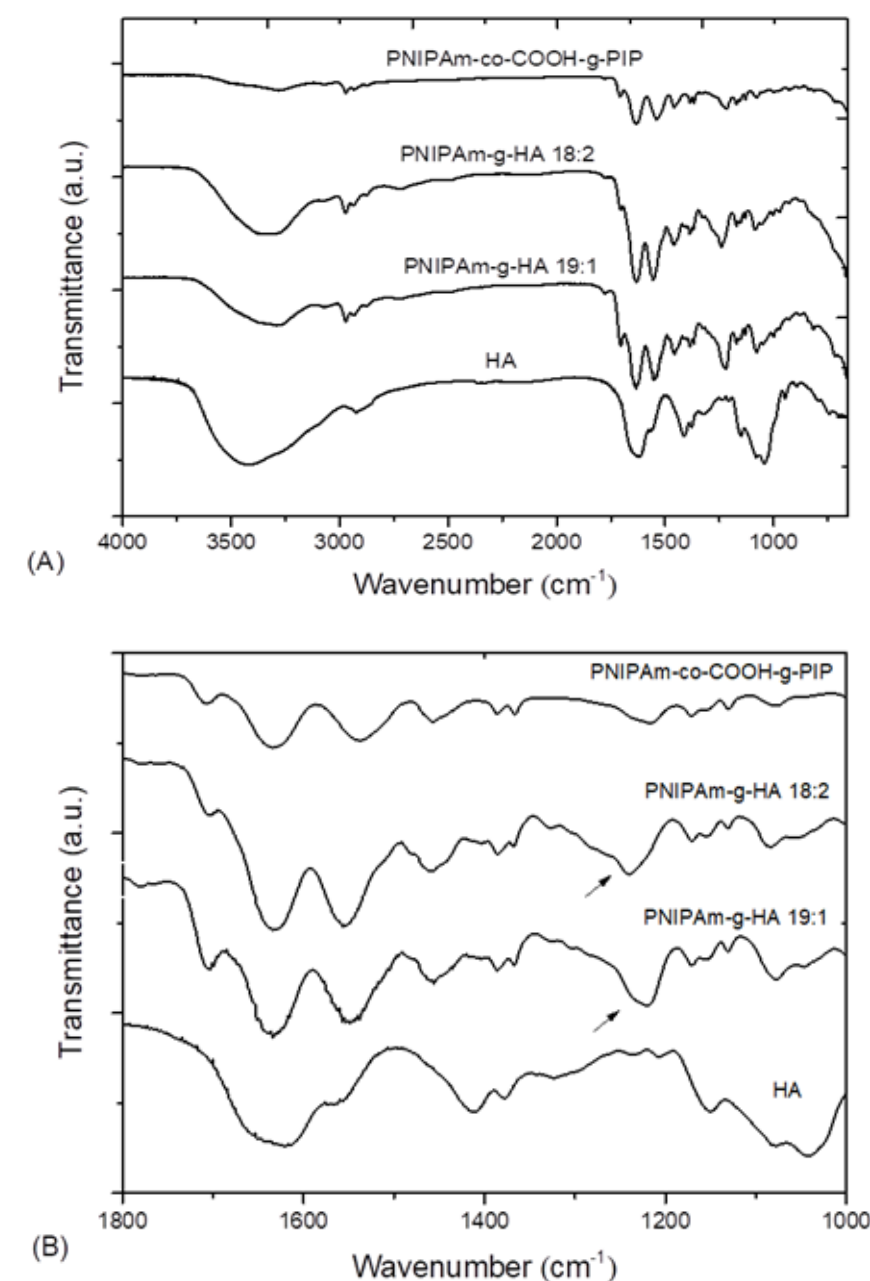


Figure 5 – FTIR spectrum of the precursor PNIPAm-co-COOH-g-PIP, HA and PNIPAm-g-HA grafts in formulations 19:1 and 18:2 in the region (A) $4000-500\text{ cm}^{-1}$ and (B) $1800-1000\text{ cm}^{-1}$.

have a transition temperature ($T_{\text{onset LCST}}$) lower than or equal to the reference homopolymer PNIPAm synthesized (approx. 33°C).

PNIPAm-g-CS grafts, by having shorter chain ramifications (chitosan oligomers), in comparison with their similar formulation of PNIPAm-g-HA, will require less energy to increase polymer/polymer interactions as shown by the ΔH values contemplated, and resume in table 1.

The significant difference in the molecular weight of the polysaccharides used (shown by M_v of each polysaccharide), can have consequences at the time of making the chemical graft reaction, because in the case of HA, this can increase the viscosity of the system. In consequence, the process of grafting is in disadvantaged and may be less effective, as shown in the yield results reported in Table 1. Also, if grafting occurs with this biopolymer of higher molecular weight, greater molecular entanglements are generated when the system is dissolved (at $T < \text{LCST}$), but when this system begins to undergo the transition process, these entanglements make it difficult the phase segregation process, requiring a higher energy cost for to induce the thermal transition reflecting in enthalpy results.

The PNIPAm homopolymer presents an $\text{LCST}_{\text{onset}}$ around 33°C and in

the case of the copolymers obtained from the formulation grafted with HA the new products decrease this transition to around $29-30^\circ\text{C}$, but it seems to have more effective grafting despite requiring greater energy or enthalpy (ΔH). In the case of copolymer grafted with CS oligomers, not change are observed in LCST , and relate with ΔH , this value is depending of the effective anchor point and the entanglement produce for the oligomers ramifications.

It has been reported in the literature that polymers with a low LCST , which provide networks undergoing reversible phase transitions, show an enormous potential to develop useful drug delivery systems to control both the site and the release rate³. All thanks to its LCST transition that allows gelling in situ, which can also favor the design of injectable scaffolds, because ideally, the polymer solution exists in the liquid state at room temperature and forms a gel at human body temperature. Also, thermal transition induced physical crosslinked hydrogels that have several favorable properties, for example they do not need organic crosslinkers and have no thermal effect on the surrounding tissues³⁸.

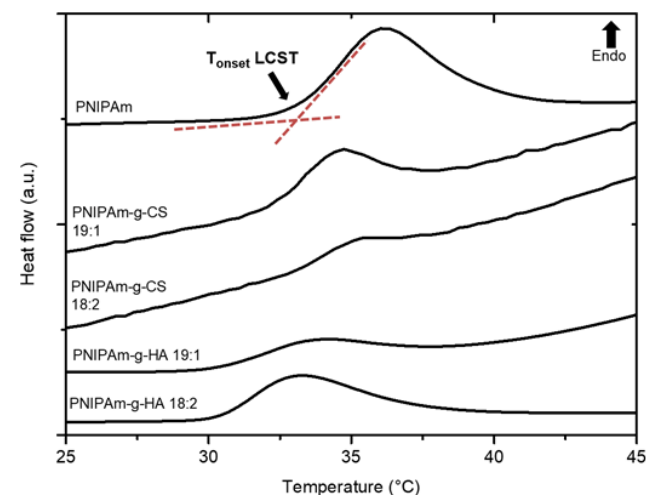


Figure 6 – Determination of the LCST transition by DSC for the PNIPAm and the grafts PNIPAm-g-CS and PNIPAm-g-HA

SAMPLE	Yield (%)	DSC	
		T _{onset} LCST (±0.1) °C	ΔH _{LCST} (±0.1) J/g
PNIPAm	-	33.1	17.9
PNIPAm-g-HA 19:1	72.5	29.4	19.2
PNIPAm-g-HA 18:2	78.1	30.5	10.5
PNIPAm-g-CS 19:1	84.4	32.6	14.8
PNIPAm-g-CS 18:2	76.6	33.1	4.5

Table 1 – Yield reaction and transition LCST of graft copolymers synthesized.

Study of copolymer morphology observed by SEM

During the development of new materials, the study of porosity is one of the most important aspects to investigate, because it allows to evaluate the potential of a new biomaterial due to its close relationship with processes of fluid exchange, biocompatibility, biodegradability, vascularization, etc.^{25,39-41}. Consequently, the size of the pore and the interconnection of the network determine how is the interaction process: hydrogel-organism, and are increasingly used in the development of scaffolds with applications in tissue engineering^{42,43}. The porosity and interconnectivity of the network are responsible for the response of the tissues where they can be implanted⁴⁴. When the pores are larger, there is a greater amount of surface exposed to the biological environment, so the interaction of the biomaterial with the organism is also favored. Further the pore size, another variable of great importance is the interconnection of the network, since if a 3D network presents interconnected channels, a better flow and greater reach of the aqueous medium (therefore of nutrients) will be obtained in the new material²⁹.

The injectability process was simulate, to see how the shear stresses could generate a morphological change in the final structure of the gels. In this way, when the gel is going through the needle of an injector, and after the sample pass the limit temperature for the LCST transition, some porosity could be create permanently. It can be observe in figure 7. The formulations 19:1 and 18:2 of the PNIPAm-g-CS graft-copolymers present a homogeneous morphology as a “honeycomb” (due to the shape of their interconnected pores). While the PNIPAm-g-HA micrograph shows a high porosity with less homogeneity and continuity. This evidence can be interpreting taking into account the molecular size (*M_v*) of both grafted polysaccharides. From which it can be inferred that the smaller the size of

the grafted chain, there will be minor molecular entanglements with the backbone of the copolymer, which may result in a certain ordering in the solid gel state, which confers a greater size of the pores formed among them. In the case of HA, with large *M_v*, all the entanglement could be non-favorable for the generation of pores and interconnectivity; or because the LCST transition occur first and can not give time to the molecules to get certain order in the xerogel state.

In general, the synthesized materials show scaffolding structures with interconnected pores, whose homogeneity varies depending on the formulation and the molecular weight of the polysaccharide. The observed morphology is an important requirements to be able to estimate the biomedical or tissue engineering applications that these graft copolymers could have.

Cytotoxic studies

The cytotoxic studies by hemolysis performed in an agar / blood system allowed to evaluate the hemocompatible character of the synthesized materials. Noting that graft copolymers obtained are not toxic, since none of them shows evidence of cell lysis, as shown in Figure 8.

The tests of cytotoxicity through the use of agar gels enriched with blood, allow the verification of the degradative activity by the action of the cytotoxic components present in a given biomaterial⁴⁵. In case of the possible diffusion of cytotoxic components present in prepared hydrogels or gels, in a certain time, there would be evidence of lysis or decomposition by the rupture of red blood cells (call this process hemolysis)⁴⁶. If, after 48 h of contact between the agar/blood and the biomaterial, hemolysis does not occur, the biomaterial is consider non-cytotoxic⁴¹. When in the presence of a cytotoxic material, hemolysis is evidenced by the formation of a whitish halo around the contact area of the material seeded in the

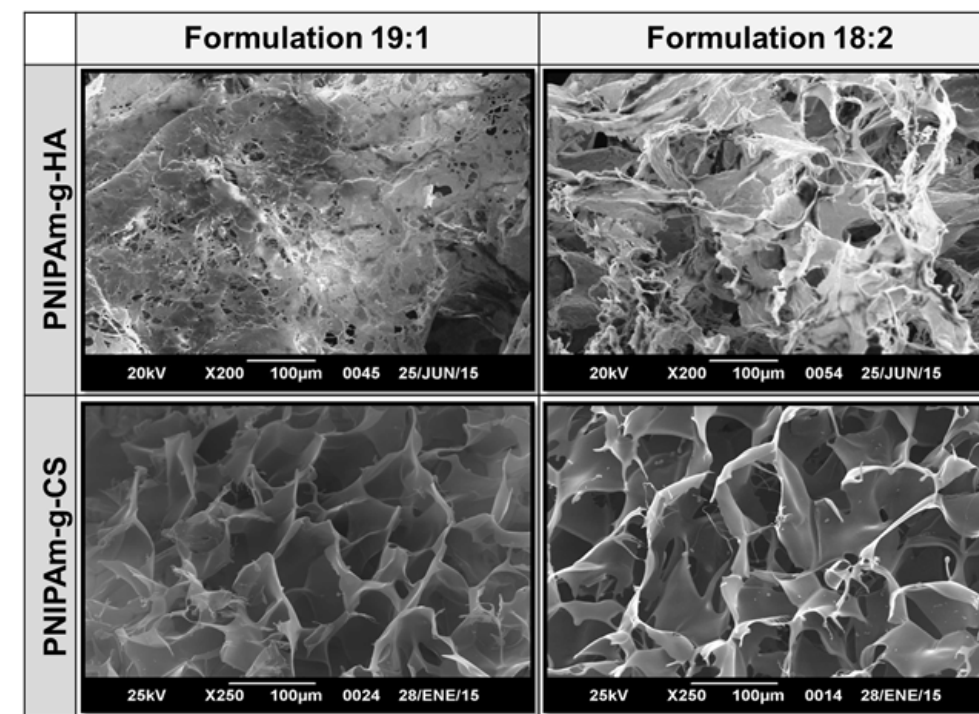


Figure 7 – Micrographs of PNIPAm-g-CS and PNIPAm-g-HA grafts copolymers.

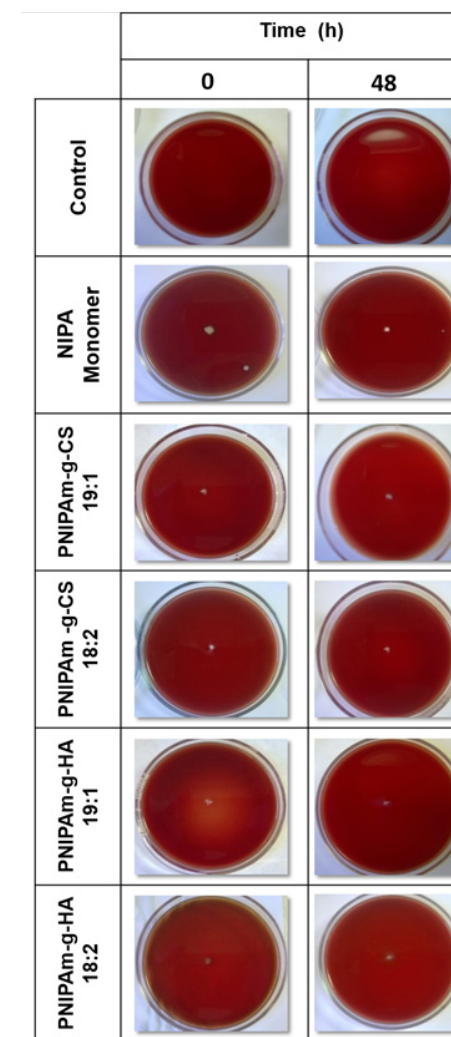


Figure 8 – Non-cytotoxic evidence of the PNIPAm-g-CS and PNIPAm-g-HA grafts in contact with the agar/blood at time 0 and after 48h.

agar/blood, an indication that a lysis process has occurred as a cytotoxic response^{29,46}.

Figure 8, resume the hemo-compatibility test results, and the formation of the white halo around the surface of the copolymers gel is not observe (after 48 h), therefore, the synthesized copolymeric gels can be considered non-cytotoxic compounds. As a control, the NIPA monomer was used, in which it is possible to observe, after 48 h, a slight halo formed at the border of the sample and the agar/blood medium.

Conclusions

The results obtained in this study, such as the thermal transition LCST at temperatures close to the human body of the graft copolymers PNIPAm-g-HA and PNIPAm-g-CS, as well as their injectable character and the porous morphology observe, are indicative that these new water-soluble biomaterials have a high potential to be used in applications such as: injectable scaffolds for tissue engineering and/or encapsulation/controlled release of drugs. Additionally, the results of non-toxicity on contact with blood give to these copolymers a hemocompatible character.

Acknowledgment

The authors would like to express their thanks to the following laboratories in the University Simón Bolívar: B5IDA research group, Polymer research group GPUSB-1, Laboratory of Surfaces for SEM analysis (Laboratory E), Laboratory of Microbiology of the Department of Cell Biology and Laboratory of instrumental analysis of Chemistry Department.

Reference

- Fu G and Soboyejo W, Swelling and diffusion characteristics of modified poly (N-isopropylacrylamide) hydrogels, *Materials Science and Engineering C*. **30**: 8–13 (2010).
- Haq MA, Su Y, Wang D. Mechanical properties of PNIPAm based hydrogels: A review. *Materials Science and Engineering C*, **70**: 842–55 (2017).
- Alvarez-Lorenzo C, Concheiro A, Dubovik A, Grinberg N, Burova T, Grinberg V. Temperature-sensitive chitosan-poly(N-isopropylacrylamide) interpenetrated networks with enhanced loading capacity and controlled release properties. *Journal of Controlled Release*, **102**: 629–641 (2005).
- Guo H, Brület A, Rajamohanam P, Marcellan A, Sanson N, Hourdet D. Influence of topology of LCST-based graft copolymers on responsive assembling in aqueous media. *Polymer*, **60**: 164.175 (2015).
- Zhang W, Shi L, Wu K, An Y. Thermoresponsive Micellization of Poly (ethylene glycol)-b-poly (N-isopropylacrylamide) in Water. *Macromolecules*, **38** (13): 5743–5747 (2005).
- Conzatti G, Cavalie S, Combes C, Torrisani J, Carrere N, Tourrette A. PNIPAm grafted surfaces through ATRP and RAFT polymerization: Chemistry and bioadhesion, *Colloids and Surfaces B: Biointerfaces*. **151**: 143–55 (2017).
- Davis K, Matyjaszewski K. Statistical, Gradient and Segmented Copolymers by Controlled/Living Radical polymerizations. In: *Advances in polymer Science*. Springer-Verlag Berlin Heidelberg (2002).
- Feng C, Li Y, Yang D, Hu J, Zhang X, Huang X, Well-defined graft copolymers: from controlled synthesis to multipurpose applications, *The Royal Society of Chemistry*, **40**: 1282–1295 (2011).
- Malviya R, Sharma PK, Dubey SK, Modification of polysaccharides: Pharmaceutical and tissue engineering applications with commercial utility (patents). *Materials Science & Engineering C*, **68**: 929–938 (2016).
- Pino V, Meléndez H, Ramos A, Bucio E. Radiation Grafting of Biopolymers and Synthetic Polymers: Synthesis and Biomedical Applications. In: *Biopolymer Grafting: Applications*, Elsevier Inc (2018).
- Le P, Huynh C, Tran N. Advances in thermosensitive polymer-grafted platforms for biomedical applications. *Materials Science and Engineering: C*, **92**: 1016–1030 (2018).
- Soni S, Ghosh A. (2018). Grafting Onto Biopolymers: Application in Targeted Drug Delivery. In: *Biopolymer Grafting: Applications*, Elsevier Inc (2018).
- Bhavsar C, Momin M, Gharat S, Omri A. Functionalized and graft copolymers of chitosan and its pharmaceutical applications. *Expert Opinion on Drug Delivery*, **14**(10):1189–1204 (2017).
- Ohya S, Kidoaki S, Matsuda T. Poly(N-isopropylacrylamide) (PNIPAM)-grafted gelatin hydrogel surfaces: interrelationship between microscopic structure and mechanical property of surface regions and cell adhesiveness. *Biomaterials*, **26**(16):3105–3111 (2005).
- Işıklıan N and Tokmak S. Microwave based synthesis and spectral characterization of thermo-sensitive poly(N,N-diethylacrylamide) grafted pectin copolymer. *International Journal of Biological Macromolecules*, **113**: 669–680 (2018).
- Ciocoiu O, Staikos G, Vasile C. Thermoresponsive behavior of sodium alginate grafted with poly(N-isopropylacrylamide) in aqueous media. *Carbohydrate Polymers*, **184**: 118–126 (2018).
- Conzattia G, Cavalie S, Gayet F, Torrisani J, Carrère N, Tourrette A. Elaboration of a thermosensitive smart biomaterial: From synthesis to the ex vivo bioadhesion evaluation. *Colloids and Surfaces B: Biointerfaces*, **175**: 91–97 (2019).
- Vihola H, Laukkanen A, Valtola L, Tenhu H, Hirvonen J. Cytotoxicity of thermosensitive polymers poly(N-isopropylacrylamide), poly(N-vinylcaprolactam) and amphiphilically modified poly(N-vinylcaprolactam). *Biomaterials*, **26**(16): 3055–3064 (2005).
- Cooperstein M and Canavan H. Assessment of cytotoxicity of (N-isopropyl acrylamide) and Poly(N-isopropyl acrylamide)-coated surfaces. *Biointerphases*, **8**(19): 1–12 (2013).
- Tsitsilianis C, Lencina S, Iatrídi Z, Villar M, Thermoresponsive hydrogels from alginate-based graft copolymers. *European Polymer Journal*, **61**: 33–44 (2014).
- Rueda J, Zschoche S, Komber H, Schmaljohann D, Voit B, Síntesis y caracterización de hidrogeles termosensibles. *Revista de QUÍMICA*, **41**–46 (2006).
- Rejinold NS, Sreerexha PR, Chennazhi KP, Nair SV, Jayakumar R, Biocompatible, biodegradable and thermo-sensitive chitosan-g-poly (N-isopropylacrylamide) nanocarrier for curcumin drug delivery. *Macromolecules*, **49**: 161–172 (2011).
- Isıklan N and Küçükbalcı G, Microwave-induced synthesis of alginate-graft-poly(N-isopropylacrylamide) and drug release properties of dual pH- and temperature-responsive beads. *European Journal of Pharmaceutics and Biopharmaceutics*. **82**:316–331 (2012).
- Stile R, Burghardt W, Healy K, Synthesis and Characterization of Injectable Poly(N-isopropylacrylamide)-Based Hydrogels That Support Tissue Formation in Vitro. *Macromolecules*. **32**: 7370–7379 (1999).
- Vieira J, Posada J, Rezende R, Sabino M, Starch and chitosan oligosaccharides as interpenetrating phases in poly(N-isopropylacrylamide) injectable gels. *Materials Science and Engineering C*. **37**: 20–27 (2014).
- Benrebouh A, Avoce D, Zhu X, Thermo- and pH-sensitive polymers containing cholic acid derivatives. *Polymer*. **42**: 4031–4038 (2001).
- Zhu J and Marchant R, Design properties of hydrogel tissue-engineering scaffolds. *Expert Rev. Med. Devices*. **8**(5): 607–626 (2011).
- Carrero M, Posada J, Sabino M, Intelligent copolymers based on poly (N-isopropylacrylamide) PNIPAm with potential use in biomedical applications. Part I: PNIPAm functionalization with 3-butenoic acid and piperazine. *International Journal Of Advances In Medical Biotechnology*. **1**(1):23–31 (2018).
- Coronado R, Pekerar S, Lorenzo A, Sabino M, Characterization of thermo-sensitive hydrogels based on poly (N-isopropylacrylamide)/hyaluronic acid. *Polymer Bulletin*, **67**: 101–124 (2011).
- Brugnerotto J, Lizardi J, Goycoolea FM, Argüelles-Monal W, Desbrières J, Rinaudo M, An infrared investigation in relation with chitin and chitosan characterization. *Polymer*. **42**: 3569–3580 (2001).
- Povea M, Argüelles-Monal W, Cauich-Rodríguez J, May A, Badas N, Peniche C, Interpenetrated chitosan-poly(acrylic acid-co-acrylamide) hydrogels. Synthesis, characterization and sustained protein release studies. *Materials Sciences and Applications*. **2**: 509–520 (2011).
- Sestak J, Mullins M, Northrup L, Thati S, Forrest ML, Siahaan TJ, Berkland C. Single-step grafting of aminoxy-peptides to hyaluronan: A simple approach to multifunctional therapeutics for experimental autoimmune encephalomyelitis. *Journal of Controlled Release*. **168**: 334–340 (2013).
- Chang KH, Liao HT, Chen JP, Preparation and characterization of gelatin/hyaluronic acid cryogels for adipose tissue engineering: In vitro and in vivo studies. *Acta Biomater*. **9**(11): 9012–9026 (2013).
- Jagadeeswara R, and Karunakaran K, Purification and characterization of hyaluronic acid produced by *Streptococcus zooepidemicus* strain 3523-7. *J. BioSci. Biotech.*, **2**(3): 173–179 (2013).
- Khanmohammadi M, Baradar A, Eskandarneshad S, Feyze N, Ebrahimi S, Sequential optimization strategy for hyaluronic acid extraction from eggshell and its partial characterization. *Journal of Industrial and Engineering Chemistry*, **20**(6): 4371–4376 (2014).
- Zhang J, Ma X, Fan D, Zhu C, Deng J, Hui J, Ma P, Synthesis and characterization of hyaluronic acid/human-like collagen hydrogels. *Materials Science and Engineering C*. **43**:547–554 (2014).
- Ha D, Lee S, Chong M, Lee Y, Preparation of Thermo-Responsive and Injectable Hydrogels Based on Hyaluronic Acid and Poly(N-isopropylacrylamide) and Their Drug Release Behaviors. *Macromolecular Research*, **14**(1): 87–93 (2006).
- Chang B, Ahuja N, Ma C, Liu X, Injectable scaffolds: Preparation and application in dental and craniofacial regeneration. *Materials Science and Engineering R*, **111**: 1–26 (2017).
- Xiang Y, Peng Z, Chen D, A new polymer/clay nano-composite hydrogel with improved response rate and tensile mechanical properties. *European Polymer Journal*, **42**(9): 2125–2132 (2006).
- Koo H, Jin G, Kang H, Lee Y, Nam H, Jang H, Park J, A new biodegradable crosslinked polyethylene oxide sulfide (PEOS) hydrogel for controlled drug release. *International Journal of Pharmaceutics*, **374**: 58–65 (2009).
- Coronado R, Pekerar S, Lorenzo A, Sabino M, Obtención y caracterización de hidrogeles inteligentes del tipo red interpenetrada basados en Poli(N-Isopropilacrilamida). *Suplemento de la Revista Latinoamericana de Metalurgia y Materiales*, **52**(1): 65–66 (2009).
- Mao Y, Pravansu M, Gargi G, Morphology and properties of poly vinyl alcohol (PVA) scaffolds: Impact of process variables. *Materials Science and Engineering*, **42**: 289–294 (2004).
- Khademhosseini A, Langer R, Microengineered hydrogels for tissue engineering. *Biomaterials*, **28**: 5087–5092 (2007).
- Sabino M, Feijoo J, Nuñez O, Ajami D, Interaction of Fibroblast with Poly(p-dioxanone) and its degradation products. *Journal of Materials Science*, **37**(1): 35–40 (2002).
- Khan A, Husain T, Ahamed M, Mohamed A, Aldabahi A, Alam J, Ahamad T. Temperature-Responsive Polymer Microgel-Gold Nanorods Composite Particles: Physicochemical Characterization and Cytocompatibility. *Polymers*, **10**(1): 1–13 (2018).
- Rodríguez E, Gamboa M, Hernández F, García J, *Bacteriología General: Principios y Prácticas de Laboratorio*. Universidad de Costa Rica, pp. 498–499 (2005).



3D electrospinning used in medical materials

Natasha Maurmann^{1,2*}, Juliana Girón^{1,2}, Bruna Borstmann Jardim Leal¹, Patricia Pranke^{1,2,3*}

*Corresponding author: E-mail address: natasha.maurmann@ufrgs.br; patriciapranke@ufrgs.br

Abstract: Electrospinning (ES) is an interesting and efficient technique for biomedical use. This is a method used for the fabrication of polymer fibers used in tissue engineering (TE). The electrospun nano- and microfibers biomaterial, called scaffolds, are also used for regenerative medicine. The aim of the present mini-review is to present methods used to fabricate 3D fibers by electrospinning and their applications in TE. Also, discussed here are issues regarding the electrospinning limitations and research challenges.

Keywords: Biomaterials; Electrospun; Three dimensional (3D) culture; Tissue Engineering.

Introduction

New frontiers in the application of techniques involving the production of medical products have been recently investigated. Electrohydrodynamic techniques, as electrospinning (ES), are very powerful tools for developing and producing materials with the structural features necessary for tissue engineering (TE) applications^{1,2}.

The conventional setup of an electrospinning process is illustrated in Fig. 1a. The equipment used for the electrospinning technique consists of a syringe with a needle attached to its tip, connected to an electrode, a hydrostatic pump, and an electrical source. In the syringe, a polymer solution is packaged and then, through the hydrostatic pump, this polymeric solution is directed to a metal collecting plate, which acts as a support for collecting the material produced^{2,3}. When the applied voltage is increased beyond a critical value, where the electrostatic forces are balanced by the

surface tension of the polymer solution drop at the tip of the capillary, Taylor's cone formation occurs (Fig. 1b)⁴. The potential difference between tip and metal collector induces stretching in a polymer solution from the apex of the Taylor cone. The electrospun process is divided into two stages: first, the drop geometry distortion occurs due to the action of the electric field and then a continuous jet formation occurs from the end of the drop⁵. Between the spinneret and the collector, the solvent is evaporated and fibers with smaller significant diameters than the spinneret are deposited in the collector⁴. Another monoaxial electrospinning process (with just one capillary) is emulsion electrospinning (Fig. 1c). An experimental setup with coaxial nozzle electrospinning (Fig. 1c) consists of two independent solutions simultaneously electrospun forming fibers with core-shell morphology^{4,6}.

In TE, the produced biomaterials are known as scaffolds. Scaffolds

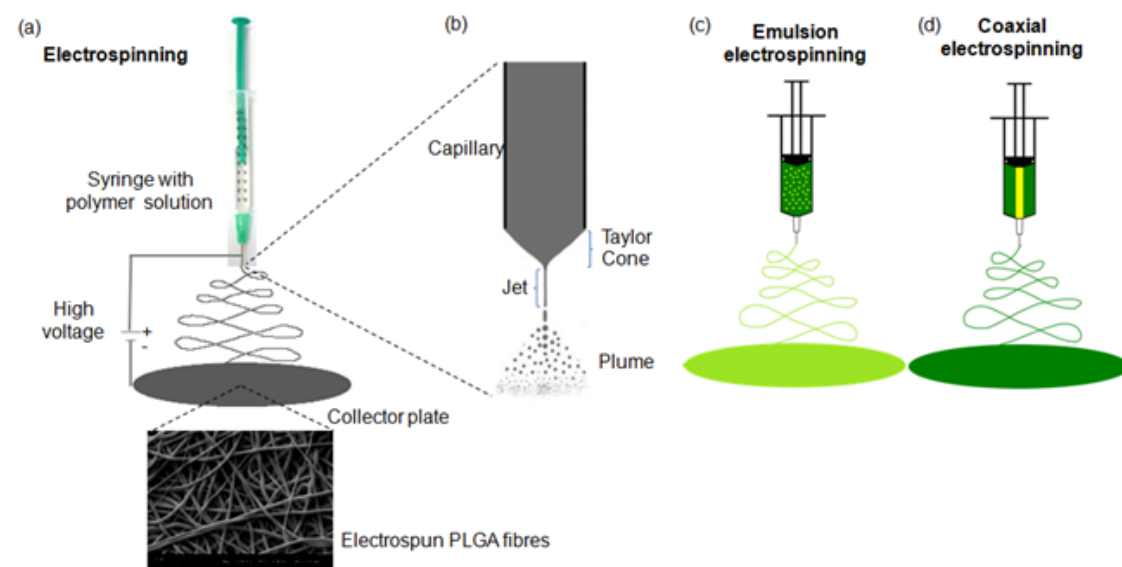


Figure 1 – Schematic diagram of the electrospinning processes for the production of nano- or microfibers. (a) The polymer solution is pumped into the syringe and passes through a spinneret. The nozzle is connected to a terminal of the power supply and a metal collector to the opposite terminal. The jets of polymer solution ejected from the capillary tube can form polymeric particles or filaments, depending on the physical properties of the polymer solution. (b) Schematic illustration of the Taylor cone (https://commons.wikimedia.org/wiki/File:Taylor_cone.jpg). (c) emulsion electrospinning and (d) co-axial electrospinning. Adapted, with permission, from Ref.².

produced by ES technique are formed by nano- or microfibers, pretending to be similar to native extracellular matrix (ECM). Natural ECM where the cells are attached contain nanofibrous proteins and proteoglycans⁷. Thus, the scaffolds produced by ES have special characteristics for use in TE since they are biomimetic materials. In TE, the scaffolds are associated with cells and bioactive molecules, a strategy for a better cellular response on the surface of the biomaterial^{8,9}. Some requirements of scaffolds for use in TE are illustrated in Fig. 2.

Several biomaterials are used for the production of medical structural supports by ES. Some examples are the FDA-approved synthetic polyesters poly(ϵ -caprolactone) (PCL) and poly(lactic-co-glycolic acid) (PLGA). PCL scaffold fibers produced by ES are shown in fig. 3a. In this case, 1.2 ml was used of a polymer solution composed of 15% PCL in tetrahydrofuran:methanol (3:1) with the injection rate of 1.41 ml/h, distance of 15 cm between the tip and the plate and supply voltage of 20kV. Fig. 3b shows scaffolds of PLGA (18%) in acetone:hexafluoro (9:1) produced by ES. The procedure for producing PLGA scaffolds was similar to that used for producing PCL scaffolds except for a voltage of +13 kV and flow 1.74ml/h. When scanning electron microscopy (SEM) was realized in the PCL and PLGA electrospun fibers using a JSM-6060 – JEOL microscope, the density of the web uniform fibers was shown. The mean diameter (μm) and the standard deviation was of 1.35 ± 0.50 for PCL and 1.21 ± 0.25 for PLGA.

Additionally, natural polymers such as gelatin, collagen and chitosan, as well as compositions of the polymers can be formed by ES¹⁰.

Research studies involving the use of ES have increased considerably over the last few years. The number of publications in the “PubMed” database (<http://www.pubmed.gov>) with the keywords “electrospinning” or “electrospun” in the field search Title/Abstract was 10,708 from 2001 until today. When the term “medical” or “tissue engineering” was added to ES searches, the number decreased to 254 and 2,920, respectively. Although in 2001 the numbers of articles were similar, over the years, research with ES has increased more than ES with TE, showing that this technique is being used for other purposes, mainly in batteries and filtration membranes studies. When the term “3D” (three-dimensional) was added to the search with ES and TE, the number fell to 375 articles (Fig. 4). Between these 375 papers, 54 correspond to reviews and 321 to original articles. The major applications of ES for TE are bone, soft tissue and vessels^{2,10}.

The traditional electrospun nanofibrous mats are two-dimensional (2D) and have some disadvantages regarding the lack of a 3D structure^{3,11}. Although they have a high number of pores, the ES scaffolds have a small pore size ($<10 \mu\text{m}$) between the closely packed nanofibers^{11–13}. These 2D biomaterials cause limited cell infiltration since the cells can only proliferate on the surface of the scaffolds, limiting the number of cells grown in and on the scaffolds¹¹.

Studies have shown that 3D biomaterials, when compared to 2D, serve as ideal scaffolds for cell delivery, providing a support structure and cell encapsulation, thus facilitating cell release at the target destination¹¹.

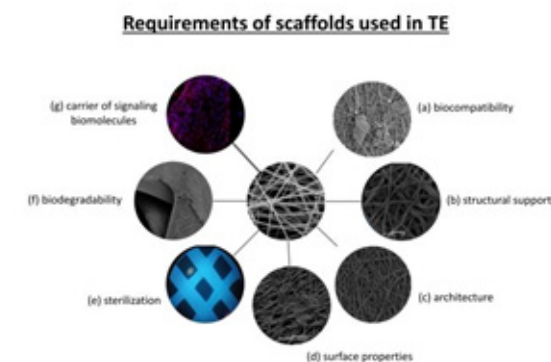


Figure 2 – Illustration of some requirements of scaffolds for use in TE. Adapted, with permission, from Ref.⁸.

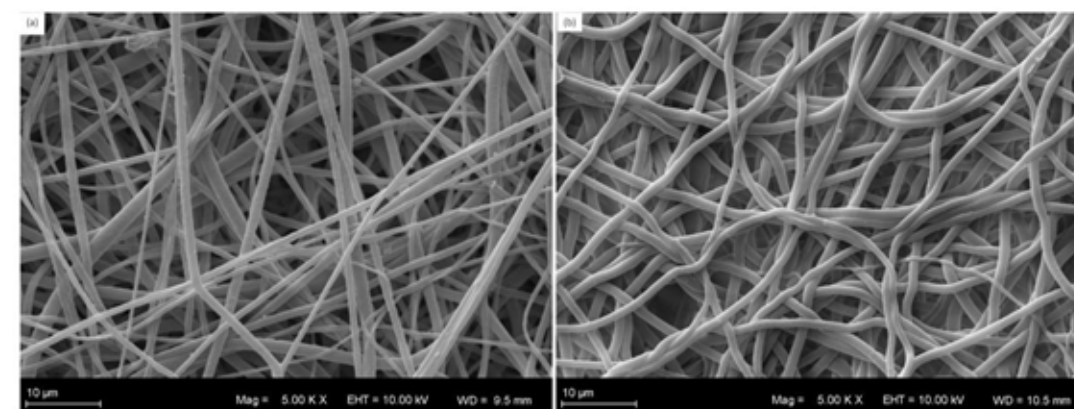


Figure 3 – SEM of fibers electrospun from different polymers. (a) PCL and (b) PLGA. Photographs kindly provided by the Stem Cell Laboratory archives, Universidade Federal do Rio Grande do Sul.

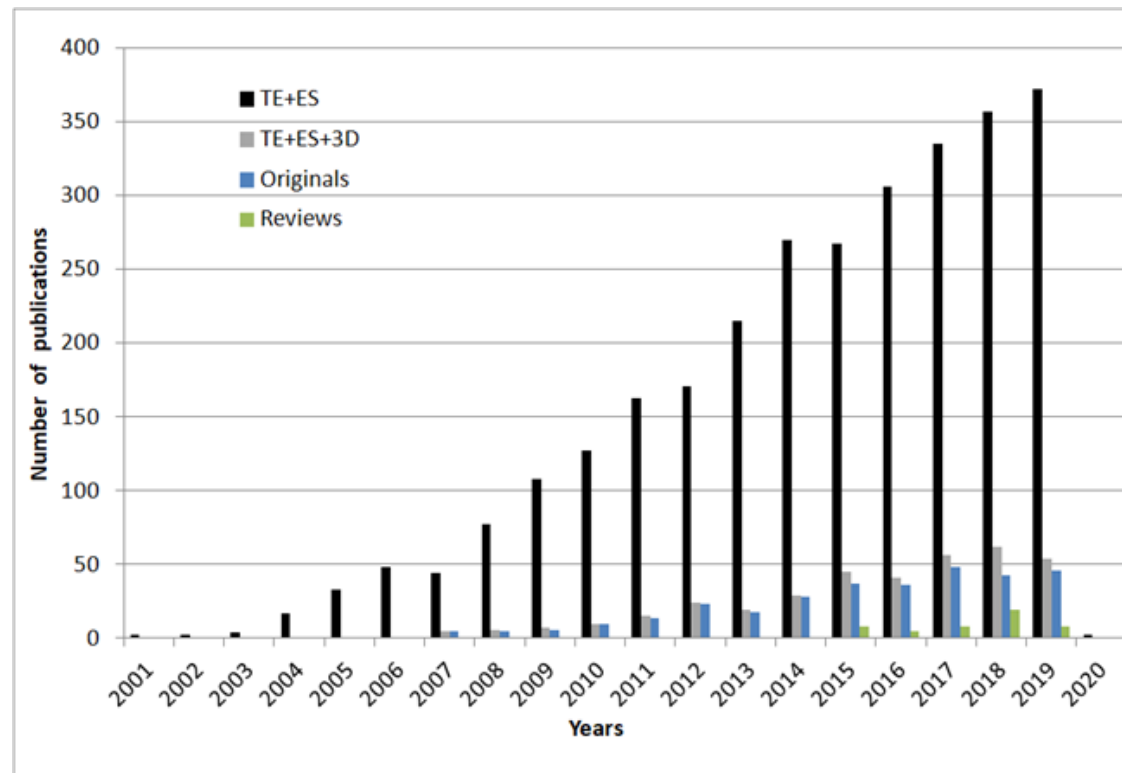


Figure 4 – The number of annual publications in the “PubMed” database from 2001 to November 2019. The black columns indicate the use of keywords “tissue engineering” and “electrospinning” or “electrospun”, the gray columns indicate the addition of the keywords “3D”, the blue columns indicate the originals and the green columns indicate the review papers (searches realized on 2nd November 2019).

3D electrospinning

In order to enhance the ideal pore size and a 3D structure in nanofibrous scaffolds to improve cell infiltration, some modifications in the ES method have been proposed. Some of the variations are the use of different salts and surfactants molecules, modifications on the collecting plate, the use of sacrificial elements, the gas foaming technique, extra metal as a positive electrode, the simple layer-by-layer ES, as well as the association between 3D techniques and electrospinning³.

The use of sacrificial elements involves the use of soluble components that are mixed with insoluble polymers. The function of the soluble component (sacrificial element), that could be a polymer or particles, is to leave a bigger pore when it is removed by rinsing in water. Wang and colleagues fabricated an electrospun silk fibroin scaffolds with macropores and high porosity using electrospinning-generated poly (ethylene oxide) (PEO) microparticles as porogen. The scaffolds with a greater diameter allowed the cells to be infiltrated with up to 550 μm , while those on the control scaffolds remained on the surface¹⁴. Moreover, Zander and colleagues compared two methods to reach a bigger pore size, one fabricating aligned fibers by co-electrospinning of PCL with a sacrificial polymer PEO, and the other, fabricating a scaffold with various concentrations of PCL to obtain different fibers diameters and porosity. The last was the better method; however, a better infiltration only was achieved for the micron-sized fibers obtained from a 40 wt% PCL solution¹⁵.

Another interesting method to improve the pore size is the cold-plate electrospinning technique (CPE), wherein humid conditions, polymer fibers are deposited in a cryogenic mandrel while the formation of ice crystals occur due to the condensation of humidity. Sheikh and colleagues produced 3D silk fibroin nanofibers with high porosity using the cold-plate technique and compared this technique to salt leaching electrospinning (SLE). Results showed that CPE can produce nanofibers with a higher porosity than those achieved using the TE and SLE techniques. Additionally, nanofibers had more regular pore architecture and consequently an intense cell infiltration, in contrast with the SLE, when there was a mild cell infiltration¹⁶.

On the other hand, researchers have developed nanofibrous scaffolds with bigger pore size processing the electrospun scaffolds after its con-

ventional production. In the study of Lee JB and colleagues, a 3D nanofibrous scaffold of poly-L-lactic acid (PLLA) was fabricated by subjecting a conventional PLLA electrospun scaffold, with densely packed nanofibers, to ultrasonication. The results showed highly porous scaffolds with over 98% porosity, which was dependent on the ultrasonic exposure time. The increase in the pore size and porosity allows a maximum 3D cell infiltration of 28% of the total depth of the scaffold in 7 days *in vitro*¹⁷.

The gas foaming technique is another way used to increase the pore size and porosity. This method takes advantage of gas at high pressure to produce harsh solvents instead of the often used particle-leaching methods¹⁸. Jiang and colleagues used this technique, where hydrogen gas bubbles generated from the sodium borohydride (NaBH₄) hydrolysis reaction, expanded aligned electrospun nanofiber PCL mats in 3 dimensions, with an increased porosity of 84 to 99 %¹⁹. Hematoxylin–eosin (H&E) staining of cell-seeded scaffolds suggested that cells successfully infiltrated and proliferated throughout the bulk of expanded nanofiber scaffolds¹⁹.

A simple way to produce 3D scaffolds with ES is to make rectangular scaffold mats which a glued forming a 3D conduit (Fig. 5a)²⁰. In addition, a similar 3D conduit (Fig. 5b) can be produced by the electrospinning technique utilizing a cylinder grounded as a collection rotating mandrel^{21–23}. This method involves the deposition of the fibers in the tubular collection, represented by “sa” and “pa” (Fig. 5b). The appearance of the scaffold (tubular conduit) is shown in Figure 5b. Sell and colleagues described the production of scaffolds for vascular grafts with a view towards the cardiovascular tissue engineering²¹. Lee et al developed this scaffold composite of PCL/collagen with adequate elasticity and burst pressure larger than with the PCL scaffolds alone, which is appropriate for vascular TE²¹.

It is also possible to combine techniques such as ES and rapid prototyping. The 3D printing assists in the rapid fabrication of tissue engineering biomaterials for complex shapes and cells can be easily associated¹¹. The association between 3D techniques and electrospinning is of great relevance, and electrospun nanofibers in association with 3D printed matrices have been developed (Fig. 5b)⁹. These scaffolds can be used for tissue engineering of cartilage and bone.

In a study with the laser-based 3D printing system, Lee and colleagues used stereolithography capable of fabricating 3D constructions through a

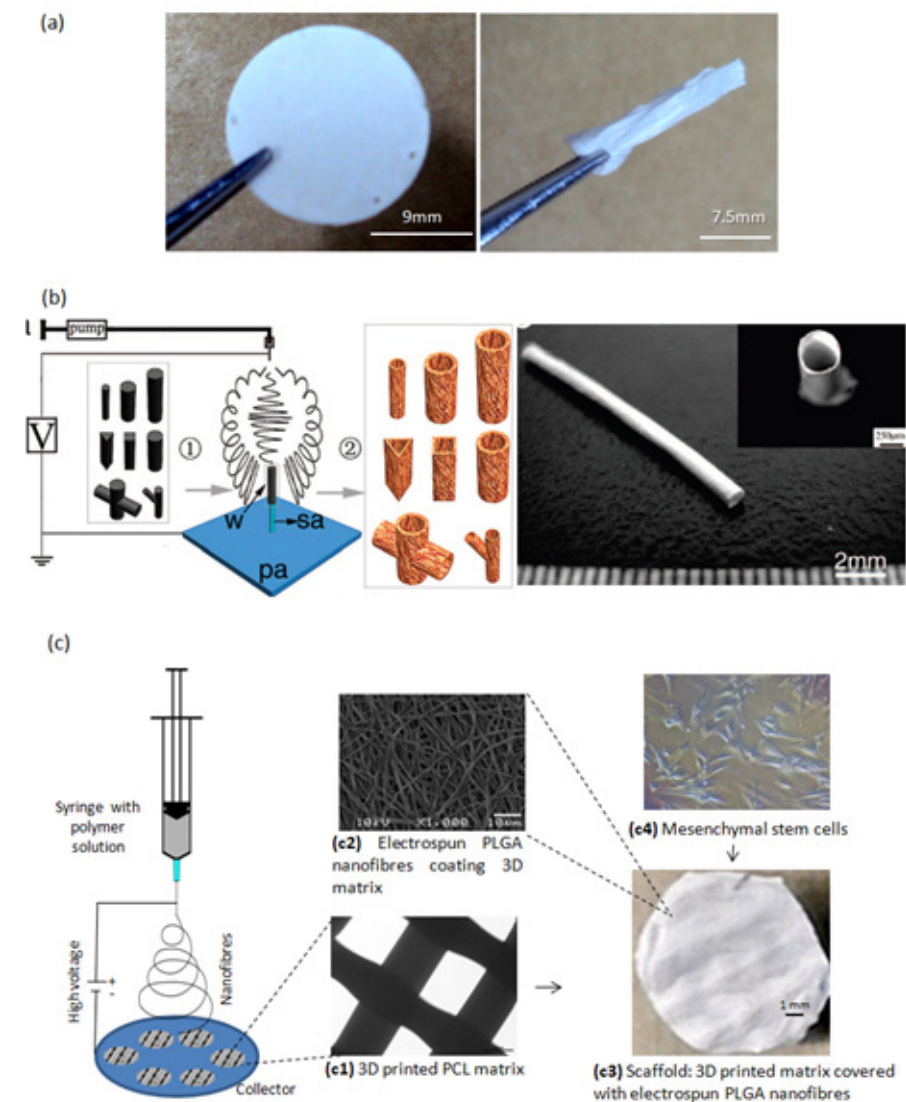


Figure 5 – 3D making scheme. (a) Production of 3D conduit. Adapted, with permission, from Ref. 20. (b) Fabrication of tubes by the electrospinning technique using 3D columnar collectors. 1: 3D columnar collectors. 2: fibrous tubes. (w: working collector; pa: plate assistant collector; sa: stick assistant collector) and an optical photograph of a tube fabricated using this method. Adapted with permission from Ref. 22. Copyright (2019) American Chemical Society. (c) ES at par 3D printed matrices. Adapted, with permission, from Ref. 8.

layer assembly method. The association of this technique with electrospinning developed a 3D biomimetic neural scaffold associated with bioink to improve biocompatibility and mechanical properties²³.

In another study, hierarchical scaffolding supplemented with cellulose alginate hydrogel microfibers was developed to evaluate the effect of diameter and thickness on cell activity. The bioink used was associated with alginate solution MG63 cells and is overlaid with PCL nanofibers and 3D printed PCL microstructure by 3D printing. They concluded that the MG63-associated microfibers assisted in the process of proliferation, release efficiency and osteogenic differentiation, and are promising for soft tissue and hard tissue regeneration²⁴.

Lately, both 3D printing and electrospinning technologies have been associated to develop an efficient scaffold, capable of supporting the culture of tissues like skin. Miguel and colleagues produced a 3D skin asymmetric construct by using electrospinning and 3D bioprinting techniques. To develop the epithelium like a layer, a PCL/silk serin scaffold was electrospun and placed at the top of a dermis like layer formed by printing a layer by layer chitosan/sodium alginate hydrogel. Results showed that the epithelium layer, developed with the electrospun scaffold, provided a protective barrier against dehydration and potentially dangerous elements. On the other hand, the printed dermis exhibited an adequate porosity, wettability and biological properties for supporting cell adhesion, migration and proliferation²⁵.

Other 3D electrospun materials could be used in bone, skin and cartilage regeneration. On the skin, the biomaterials have crucial performance in body defence. They can be used as autologous and allogeneic keratinocyte grafts, and cellular biological matrix and there is also the possibility of including biological substances that can assist in the regeneration process. For bone use, calcium phosphate or growth factors associated with bone marrow or osteoblast-like stromal cells are used. Cartilage provides a structure to the body without bone stiffness, consisting mainly of chondrocytes incorporated into the non-vascularized extracellular matrix. One study used electrophilic silk matrices, which resulted in increased binding and proliferation of the chondrocytes⁴.

Conclusions

The electrospinning to produce nonwoven fibers, from both natural and synthetic biomaterials, have been used in tissue engineering. Moreover, fibrous scaffolds confer better cell adhesion, proliferation, migration and differentiation for the cells.

These scaffolds produced by ES are formed by structures that mimic the fibrous structure of the ECM two-dimensionally making this technique an effective and simple method for producing micro- and nanofibers with a wide variety of biodegradable polymers. Although there are many techniques for obtaining biomimetic 2D structures, the production of true 3D microenvironments for tissue regeneration is just beginning. There

has been an increase in the number of annual publications in the field of electrospinning with applications in medicine. When the keyword 3D was added to research, the number decreased (about 10x less), indicating that the papers do not address the three-dimensional aspect. Between the papers that focus on TE + ES + 3D, most refer to original articles and 14% review the topic.

Electrospinning has been recognized as a versatile approach for obtaining variously shaped structures from a range of biomaterials for possible applications in tissue engineering and regenerative medicine. However, the dense bundling of fibers is a major setback, where the cells do not form a real three-dimensional environment. To this end, various strategies have been reported on electrospun scaffolding which thus improve cellular response. Key challenges include the development of ES-based 3D scaffolds that have an appropriate structure similar to native tissue to aid in cell adhesion and proliferation. The 3D approach offers advantages regarding the promotion of cell infiltration; increased cell numbers mimic better ECM and allows for the production of scaffolds which are more similar to living tissue. As each tissue and organ have different organizations, the fabrication of standardized scaffolds is not possible, and the optimization of each cell type is necessary.

Several electrospinning parameters affect the fibers, porous and consequently the formation of the 3D scaffolding structure, such as the solvent, polymer, processing additives, flow rate, applied voltage, needle size, spinner to the collector distance, ambient temperature and humidity. Some setups with electrospinning allow for the production of 3D scaffolds. For example, the use of layer-by-layer ES; the association between 3D techniques and electrospinning; an extra metal as the positive electrode or the modifications on the collecting plate; salts, surfactants and others sacrificial elements and gas foaming technique. The ES method with 3D collection is a versatile and extensively used technique for manufacturing fibrous tubes in biomedical applications.

It is necessary to fine-tune the process to create reproducible scaffolds with ideal fiber and pore sizes. Thus, innovative and alternative approaches in TE research and development are still seeking to understand the in vivo behavior of these materials, their rate of degradation and remodeling in situ, as well as their inflammatory and immunological responses.

Acknowledgments

The authors would like to acknowledge the support of the Ministry of Science, Technology, Innovation and Communication (MCTIC), the National Council of Technological and Scientific Development (CNPq) Coordination for the Improvement of Higher Education Personnel (CAPES) and the Stem Cell Research Institute (IPCT, Instituto de Pesquisa com Células-tronco).

References

- Huang Z-M, Zhang Y-Z, Kotaki M, Ramakrishna S. A review on polymer nanofibers by electrospinning and their applications in nanocomposites. *Compos Sci Technol* **63**(15):2223–53 (2003). DOI: 10.1016/S0266-3538(03)00178-7.
- Maurmann N, Sperling L, Pranke P. Electrospun and Electrospayed Scaffolds for Tissue Engineering, in *Cutting-Edge Enabling Technologies for Regenerative Medicine, Advances in Experimental Medicine and Biology*, ed by H. J. Chun et al. Springer Nature Singapore, pp 79–100 (2018). DOI: 10.1007/978-981-13-0950-2.
- Agarwal S, Burgard M, Greiner A, Wendorf J. In *Electrospinning: A Practical Guide to Nanofibers*. Ed by Walter de Gruyter GmbH, Berlin/ Boston 2016. 189 pgs (2016).
- Zhang X, Reagan M, Kaplan D. Electrospun silk biomaterial scaffolds for regenerative medicine. *Adv Drug Deliv Rev* **61**: 988–1006 (2009). DOI: 10.1016/j.addr.2009.07.005.
- Costa RGF, Oliveira JE de, Paula GF de, Picciani PH de S, Medeiros

ES de, Ribeiro C, et al. Eletrofiiação de Polímeros em Solução: parte I: fundamentação Teórica. *Polímeros* **22**:170–177 (2012). DOI: 10.1590/S0104-14282012005000026.

- Hu W, Huang ZM, Liu XY. Development of braided drug-loaded nanofiber sutures. *Nanotechnology* **21**(31):315104 (2010). DOI: 10.1088/0957-4484/21/31/315104.
- Nagle AR, Fay C, Xie Z, Wang X, Wallace GG, Higgins MJ. Patterning and process parameter effects in 3D suspension near-field electrospinning of nanoarrays. *Nanotechnology* (2019). DOI: 10.1088/1361-6528/ab3c87.
- Maurmann N, Pereira DP, Burguez D, Pereira FDADS, Neto PI, Rezende RA, et al. Mesenchymal stem cells cultivated on scaffolds formed by 3D printed PCL matrices, coated with PLGA electrospun nanofibers for use in tissue engineering. *Biomed Phys Eng Express* **3**:045005 (2017). DOI: 10.1088/2057-1976/aa6308.
- Sousa RB De, Vieira EG, Osajimafurti JA et al. Recent advances in methods of synthesis and applications of bacterial cellulose/calcium phosphates composites in bone tissue engineering. *IJAMB* **1**:33–42 (2018). DOI: 10.25061/2595-3931/IJAMB/2018.v1i2.16.
- Steffens D, Braghirolli DI, Maurmann N, Pranke P. Update on the main use of biomaterials and techniques associated with tissue engineering. *Drug Discov Today* **23**:1474–1488 (2018). DOI: 10.1016/j.drudis.2018.03.013.
- Lin W, Chen M, Qu T, Li J, Man Y. Three-dimensional electrospun nanofibrous scaffolds for bone tissue engineering. *J Biomed Mater Res Part B* (2019). DOI: 10.1002/jbm.b.34479.
- Dhandayuthapani B, Yasuhiko Y, Maekawa T, Kumar DS. Fabrication and characterization of nanofibrous scaffold developed by electrospinning. *Mat Res* **14**:317–325 (2011). DOI: 10.1590/S1516-14392011005000064.
- Chen W, Xu Y, Liu Y, Wang Z, Li Y, Jiang G, et al. Three-dimensional printed electrospun fiber-based scaffold for cartilage regeneration. *Materials & Design* **179** (2019). DOI: 10.1016/j.matdes.2019.107886.
- Wang K, Xu M, Zhu M, Su H, Wang H, Kong D, et al. Creation of macropores in electrospun silk fibroin scaffolds using sacrificial PEO-microparticles to enhance cellular infiltration. *J Biomed Mater Res Part A* **101**(12):3474–81 (2013). DOI: 10.1002/jbm.a.34656.
- Zander NE, Orlicki JA, Rawlett AM, Beebe TP. Electrospun polycaprolactone scaffolds with tailored porosity using two approaches for enhanced cellular infiltration. *J Mater Sci Mater Med* **24**(1):179–87 (2013). DOI: 10.1007/s10856-012-4771-7.
- Sheikh FA, Ju HW, Lee JM, Moon BM, Park HJ, Lee OJ, et al. 3D electrospun silk fibroin nanofibers for fabrication of artificial skin. *Nanomedicine* **11**(3):681–91 (2015). DOI: 10.1016/j.nano.2014.11.007.
- Lee JB, Jeong SI, Bae MS, Yang DH, Heo DN, Kim CH, et al. Highly Porous Electrospun Nanofibers Enhanced by Ultrasonication for Improved Cellular Infiltration. *Tissue Eng Part A* **17**(21–22):2695–702 (2011). DOI: 10.1089/ten.TEA.2010.0709.
- Lakhtakia A, Martín-Palma RJ, Carter P, Bhattarai N. Bioscaffolds: Fabrication and Performance. *Eng Biomimicry* 161–88 (2019). DOI: 10.1016/B978-0-12-415995-2.00007-6.
- Jiang J, Carlson MA, Teusink MJ, Wang H, MacEwan MR, Xie J. Expanding Two-Dimensional Electrospun Nanofiber Membranes in the Third Dimension By a Modified Gas-Foaming Technique. *ACS Biomater Sci Eng* **1**(10):991–1001 (2015). DOI: 10.1021/acsbio-materials.5b00238.
- Dos Santos FP, Peruch T, Katami SJV, Martini APR, Crestani TA, et al. Poly (lactide-co-glycolide) (PLGA) scaffold induces short-term nerve regeneration and functional recovery following sciatic nerve transection in rats. *Neuroscience* **396**:94–107 (2019). DOI: 10.1016/j.neuroscience.2018.11.007.
- Sell A, Michael J, Garg K, Wolfe P, Bowlin G. Electrospinning of collagen/biopolymers for regenerative medicine and cardiovascular tissue engineering. *Adv Drug Deliv Rev* **61**:1007–1019 (2009). DOI: 10.1016/j.addr.2009.07.012.
- Zhang D, Chang J. Electrospinning of Three-Dimensional Nanofibrous Tubes with Controllable Architectures. *Nano Letters* **8**:3283–3287 (2008). DOI: 10.1021/nl801667s.
- Lee SJ, Nowicki M, Harris B, Zhang LG. Fabrication of a Highly Aligned Neural Scaffold via a Table Top Stereolithography 3D Printing and Electrospinning. *Tissue Eng Part A* **23**(11–12):491–502 (2017). DOI: 10.1089/ten.TEA.2016.0353.
- Yeo M, Kim G. Cell-printed hierarchical scaffolds consisting of micro-sized polycaprolactone (PCL) and electrospun PCL nanofibers/cell-laden alginate struts for tissue regeneration. *J Mater. Chem. B.* **2**:314–324 (2013). DOI: 10.1039/C3TB21163K.
- Miguel SP, Cabral CSD, Moreira AF, Correia IJ. Production and characterization of a novel asymmetric 3D printed construct aimed for skin tissue regeneration. *Colloids Surfaces B Biointerfaces* **181**:994–1003 (2019). DOI: 10.1016/j.colsurfb.2019.06.063.



The Brazilian sectoral innovation system in the field of Tissue Engineering and Bioprinting: actors, challenges and perspectives

Pedro Massaguer¹, Ana Luiza Millás¹

*Corresponding author: E-mail address: pedrodroxrm@3dbs.com.br; anamillas@3dbs.com.br

Abstract: The objective of this work is to map the main actors within the Brazilian innovation system framework in the field of tissue engineering and bioprinting, and analyze the main conditioners related to entrepreneurship and innovation. While keeping as a backdrop, the history of 3D Biotechnology Solutions startup, its challenges and projects. Tissue engineering is a subcategory of regenerative medicine with the purpose of repairing or substituting, partially or completely, tissues or organs that have been affected by some disease or lesion. The conventional methods used for the production of these biomaterials via tissue engineering do not have the capacity to mimic the reality of native structures in the nano, micro and macro scales, while guaranteeing the reproducibility and scalability of the materials. Technologies such as 3D bioprinting or additive manufacturing could change the way that many diseases are treated in the medium term by replacing the damaged tissues with custom bio-similar constructs. Mapping and reflections based on the innovation systems framework contribute to organize stimulus policies, stimulate interaction between actors, identify gaps and technological demands and periodically organize the analysis and expansion of this system in Brazil.

Keywords: Bioprinting; Tissue engineering; Biofabrication; Sectoral Innovation systems.

Introduction

3D bioprinting has emerged as a technological platform with great potential to meet the growing demands of regenerative medicine. Tissue engineering (TE) as a subcategory within the field of regenerative medicine was defined by Langer and Vacanti¹ as a “an interdisciplinary field that applies the principles of engineering and life sciences to the development of replacements that restore, maintain or improve tissue function”. TE develops alternatives to induce a tissue regeneration process, overcoming some disadvantages found in organ transplantation, such as the lack of donors and the need for immunosuppressive therapy. TE applications also have potential for the conception of in vitro models of healthy or pathological tissues and organs, assisting in drug screening, evaluation of new therapies, as well as the investigation of complex phenomena that occur within the progression of a disease such as cancer².

In addition to their high scientific potential, these models run into ethical questions, the issue of using animals for drug testing is a practical example of how TE is a disruptive technology platform. In Brazil, as of this year (2019), comes into force the Normative Resolution of the National Council for the Control of Animal Experimentation (Concea) that obliges the mandatory substitution of the original method performed on animals by the alternative method for research activities. This resolution, which seeks to apply the replacement, reduction and refinement (3Rs) principle in the country³ encourages the research community to recognize the importance of well-being for animals used in science, and was also officially endorsed by the National Health Surveillance Agency (ANVISA) so that these methods could be applied for regulatory purposes. The European Union has determined, since 2004, the transfer of tests for toxicity assessment to in vitro systems. In 2013, it also banned the import of animal-tested cosmetic products (Amendment 2003/15 / EC of Directive 76/768 EEC).

The potential use of bioprinters is high because repair of damaged or lost tissue is a worldwide concern, as well as the increase in the rates of obesity, diabetes and the elderly population. To give you an idea, Brazil today has 20.6 million elderly, a figure that represents 10.8% of the population. By 2060, the country is expected to have 58.4 million elderly (Brazilian Institute of Geography and Statistics-IBGE). A point to note is that the list of patients awaiting some type of transplant in Brazil is around 33,000. Even

though there is an annual increase in the number of transplants performed, the demand for organs has been growing at a higher rate.

Hence, with the growing interest of the medical and pharmaceutical communities, the demand for these bioproducts has increased and a wide range of bioprinting equipment have been developed within the labs of research institutions and also by startups⁴. Therefore, although the number of technologies, design and applications have grown as research advances to create increasingly complex fabric, a series of scientific technical challenges need to be overcome such as equipment precision, aseptic conditions, amongst others.

From a market perspective, the BCC Research report⁵ predicts that by 2021 this field will reach US\$ 1.8 billion. This growth is estimated at a compound annual growth rate of 4.3% from 2016 to 2021. Another report from the consultancy Grand View Research⁶ estimated the global bioprint market at US\$ 682 million in 2016 expected to reach US\$ 2.6 billion by 2024. Growth should be driven by new printing technologies as well as by the expansion of new applications within the medical field such as vascularized tissues, vascular grafts, cartilage, bone, skin and other applications.

From a business strategy perspective it is only natural that companies offering products for bioprinting will gradually come to provide bioprinting products, given the different business possibilities that open up with this technological platform. A representative case is of the American company Organovo, founded in 2007 it initially focused in products for bioprinting (bioprinters, bioinks, etc.) and today is a leader in the co-development of bioprinting products, with patent requests for different therapeutic applications. It is also natural that important ethical, moral and social questions have to be analyzed so that an appropriate regulatory framework can be put in practice and make possible for bioprinting products to find their way to the market and improve patients' quality of life, as discussed by Li⁷.

In this regard, it is important to highlight that other countries for some years now have been working toward providing an adequate regulatory environment to foster the development of therapeutic applications with cells using TE and bioprinting. The creation of an environment conducive to research and development can provide companies and institutions an advantage in these countries, demanding a robust strategy so that Brazil does not lag behind and positions itself as a protagonist in this type

of vanguard technology. In this sense, mapping actors can support the organization of policies and funding mechanisms, stimulate cooperation and interaction, identify demands and provide a systemic platform for periodically analyzing the evolution of this system.

The article is organized into four items other than this introduction. In the next two items, the analysis referential based on the innovation systems and the characterization of the Brazilian sectoral system will be analyzed. Next, we will present the case of 3D Biotechnology Solutions startup, its history and projects. Finally, we will present some reflections regarding the entrepreneurship in this emerging sector. It is noteworthy to highlight right away, that the mapping exercise carried out was not exhaustive and should not be complete, and that we encourage the constant addition of new actors.

The Innovation Systems Approach to Characterize Leveraging of Skills in Research Development and Innovation

Innovation system (IS) models have traditionally been applied on a national innovation system (NIS) approach. This approach has also been applied to analyze industry sectors and specific enabling of sectoral technologies. This approach has also been applied to analyze industry sectors and sector specific technology capabilities. These approaches share the view that the innovative process can best be explained by characterizing system components and how they interact. Specifically, its actors, networks and institutions, including regulatory norms.

The IS approach makes explicit the importance of systemic interactions between various components of an invention, of the research, technical change, learning, and innovation. Such interactions have multiple internal and external sources of information and knowledge coming from different classes of actors and institutions. These interactions have created an informal systemic interdependence in the production systems of the respective actors, giving rise to what is now called the “Innovation System”. The central idea of the IS approach is the notion that what appears as innovation at the aggregate level is in fact the result of an interactive process that involves several actors at the micro level, and that alongside

The Brazilian sectoral innovation system in...

market forces many of these interactions are governed by non-market institutions. The efficiency of this process observed at the macro level thus depends on the behavior of individual actors, in addition to the institutions that govern their interaction.

It is no surprise that economists in the institutional tradition of innovation studies^{8,9} and scholars of evolutionary theories¹⁰, became the strongest supporters of the notion of innovation systems as this point of view refers to a continuous process in which institutions (habits, practices and rules) coevolve through learning processes, while playing a central role in generating innovation and technological change.

From an analytical perspective, the Sectoral Innovation Systems (SIS)¹¹ approach takes a multidimensional and dynamic cut of a given industrial sector, composed of the following elements:

(i) its products, (ii) agents, such as companies, universities, financial institutions, central and regional governments, (iii) knowledge and learning systems (group courses and research lines) (iv) interrelationships and complementarities of basic technologies, supplies and demands, (v) mechanisms of interaction between external and within the sector companies, involved in both market and non-market processes, (vi) competition and selection processes, (vii) institutions, understood as production standards, regulations and the job market. This framework serves as a practical tool for the design and implementation of innovation policies.

In this sense, Chaminade and Edquist¹² affirm that the innovation policies based on the Innovation Systems perspective aim to solve systemic problems or failures, which are not automatically resolved by private actors. The authors highlight some possible systemic failures, such as (i) the provisioning of infrastructure and investment failures, (ii) failures in the technological paradigm transition (iii) lock-in problems, (iv) failures in “hard” and “soft” institutions, (v) networking failures, (vi) learning and competency failures and (vii) complementarity failures. In practice, this approach allows the analysis of blocking and induction mechanisms and to delimit the main functions which this system should provide to develop virtuously. Table 1 summarizes induction and blocking mechanisms and functions of these systems.

Induction Mechanisms	Functions	Blocking mechanisms
<ul style="list-style-type: none"> Governmental R&D Programs Investments Subsidies Measures that affect relative prices Public purchase notices 	<ul style="list-style-type: none"> Knowledge creation and propagation Influences in the direction of R&D Business experimentation Market development Resource Mobilization Legitimation of new technologies Development of positive externalities 	<ul style="list-style-type: none"> Features of the new technology Weak institutional power Lack of customer competence Weak links within the collaboration network Established Lock-in Technology Lack of long-term government vision

Adapted from Jacobsson e Bergek¹³

Table 1 – Characteristics of Technological Innovation Systems.

¹ 3D Biotechnology Solutions CEO – Innovation Strategist, Brazil.

The sectoral system of innovation in Brazilian Bioprinting and tissue engineering

The sectoral system of innovation in the Brazilian field of bioprinting is in an emerging phase, that is, innovative applications based on this technological platform begin to be explored economically. This system is made

up mostly by: university research groups, research institutes, companies and startups. In addition, the regulatory agency ANVISA. The analysis performed based on the data available from the group research Directory of the Lattes² platform identified 60 research groups and 71 threads of research hosted in 30 universities, 2 hospitals and 3 research institutes.

Search Query:
 Date: 07/31/2019
 Terms: Bioprinting, Tissue engineering and Biofabrication – Exact search: Group name, research field name, research field keyword

Actors	
Universities	Federal Center of Technological Education of Minas Gerais Brazilian Agricultural Research Company Porto Alegre Clinical Hospital Little Prince Children's Hospital Paraíba Federal Institute of Education, Science and Technology Federal Institute of Ceará – Rectory Pontifical Catholic University of Rio Grande do Sul Brazil University Araraquara University University of Brasilia University of Pernambuco University of Sao Paulo State University of Minas Gerais Campinas State University Paulista State University Julio de Mesquita Filho Federal University of Southern Frontier Federal University of Campina Grande Federal University of Itajubá Federal University of Mato Grosso do Sul Federal University of Minas Gerais Federal University of Pernambuco Federal University of Santa Catarina Federal University of São Carlos Federal University of Sao Paulo Federal University of Sergipe Federal University of Viçosa Federal University of ABC Federal University of Espirito Santo Federal University of Piaui Universidade Federal do Rio de Janeiro Universidade Federal do Rio Grande do Sul Universidade Federal do Vale do São Francisco Universidade Federal dos Vales do Jequitinhonha e Mucuri – Campus JK Universidade Federal Fluminense Universidade Ibirapuera



		Bioprinting areas of practice
Research Institutes	CTI Renato Archer	Biofabrication, prosthesis, software applications and systems
	IPEN	Applications
	CNPEM LNBio	Organoids
	INCT Biofabris	Development of biomaterials
	Dante Pazzanese Institute	Cardiovascular therapeutic applications
	The Heart Institute (Incor)	Cardiovascular therapeutic applications
Startups	InSitu Cellular Therapy (2016),	Bioprinting Products: Biocuratives
	3D Biotechnology Solutions (2017),	Products for Bioprinting: equipment and supplies Bioprinting Products: InVitro Models
	BioCellTiss (2017),	Bioprinting Products: InVitro Models
	BioEdTech (2018),	Products for Bioprinting: Low cost equipment and educational area
	TissueLab (2018),	Products for Bioprinting: Bioinks
	Bioprint3D (2019),	Products for Bioprinting: Low cost equipment
	GCell (2019)	Spheroids
Companies	Embrapa Genetic Resources	Bioprinting applications: biomaterials, nanopigments, and applications in agriculture
	Natura Cosmetics	InVitro Skin models
	AC Camargo Câncer Hospital	In Vitro models to fight Cancer
Government Agencies	ANVISA	Advanced Therapy Regulation

Source: Self Developed

Table 2 – Main actors of the Sectoral System of Bioprinting Innovation

Among the main research centers in Brazil we can highlight the pioneering work of the Biofabrication Research Group of the Information Technology Center CTI Renato Archer, which has been using additive manufacturing technologies for the creation of prostheses since 1994. Also, the research lines by the Embrapa Nanobiotechnology Laboratory, in the development of biomaterials originating from agriculture. Finally, the cutting edge research by the National Center for Materials Research CNPEM on organoid development, amongst others. Moreover, the essential role of universities in providing the appropriate environment that allows connection with this cutting edge area under different lines of research.

An example of a large Brazilian company that comes to view applications in the field of bioprinting is Natura Cosmetics. One of its ongoing projects aims to develop a dermo skin equivalent from the 3D bioprint technique to serve as an in vitro platform for cosmetic product evaluation. Fibroblasts, keratinocytes and melanocytes will be co-cultured on layer-by-layer polymeric support, following the trend of alternative in vitro models, which serve as an alternative to the use of animals for effectiveness and safety for the testing of cosmetics. The arrangement for the execution of this project includes leading researcher at startup 3D Biotechnology Solutions, Dr. Ana Luiza Millás under the supervision of Prof. Silvy Maria-Engler Stucchi, from the School of Pharmaceutical Sciences, University of São Paulo / USP. Figure 1 below shows the geographical distribution of groups, research lines and startups in Brazil.

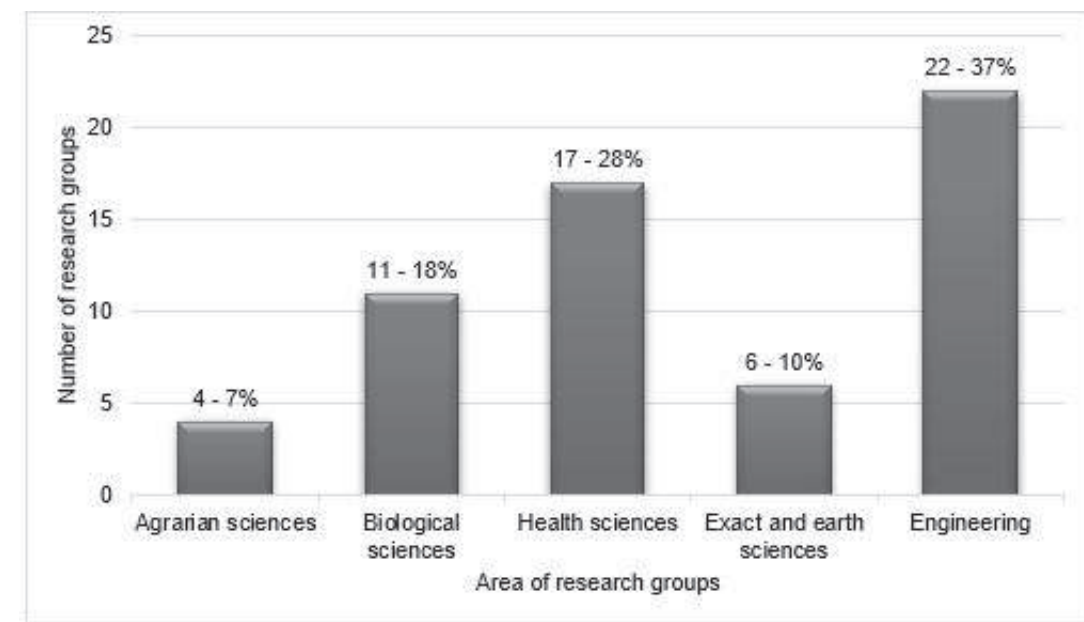
Most of the system is located in universities and research institutes that are concentrated in the states of São Paulo, Minas Gerais, Rio Grande

do Sul, Santa Catarina, and Rio de Janeiro. In general it can be said that all startups come from centers of excellence in this field which demonstrates the important function of any innovation system that is the dissemination of knowledge. The emergence of startups is an indication that resource mobilization toward enterprise experimentation is also taking place.

It is also worth noting that the groups as well as lines of research predominantly have an area of activity classified as "Engineering" followed by "Health Sciences" and "Biological Sciences", as shown in Graph 1 below. This indicates the interdisciplinary character of the field as researchers are encountering TE and Bioprinting from different disciplines and under different approaches and lines of research.

As for induction mechanisms and support for innovation, we did not identify any specific support line for the development of the field. The available support mechanisms are the same for other technology-based and innovation-promoting enterprises; however, an important point to highlight is the vital role of the São Paulo State Research Foundation - FAPESP, which through its PIPE program funded / funds projects in three of the four startups in this state.

From the regulatory point of view, it is worth highlighting the position of ANVISA, that approved the Resolution of the Collegiate Board (RDC 260/2018), which establishes specific criteria for studies with advanced therapy products, methods that consist of the use of genetic material (genes and cells) in various treatments. This resolution covers different application possibilities using stem cells for the field of bioprinting and tissue engineering.



Graph 1 – Predominant area of research groups.

Characteristics of innovation projects in the field of bioprinting from the perspective of a startup: The case of 3D Biotechnology Solutions – 3DBS

3DBS – 3D Biotechnology Solutions was established in December of 2017, registered with the National Register of Legal Entities (CNPJ): 29.150.401/0001-00, as the first Brazilian startup working in the field of bioprinting. Its shop is located in São Paulo, Brazil. Since its opening, it has been developing projects for customizing bioprinting equipment and consulting services in the area of tissue engineering. 3DBS' services have been in demand both for the development of equipment as well as for its *Know How* within the field of bioprinting. Since its opening it has been developing diverse projects to meet specific demands of startups, research institutes and universities. Among these we can mention, In Situ Cellular Therapy, IPEN, Embrapa, UNICAMP, INCT Biofabris, UFRGS, UFRJ, USP/São Paulo.

In these months of operation, so far it has been observed that the main client is either the researcher who develops applications or the professors in the educational field. His main need is to supply missing knowledge to

advance research since the field of bioprinting is extremely interdisciplinary and is in its early stages in Brazil. Thus, there is a need/demand for support to begin research in the field of bioprinting and personalized and close assistance to operationalize the lines of research. In addition, there are difficulties in importing equipment and resources, both from a price, as well as from a logistical and customs barrier. Among the elements that compose the value proposition of 3DBS we can highlight: reduction in the cost of bioprinting, customization for specific purposes, partnerships for the co-development of applications, possibility of printing of different materials and association with other technical methods such as electrospinning.

Among the next steps, 3DBS has been developing applications that aim to explore bioprinting products, and for this purpose it has been developing specific projects with the support of the São Paulo State Research Support Foundation (FAPESP) and partners such as the Federal School of Medicine of São Paulo (UNIFESP), the AC Camargo Cancer Center hospital, and the Faculty of Pharmaceutical Sciences of USP/São Paulo. Moving forward, we will detail the main aspects of these initiatives.



Figure 2 – 3DBS Bioprinters, models Genesis II and Octopus.

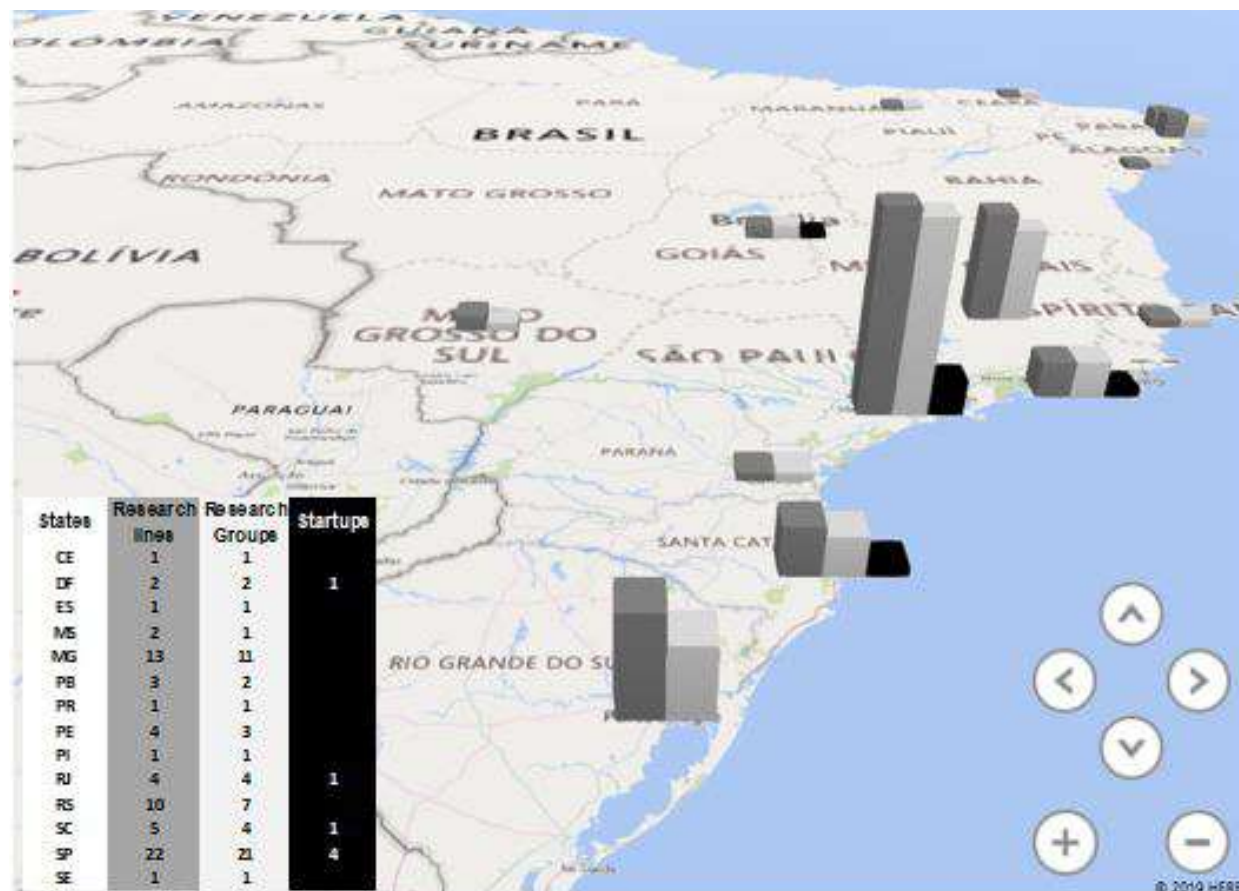


Figure 1 – Distribution of groups, research lines and startups in the field of Bioprinting and tissue engineering.

Ongoing 3DBS Projects and their impacts

Project I: Bioprinting of tubular structures and In Vitro models – Partnership with USP and FEM Unicamp – PIPE FAPESP phase II program support

Cardiovascular diseases are the leading cause of deaths in developed countries, particularly those that cause flow obstruction as is the case of atherosclerosis¹⁴. In addition to atherosclerosis, several vascular diseases and pathologies lead to aneurysmal degeneration, congenital malformation, vasculitis, and traumatic injuries requiring arterial bypass. Bypass or revascularization surgery is a surgical procedure that utilizes an autologous vascular graft, such as the patient's own saphenous vein or peripheral artery or an artificial graft¹⁵. Even today, the autologous graft is the gold standard; however, previous surgeries and medical comorbidities may limit the availability of these vessels.

Thus, synthetic vascular grafts play an important role in the treatment of these clinical conditions as 30% of patients that require bypass surgery do not possess adequate or sufficient autologous blood vessels¹⁶. Polyethylene terephthalate (PET), Dacron and expanded polytetrafluoroethylene (ePTFE) are the biomaterials commonly used in vascular prostheses, awarding satisfactory results when used to replace or bypass large blood vessels. However, due to the blood flow velocity in small caliber vessels, the clinical performance of these grafts is inferior^{17,18}. Although biologically inert, synthetic vascular prostheses are also susceptible to infections¹⁹.

Due to the poor functional performance of commonly used biomaterials, strategies have been developed to reduce the factors that influence low permeability rates, namely acute thrombus formation and intimal hyperplasia^{20,21}. Endothelialization of the luminal surface of the graft using autologous endothelial cells has become a successful procedure to improve long-term permeability rate (7 years) in artificial vascular grafts²². Studies show the use of autologous cells and genetically modified cells loaded in biological or synthetic matrices to construct tubular structures

and subject them to mechanical and chemical stimuli in an attempt to develop a small caliber vascular graft^{23,24}. As noted with the increasing demand for blood vessels and the problematic of existing therapies, tissue engineering as a multi and interdisciplinary discipline establishes three essential criteria for blood vessel development: i) to present biocompatible components with high tensile strength that provide mechanical support; ii) have a biocompatible elastic component that provides elastic reserve and prevents the formation of aneurysms (elastin fibers); iii) have a confluent endothelium that prevents intravascular thrombosis.

To achieve these goals, technologies that were previously used for other purposes have been adapted over the past decade to meet the demands of regenerative medicine and, specifically, tissue engineering. This is the case of 3D bioprinting, an adaptation of conventional 3D and electrospinning printing techniques, inherited by the textile industry, to produce nano and micro fibers.

The 3D printer used in this project was developed under the Phase I PIPE/FAPESP program by 3DBS startup. The equipment has two printer heads that allow you to work with two bioinks layer-by-layer in the same bioconstruct, as well as a photocuring system (ultraviolet light), HEPA filters, a camera for recording images during the bioprinting process and a fourth rotary axis with controlled speed and diameters for the generation of tubular structures (diameters between 2mm and 12mm) (Figure 3).

During Phase I of the PIPE program, tests were performed to validate the equipment, so we had the collaboration of the researcher Prof. Dr. Marcos Akira, from the Faculty of Mechanical Engineering at UNICAMP and Prof. Dr. Sang Won Han of the Center for Cellular and Molecular Therapy (CTCMOL) at UNIFESP. Bioinks with different compositions and rheological properties were tested analyzing printability, filament formation, injectability, the preservation of three-dimensional geometry after crosslinking and biocompatibility (cell viability) (vide Figure 4).

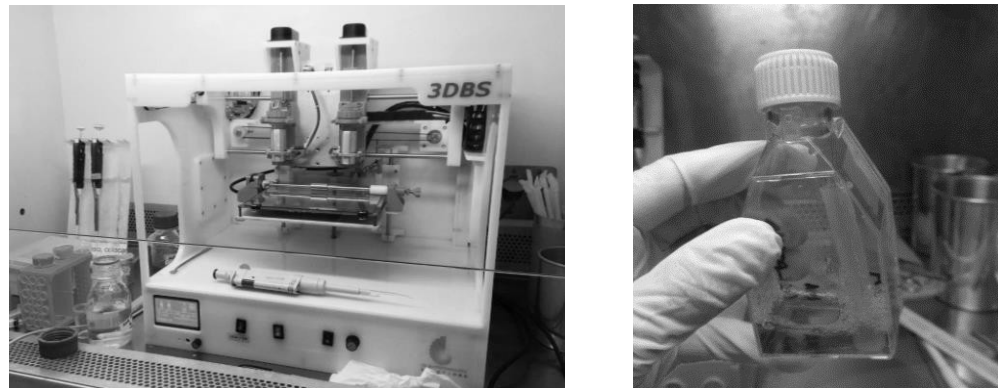


Figure 3 – 3D Bioprinter Model Genesis II from 3DBS startup. It possesses a fourth rotary axis for the generation of tubular structures (vascular grafts). Source: author.

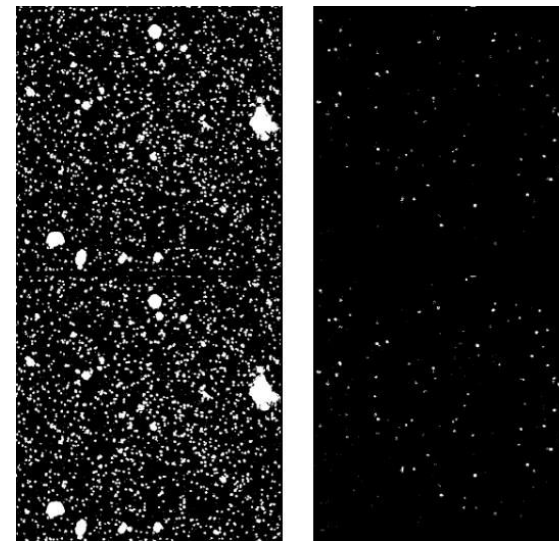


Figure 4 – On the left, tubular alginate (4%) +gelatin (2%) structures loaded with fibroblasts after 11 days of printing. On the right, tubular alginate (6%) structure loaded with fibroblasts. Cell viability is higher when gelatin is incorporated. We tested pure alginate bioink, alginate+gelatin compositions and alginate with laponite bioink. Source: author.

Project II: Bioprinting of In vitro tumor models – partnership with AC Camargo Cancer Hospital

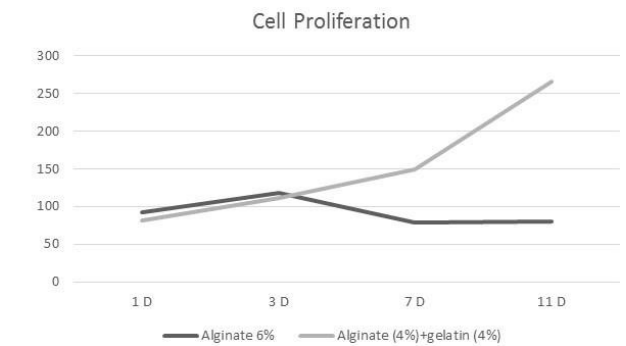
Despite substantial progress in cancer research over the past century, the World Health Organization (WHO) has reported that the incidence of cancer worldwide has increased from 12.7 million in 2008 to 14.1 million in 2012, and the estimate for the next two decades is that this incidence will increase to 25 million, with the greatest impact on low and middle income countries²⁵. Applied to oncological investigations, bioprinting allows the creation of in vitro three-dimensional structures with cellular complexity and heterogeneity similar to that found in an in vivo tumor microenvironment, characteristics that are not observed in conventional two-dimensional models²⁷. One of the mechanisms of cancer biology that can best be understood through the use of three-dimensional bioprinting models is metastasis, the leading cause of cancer death worldwide.

Accurate models of human tumors are needed to understand how complex stromal tumor interactions contribute to tumor growth, progression and therapeutic response. Models of genetically modified mice and cancer cell xenografts in immunocompromised mice have allowed the study of tumors in the presence of a tumor microenvironment, but these models are expensive, time consuming, do not include human stroma, and can be difficult to manipulate. Several advances have been made for *in vitro* culture methods in attempts to better recapitulate the complex in vivo tumor microenvironment^{28,29,30,31}.

Matrix-based models, such as collagen or Matrigel, or scaffold-free heterotypic co-culture models, including multicellular tumor spheroids, allow the integration of additional cell types into 3D culture.

Highlighting the importance of three-dimensional in vitro models for the study of cancer and cell interactions for oncogenesis, three-dimensional systems, when compared to 2D systems, demonstrated significant changes in the genic expression, proliferation, and tumorigenic phenotype profiles^{32,33,34}. 3D bioprinting has been used in a variety of approaches in an attempt to generate cancer models that simulate spatially defined microenvironments^{34,35}. The spatial orientation of cells within bioprinted tissues allows the investigation of tumorigenic phenotypes, such as cell migration, as well as the analysis of spatial heterogeneity. Together, these results suggest that bioprinted tissues may be useful for drug response studies and analysis of cytostatic versus toxic effects of therapies.

In practice the use of 3D models for cancer drug testing will promote a faster transfer of basic knowledge to the clinic, increase the effectiveness of treatments and lower the costs of drug development as effectiveness tests become more accessible. In addition, it will allow the development of



new experimental protocols for the study of tumor biology, especially the mechanisms of metastasis.

Conclusions

The sectoral innovation system of TE and bioprinting has a solid foundation within the academic circle, represented by consolidated groups and lines of research in different universities. The system is starting to present signs of commercial exploration of different application and correlate areas, among these, the supply of equipment and resources for bioprinting, consulting and specific training. The regulatory framework has also been established and implemented by ANVISA based on the regulatory experiences of other countries.

In general, it is worth mentioning that the field of bioprinting is incipient in the world, with the main commercial players beginning to consolidate in the last decade. What has been seen is a consistent expansion of mainly the number of startups emerging in the market within the last couple of years. From a perspective of actions to leverage the expansion of this system, the fact that it is an emerging market provides a wide range of opportunities to formulate strategies for the promotion of Leapfrogging, that is, the notion that areas with less developed technology or economic foundations can advance rapidly through the adoption of specific mechanisms of support without having to go through intermediate steps.

In this sense, to promote the interaction of actors with each other and with investors is an important induction mechanism, both to promote the contact between different related areas of knowledge, as well as to provide long-term financing. Having access to long-term financing is vital especially for developing applications that require clinical testing. Thus, reducing the entrepreneur's risk by providing access to public or private resources can stimulate the development of new startups by fostering bench-to-market movement. On the other hand, to stimulate the demand for applications through specific public bidding can be an interesting resource because it allows entrance in the market of innovative applications in the health field in a controlled manner. In addition, it legitimizes new technologies by supporting the initial formation of this market.

References

- 1- Langer R, Vacanti JP. Tissue engineering. Science. 1993 May 14;260(5110):920-6. DOI: 10.1126/science.8493529

- 2- Rider P, Kačarević ŽP, Alkildani S, Retnasingh S, Barbeck M. Bioprinting of tissue engineering scaffolds. *Journal of Tissue Engineering* 2018;9:204173141880209. doi:10.1177/2041731418802090.
3. Russell WMS. *The principles of humane experimental technique*. Methuen, 1959.
4. Choudhury D, Anand S, Naing MW. The Arrival of Commercial Bioprinters – Towards 3D Bioprinting Revolution! *International Journal of Bioprinting* 2018;4. doi:10.18063/ijb.v4i2.139.
5. Bergin J. Bioprinting: Technologies and Global Markets. Bioprinting: Technologies and Global Markets: BIO148A | BCC Research. <https://www.bccresearch.com/market-research/biotechnology/bioprinting-markets-technologies-report.html> (accessed March 6, 2020).
6. 3D Bioprinting Market Size, share and trends analysis report by technology (Magnetic levitation , inkjet based, syringe based, laser based), by application , and segment forecast, 2018–2024, 2018. Available from: www.grandviewresearch.com/industry-analysis/3Dioprinting-market
7. Li PH. 3D Bioprinting Technologies: Patents, Innovation and Access. *Law, Innovation and Technology* 2014;6:282–304. doi:10.5235/17579961.6.2.282.
8. Freeman C. *Technology, policy, and economic performance: lessons from Japan*. London: Pinter; 1987.
9. Lundvall Bengt-Åke. *National systems of innovation: toward a theory of innovation and interactive learning*. London: Anthem Press; 2010.
10. Nelson RR, Winter SG. *An evolutionary theory of economic change*. Cambridge, MA: The Belknap Press of Harvard Univ. Press; 2009.
11. Malerba F. Sectoral systems of innovation and production. *Research Policy* 2002;31:247–64. doi:10.1016/s0048-7333(01)00139-1.
12. Chaminade C, Esquist C. Rationales for Public Policy Intervention in the Innovation Process: Systems of Innovation Approach. *The Theory and Practice of Innovation Policy*. doi:10.4337/9781849804424.00012. 13– Jacobsson S. Transforming the energy sector: the evolution of technological systems in renewable energy technology. *Industrial and Corporate Change* 2004;13:815–49. doi:10.1093/icc/dth032.
14. Spence JD. Faculty of 1000 evaluation for Heart disease and stroke statistics--2013 update: a report from the American Heart Association. F1000 – Post-Publication Peer Review of the Biomedical Literature 2013. doi:10.3410/f.718113556.793483971.
15. Hobson RW, Mackey WC, Ascher E, Murad MH, Calligaro KD, Comerota AJ, *et al*. Management of atherosclerotic carotid artery disease: Clinical practice guidelines of the Society for Vascular Surgery. *Journal of Vascular Surgery* 2008;48:480–6. doi:10.1016/j.jvs.2008.05.036.
16. Nomi M, Atala A, Coppi PD, Soker S. Principals of neovascularization for tissue engineering. *Molecular Aspects of Medicine* 2002;23:463–83. doi:10.1016/s0098-2997(02)00008-0.
17. Hashi CK, Derugin N, Janairo RRR, Lee R, Schultz D, Lotz J, *et al*. Antithrombogenic Modification of Small-Diameter Microfibrillar Vascular Grafts. *Arteriosclerosis, Thrombosis, and Vascular Biology* 2010;30:1621–7. doi:10.1161/atvbaha.110.208348.
18. Carrabba M, Madeddu P. Current Strategies for the Manufacture of Small Size Tissue Engineering Vascular Grafts. *Frontiers in Bioengineering and Biotechnology* 2018;6. doi:10.3389/fbioe.2018.00041.
19. Antonios VS, Noel AA, Steckelberg JM, Wilson WR, Mandrekar JN, Harmsen WS, *et al*. Prosthetic vascular graft infection: A risk factor analysis using a case-control study. *Journal of Infection* 2006;53:49–55. doi:10.1016/j.jinf.2005.10.004.
20. Kannan RY, Salacinski HJ, Sales K, Butler P, Seifalian AM. The roles of tissue engineering and vascularisation in the development of micro-vascular networks: a review. *Biomaterials* 2005;26:1857–75. doi:10.1016/j.biomaterials.2004.07.006.
21. Kakisis JD, Liapis CD, Breuer C, Sumpio BE. Artificial blood vessel: The Holy Grail of peripheral vascular surgery. *Journal of Vascular Surgery* 2005;41:349–54. doi:10.1016/j.jvs.2004.12.026.
22. Meinhart J, Deutsch M, Zilla P. Eight Years of Clinical Endothelial Cell Transplantation Closing the Gap Between Prosthetic Grafts and Vein Grafts. *ASAIO Journal* 1997;43. doi:10.1097/00002480-199709000-00034.
23. Isenberg BC, Williams C, Tranquillo RT. Small-Diameter Artificial Arteries Engineered In Vitro. *Circulation Research* 2006;98:25–35. doi:10.1161/01.res.0000196867.12470.84.
24. Bleiziffer O, Eriksson E, Yao F, Horch RE, Kneser U. "Gene transfer strategies in tissue engineering." *Journal of cellular and molecular medicine* 11.2 (2007): 206–223. DOI: 10.1111/j.1582-4934.2007.00027.x
25. Dávila JL, D'Ávila MA. Rheological evaluation of Laponite/alginate inks for 3D extrusion-based printing. *The International Journal of Advanced Manufacturing Technology* 2018;101:675–86. doi:10.1007/s00170-018-2876-y.
26. Stewart BW, Wild CP., eds (2014). *World Cancer Report*, IARC
27. Langer EM, Allen-Petersen BL, King SM, Kendsersky ND, Turnidge MA, Kuziel GM, Riggers R, Samatham R, Amery TS, Jacques SL, Sheppard BC, Korkola JE, Muschler JL, Thibault G, Chang YH, Gray JW, Presnell SC2, Nguyen DG, Sears RC. Modeling tumor phenotypes in vitro with three-dimensional bioprinting." *Cell reports* 26.3 (2019): 608–623. doi: 10.1016/j.celrep.2018.12.090.
28. Jaganathan H, Gage J, Leonard F, Srinivasan S, Souza GR, Dave B, *et al*. Three-Dimensional In Vitro Co-Culture Model of Breast Tumor using Magnetic Levitation. *Scientific Reports* 2014;4. doi:10.1038/srep06468.
29. Katt ME, Placone AL, Wong AD, Xu ZS, Searson PC. In Vitro Tumor Models: Advantages, Disadvantages, Variables, and Selecting the Right Platform. *Frontiers in Bioengineering and Biotechnology* 2016;4. doi:10.3389/fbioe.2016.00012.
30. Longati P, Jia X, Eimer J, Wagman A, Witt M-R, Rehnmark S, *et al*. 3D pancreatic carcinoma spheroids induce a matrix-rich, chemoresistant phenotype offering a better model for drug testing. *BMC Cancer* 2013;13. doi:10.1186/1471-2407-13-95.
31. Park J, Morley TS, Kim M, Clegg DJ, Scherer PE. Obesity and cancer—mechanisms underlying tumour progression and recurrence. *Nature Reviews Endocrinology* 2014;10:455–65. doi:10.1038/nrendo.2014.94.
32. Fong EL, Harrington DA, Farach-Carson MC, Yu H. Heralding a new paradigm in 3D tumor modeling. *Biomaterials* 2016;108:197–213. doi:10.1016/j.biomaterials.2016.08.052.
33. Stadler M, Walter S, Walzl A, Kramer N, Unger C, Scherzer M, *et al*. Increased complexity in carcinomas: Analyzing and modeling the interaction of human cancer cells with their microenvironment. *Seminars in Cancer Biology* 2015;35:107–24. doi:10.1016/j.semcancer.2015.08.007.
34. Weigelt B, Ghajar CM, Bissell MJ. The need for complex 3D culture models to unravel novel pathways and identify accurate biomarkers in breast cancer. *Advanced Drug Delivery Reviews* 2014;69:70:42–51. doi:10.1016/j.addr.2014.01.001.
35. Zhang YS, Duchamp M, Oklu R, Ellisen LW, Langer R, Khademhosseini A. Bioprinting the cancer microenvironment. *ACS Biomaterials Sci Eng*. 2016 Oct 10;2(10):1710–1721. doi: 10.1021/acsbomaterials.6b00246.

Bio-inks for 3D extrusion-based bio-printed scaffolds: Printability assessment

Verónica E. Passamai¹; Sergio Katz¹; Vera Alvarez²; Guillermo R. Castro^{1*}

*Corresponding author: E-mail address: gcastro@gmail.com

Abstract: 3D bio-printer is a new technology that requires to be integrated into several areas, including medical technology. However, before design and apply at large scale it is required to establish several biophysical parameters and particularly printability. In the present work, general characteristics of extrusion method, bio-inks and scaffolds are reviewed. Printability analysis on 3D bio-printing are also included.

Keywords: 3D Bio-printing; Bio-inks; Printability; Hydrogels.

Introduction

3D-bioprinting (3DB) is a multilayer-based approach run on computer program designs and used to produce complex devices for several purposes in many areas such as biomedicine, biotechnology, among others.¹ The integration of technologies from bioengineering, materials science, cell biology, physical chemistry and medicine to the bio-print field ensures a promising future for this innovative technology². The most current approach of 3DB is the potential application in biomedical engineering and translational medicine, which consists on the development of customized

scaffolds of 3D porous structures with interconnected channels made of bio-inks based on biomaterials with active biomolecules containing or not cells^{3,4}. The main application of 3D scaffolds is the production of biocompatible constructs for tissue/organ regeneration.⁵ In addition; scaffolding bio-print can be applied for the development of high-throughput assays, drug discovery systems, and others⁵.

The main bio-ink properties can be grouped in biological, chemical and biophysical characteristics (Figure 1).

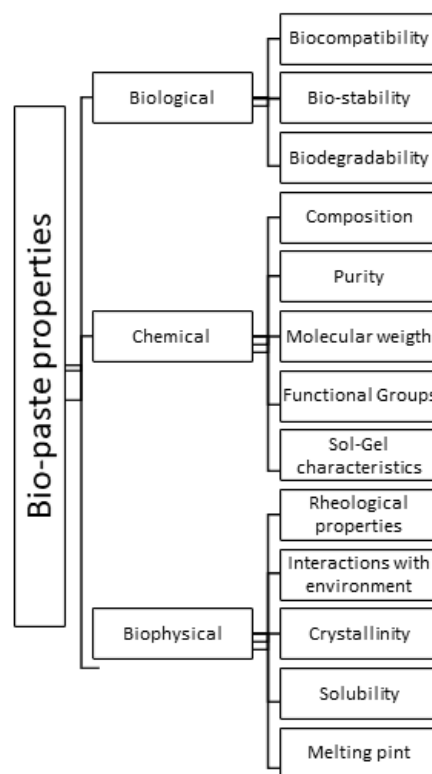


Figure 1 – Main characteristics of bioinks classified in groups of properties.

¹ Laboratorio de Nanobiomateriales, CINDEFI, Departamento de Química, Facultad de Ciencias Exactas, Universidad Nacional de La Plata (UNLP) – CONICET, Calle 47 y 115, (B1900AJI), La Plata, Buenos Aires, Argentina.

² Grupo de Materiales Compuestos Termoplásticos (CoMP), Instituto de Investigaciones en Ciencia y Tecnología de Materiales (INTEMA), Facultad de Ingeniería, Universidad Nacional de Mar del Plata (UNMDP) – CONICET, Av. Colón 10850 (B7608FDQ), Mar del Plata, Buenos Aires, Argentina.

Extrusion method, bio-inks and scaffolds general characteristics

Extrusion method is the most studied additive manufacturing technology; this is related to advantages such as precise deposition, cost-effectiveness, simplicity, process speed, homogeneous distribution of bioactive components, tailoring, versatility and predictability⁶. In this method, bio-inks are extruded through a print head using syringes with tips or specific nozzles by either pneumatic pressure or mechanical force but without heat requirements. Additive manufacturing technology has demonstrated its great potential in producing functional scaffolds for biomedical applications. All molecules used for the development of scaffolds must possess biocompatibility, no toxicity and proper biophysical properties to induce molecular bio-recognition and ensure an optimal environment for molecules and/or cells⁷.

In the extrusion methods, one of the most important factors for 3DB procedure is the rheological behavior of bio-inks. During the extrusion, the material flow from the nozzle and the fusion of layers results in scaffolds with controlled pore size, morphology, and interconnectivity¹. Apparent viscosity, defined as the ratio of shear stress to shear rate is a relevant parameter, since should be low enough to allow the extrusion process of clear filament and mechanically strong to support the deposition of upper layers without compression and/or changing the matrix shape^{4,8}. Some research groups have demonstrated the advantages of rheological characterization to systematize 3D printing methodologies and to develop mathematical models that help to gain a deep understanding of non-Newtonian fluid models⁹⁻¹⁰.

In order to facilitate tissue regeneration, scaffolds must be designed to provide a proper environment for cell growth, which generally depends on both, selection of materials but also geometrical features such as internal structures and pore size distribution. Another critical issue are the mechanical properties of the scaffold that must match those of the original tissue to be used and/or repaired¹¹. Moreover, scaffold mechanical properties such as stability and degradation kinetics must be adapted to the specific tissue application and requirements in order to guarantee the proper mechanical functions and to accomplish the rate of the new-tissue regeneration and/or formation⁸.

Printability analysis on 3D bioprinting

Recently, bio-ink research efforts have been made to develop new materials with the aims of improving biocompatibility and biofunctionality⁴. Based on the fast increase in the knowledge associated with biomaterials, cell-scaffold interactions and the ability to bio-functionalize/decorate bio-inks with cell recognition motifs (e.g. biomarkers, mucoadhesive molecules, etc.), it is also important to consider the “printability” of these novel materials¹².

Extrudability is defined as the ability to eject a paste through a nozzle without considerable cross-sectional deformation and acceptable degree of splitting/tearing of the resulting filament¹³. In fact, the extruded filament width is expected to be similar to the nozzle diameter in order to obtain a good shape fidelity and correlated to the computer aided design (CAD) model since the nozzle diameter value is included at initial set parameters of the equipment.

In previous work, seven possible filament types produced by extrusion printing of alginate-gelatin blends by varying the materials properties and operating conditions were reported. The work used continuous and defined filaments that show swelling, equivalent or stretched diameter regarding to nozzle were considered well-made filaments and they are favored for 3D printing due to the defined geometries results. Irregular filaments with rough surface, over-deposition material, compressed material or discontinuity and should be avoided due to the uncontrollability of the morphology and/or diameter of such filaments¹⁴.

There are different reasons why irregular filaments are obtained, the most frequent are low pressure of extrusion motor, nozzle obstruction due to large particles or bubbles formation in the mixture, high paste viscosity, incomplete mix of components, and excessive shear forces inside the nozzle during printing and “pinch” of the filament due to low paste

viscosity¹⁵⁻¹⁸.

The printed filament must show clear morphology with smooth surface and constant three-dimensional widths¹³. The good bio-ink printability result into regular grids and square holes displayed in linear scaffolds constructs, on the contrary, the upper layer could fuse within the lower layer creating approximately circular holes if the extruded filament showed a more sol-like state with low-viscosity⁴.

The dimensionless parameter used to characterize the extruded filament is circularity (C) of an enclosed area that can be determined by the follow equation:⁴

$$C = \frac{4\pi A}{L^2} \quad [1]$$

where L is the filament perimeter and A is the cross-section area.⁴

Circular sections have the highest circularity (C= 1). The closer the C value is to 1, the closer the shape is to a circle.

For a square shape, circularity is equal to $\pi/4$. The bio-ink printability (Pr) dimensionless parameter is based on square shape and defined using the following equation:

$$Pr = \frac{L^2}{16 A} \quad [2]$$

where L is the filament perimeter and A is the cross-section area.

For an ideal printability status, the interconnected linear channels of scaffolds display square shape with Pr value of 1⁴.

Three typical pore shapes are displayed in **Figure 2**. Scaffolds A, B and C were developed using the cartesian 3D bio-printer “NBM-FAB-CINDEFI” commanded by Arduino open hardware and Marlin firmware designed and constructed in the NBM Laboratory. The equipment was designed to extrude viscous materials using a syringe with a nozzle size

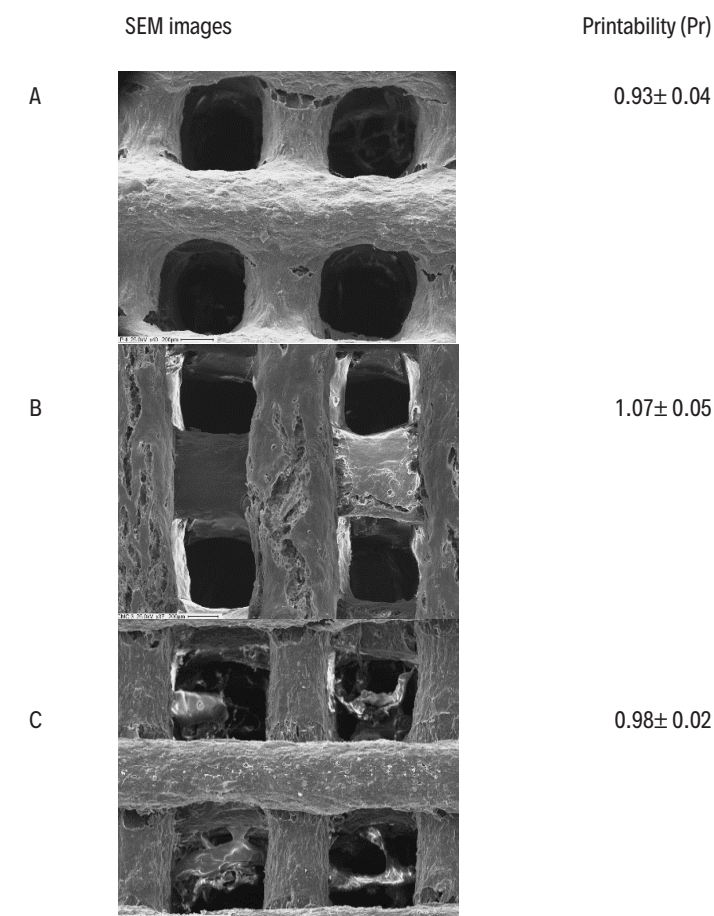


Figure 2 – SEM images and printability of pectin scaffolds under three typical pore shapes. A, pore shape closer to a circle made of pectin; B, little distorted square pore shape made of pectin and carboxymethyl cellulose and C, pore shape closer to a square made of pectin and microcrystalline cellulose.

of 0.2 mm or 0.4 mm. Scaffold A was printed with pectin bio-ink, B with pectin plus carboxymethyl cellulose and C with pectin plus microcrystalline cellulose. Pr values were analyzed by Image-J software using Scanning Electron Microscopy (SEM) images of printed scaffolds to establish the perimeter and the area of interconnected channels (n= 10). The scaffold C presents the best square interconnected channels, being it semi quantitative printability value the closest to 1 with the lowest SD. High Pr values are proportional to high bio-ink viscosity, which reveals the relevance of hydrogel rheological properties and connected with the physicochemical composition of the bio-ink paste. These parameters play an important role in controlling the resolution and shape fidelity of the 3D bio-printed structures.

Conclusions

The convergence of engineering techniques and life sciences evolved to develop the extrusion-based 3D bio-printing from a simple technique to one able to create diverse scaffolds from a wide range of biomaterials, bioactive molecules and cells types. The development and formulation of extrudable bio-inks has been a major challenge in the field of biofabrication. Bio-inks must not only display adequate rheological and mechanical properties for the chosen application but also to show high biocompatibility as well as bio-printability. Biological, and physicochemical requirements are quite studied in material science field while extrudability and printability assessing of bio-inks still needs to be carefully examined to enable robotic bio-printing. The present review summarizes printability concepts and displays some approaches to it analysis. For future, it is expected mathematical models, rheological assays, qualitative and quantitative physical analysis on 3D bioprinting applications to be standardized.

References

- Chia HN and Wu BM, Recent advances in 3D printing of biomaterials. *J. Biol. Eng.* **9**: 4. (2015). DOI: 10.1186/s13036-015-0001-4.
- Murphy SV and Atala A, 3D bioprinting of tissues and organs. *Nature Biotech.* **32**: 773–785 (2014). DOI: 10.1038/nbt.2958.
- Zhu W et al., 3D printed nanocomposite matrix for the study of breast cancer bone metastasis. *Nanomedicine* **12**: 69–79 (2016). DOI: 10.1016/j.nano.2015.09.010.
- Ouyang L et al., Effect of bioink properties on printability and cell viability for 3D bioplotting of embryonic stem cells. *Biofabrication* **8**: 3, 035020 (2016). DOI: 10.1088/1758-5090/8/3/035020.
- Peng W et al., 3D bioprinting for drug discovery and development in pharmaceuticals. *Acta Biomat.* **57**: 26–46 (2017). DOI: 10.1016/j.actbio.2017.05.025.
- Ozbolat IT and Hospodiuk M, Current advances and future perspectives in extrusion-based bioprinting. *Biomaterials* **76**: 321–343 (2016). DOI: 10.1016/j.biomaterials.2015.10.076.
- Carletti E et al., Scaffolds for tissue engineering and 3D cell culture. *Meth. Mol. Biol.* **695**: 17–39 (2011). DOI: 10.1007/978-1-60761-984-0_2.
- Tian XY et al., Characterization of the flow behavior of alginate/hydroxyapatite mixtures for tissue scaffold fabrication. *Biofabrication* **1**: 4, 045005 (2009). DOI: 10.1088/1758-5082/1/4/045005.
- Li H et al., Rheological study on 3D printability of alginate hydrogel and effect of graphene oxide. *Int. J. Bioprint.* **2**: 54–66 (2016). DOI: 10.18063/IJB.2016.02.007.
- Sarker M and Chen XB, Modeling the flow behavior and flow rate of medium viscosity alginate for scaffold fabrication with a 3D bioplotter. *J. Manuf. Sci. Eng.* **139**: 8, 81002 (2017). DOI: 10.1115/1.4036226.
- Liu J and Yan C, 3D printing of scaffolds for tissue engineering. In *3D Printing*, ed. by Cvetković D., Intech Open, UK, **7**: 137–154 (2018) DOI: 10.5772/intechopen.78145.
- Kyle S et al., 'Printability' of candidate biomaterials for extrusion based 3D printing: State-of-the-art. *Adv. Health Mat.* **6**: 16 (2017). DOI: 10.1002/adhm.201700264.
- Buswell RA et al., 3D printing using concrete extrusion: A roadmap for research. *Cement Concrete Res.* **112**: 37–49 (2018). DOI: 10.1016/j.cemconres.2018.05.006.
- Jin Y et al., Printability study of hydrogel solution extrusion in nanoclay yield-stress bath during printing-then-gelation biofabrication. *Mat. Sci. Eng. C* **80**: 313–315 (2017). DOI: 10.1016/j.msec.2017.05.144.
- Pati F et al., Extrusion Bioprinting. *Essentials of 3D Biofabrication and Translation*. A. Atala and J.J. Yoo (Editors), Elsevier. Pp. 123–152 (2015). DOI: 10.1016/B978-0-12-800972-7.00007-4.
- Zhang X et al., Tissue engineering applications of three-dimensional bioprinting, *Cell. Biochem. Biophys.* **72**: 777–782 (2015). DOI: 10.1007/s12013-015-0531-x.
- DeSimone E et al., Biofabrication of 3D constructs: Fabrication technologies and spider silk proteins as bioinks. *Pure Appl. Chem.* **87**: 737–749 (2015). DOI: 10.1515/pac-2015-0106.
- Jun Y et al., Trends on physical understanding of bioink printability. *Bio-Design Manufact.* **2**: 50–54 (2019). DOI: 10.1007/s42242-019-00033-y.



Fluid flow in a Porous Scaffold for Microtia by Lattice Boltzmann Method

Pedro J. Boschetti^{1*}; Orlando Pelliccioni^{2,3}; Mariángel Berroterán³; María V. Candal^{2,3}; Marcos A. Sabino⁴

*Corresponding author: E-mail address: pboschetti@usb.ve

Abstract: The birth deformity of ear, known as microtia, varies from a minimal deformed ear to the absence of auricular tissue or anotia. This malformation has been treated by reconstructing the external ear, mainly by autogenous rib cartilage in auricular repair. The fabrication of the ear framework is a prolonged reconstructive procedure and depends of the surgeon's skill. In order to avoid these inconveniences and reduce surgery time, it was proposed in a previous work to use implants made with biocompatible materials. One of these is a scaffold made by fused deposition modeling using PLA based in the three-dimensional geometry of the ear cartilage. The aim of this work is to evaluate the feasibility of this scaffold to perform cell culture in a perfusion biorreactor by estimating the flow transport characteristics in porous media using a scaffold with the porous geometry of the human auricular cartilage for microtia. Flow and heat transfer through the scaffold were simulated by the lattice Boltzmann method, and permeability and shear stress distribution were obtained at different Reynolds numbers. The permeability values of the scaffold achieved are in the order of magnitude of scaffolds used for cell culture. Linear dependencies between maximum shear stress and Reynolds number, and between maximum shear stress and permeability were obtained. The values of shear stress achieved correspond to high percentage of cell viability. The scaffolds for microtia treatment with the proposed filling pattern select is appropriate for cell culture in a perfusion biorreactor with characteristics similar to those described herein.

Keywords: Microtia treatment; Lattice Boltzmann method; Perfusion biorreactor; Scaffold; Shear stress in porous media.

Introduction

The birth deformity of ear is known as microtia, which varies from a minimal deformed ear, known as grade 1, to the absence of auricular tissue or anotia.¹ The more frequent cases of microtia are grade 3 and these look "like a little sausage-shaped Wrinkle of skin"¹. Microtia grade 2 looks like a miniature ear¹. This malformation occurs once in every 6,000 births, 2 only one side is involved in 90 percent of the cases, and 63.1 percent of the patients are males and the other 36.9 percent are females².

This malformation has been treated by reconstructing the external ear. In 1959, Tanzer made a successful reconstruction employing an autogenous rib cartilage as framework³. The use of autogenous rib cartilage in auricular repair has been used since that date and the results in a long term had reported^{4,5}. The fabrication of the ear framework is a prolonged reconstructive procedure and depends of the surgeon's skill. In order to avoid these inconveniences and reduce surgery time, Berroterán⁶ proposed to use implants made with biocompatible materials to treat microtia. One of these is a scaffold made by fused deposition modeling (FDM) using polylactic acid (PLA) based in the three-dimensional geometry of the ear cartilage.⁶ This must have the appropriate conditions to develop a cell culture.

The objective of the present research is to evaluate the feasibility of a scaffold proposed in a previous work to perform cell culture in a biorreactor by estimating the flow transport characteristics in porous media using a scaffold with the porous geometry of the human auricular cartilage for microtia. The micro-fluid dynamics through a scaffold is simulated by three-dimensional lattice Boltzmann method. The characteristic properties in porous media are the Darcy permeability and the shear stress distribution, because the feasibility of a specific scaffold to perform in vitro cell culture could be set knowing these characteristic properties.

One of the scopes of previous research works is to evaluate charac-

teristic properties of fluid flow in porous media of the employed scaffold by computational fluid dynamics. Some of these works simulated flow in a geometry of the employed scaffold obtained by microtomography,⁷⁻¹³ and when the geometry of the scaffold is built by three-dimensional printing, the model used in the simulations is draw using of the same parameters of the printing.¹⁴⁻¹⁶ For this application the flow field has been modeled by the finite volume method,^{8,9,14,17} the finite element method,^{15,16,18} and the lattice Boltzmann method^{7,8,10-13,19} with results similar to experimental data, however not precise to these. Pennella *et al.*¹³ explain some causes of the difference between the permeability values obtained experimentally and those calculated by computational fluid dynamic among which are the reconstructed scaffold volumes are in different orders of magnitude than the experimental samples and the resolution of the microtomography images used to reconstruct the three-dimensional models is not adequate. These previous publications differ in the way that they model the flow through the porous media and in the characteristic properties due to the specific objectives of each research. For example, Ferroni *et al.*²⁰ in addition to simulate flow through the porous scaffold, they also studied the oxygen consumption in this, and Alam *et al.*¹⁴ present a tool to simulate cell growth in bone tissue. Table 1 shows details about each referenced work.

The shear stress produced by the flow at the internal walls of the scaffold has been studied due to shear stress is an important regulator in cell function⁷. Croughan and Wang²¹ describe the shear stress effects on metabolism of living animal cells in biorreactors, and Liu, *et al.*²² demonstrated that shear stress induced by laminar flow can promote autophagy in vascular endothelial cells. According to its magnitude, shear stress could have a beneficial effect on cell growth²³, can damage cells²⁴ or prevents attachment of the cells to the scaffold^{15,16}. Computational fluid dynamics have been employed to obtain shear stress values in scaffolds concluding that shear stress is a function of the porous geometry and flow regime¹⁵,

¹Departamento Tecnología Industrial, Universidad Simón Bolívar, Camurí Grande Valley, Naguayá, 1160, Venezuela.

²Departamento de Mecánica, Universidad Simón Bolívar. AP 89000, Caracas, Venezuela.

³Grupo de Biomecánica, Universidad Simón Bolívar. AP 89000, Caracas, Venezuela.

⁴Grupo B5IDA, Departamento de Química, Universidad Simón Bolívar. AP 89000, Caracas, Venezuela.

and more specific of the Darcy permeability coefficient¹⁶.

Generally, cell cultures are performed at constant temperature around 37 degrees Celsius, the initial conditions are at room temperature (around 21 degrees Celsius). Schuerlein *et al.*²⁵ report a variation of temperature in the medium in tissue chamber from initially 21 to 36 degrees Celsius within 60 min in a perfusion bioreactor. These temperature variations could change the flow properties in the scaffold and are studied herein.

The lattice Boltzmann method has been very useful to solve flow in porous media because of it avoids to create an intricate mesh in this media, required by other computational fluid dynamic methods, besides this method allows multi-physics applications like flow and heat transfer. In this case, the open access code Palabos²⁶, based in this method, is chosen to perform the simulations. This code is capable of modeling three-dimensional, unsteady, low Reynolds flow.

Methodology

Geometry employed

Berrotecan6 built six different samples of scaffolds with the geometry of the human auricular cartilage by fused deposition modeling (FDM) using a thread of polylactic acid (PLA) fibers. These samples differ in orientation (horizontal, vertical, and lateral), fill pattern (honeycomb, line, and rectilinear), layer thickness, and fill density. To print these scaffolds was used

FDM machine brand RepRapBCN®, Esun 3D filament PLA as building material (Esun 3D filament PVA as support material). Two of these scaffolds were selected and reported an average pore size between 200 and 500 μm, which is considered appropriate for the adequate cellular proliferation in the scaffold according to Wu *et al.*²⁷ and Sobral *et al.*²⁸ These two scaffolds were printed with orientation and fill pattern horizontal honeycomb and lateral rectilinear, layer size of 0.4 and 0.2 mm, respectively, and both with a fill density of 60%. The resultant average pore sizes are 471±19 and 487±36 μm, respectively.

Using the data of the scaffold printed with orientation lateral and fill pattern rectilinear, a digital geometry with the same orientation and fill pattern, layer size of 0.2 mm and pore size 487±36 μm was created in order to simulate fluid flow in a small sample of the complete scaffold geometry. Figure 1 presents photographs of this scaffold. The digital geometry of the test scaffold has twelve layers of depth, due to this is the maximum resultant number of layers depth of the printed scaffold of the human auricular cartilage at its thickest point. Its dimensions are height 4.925 mm, width 5.225 mm and length 2.675 mm. The geometry was drawn using the design program Rhinoceros²⁹ joint with the plugin Intralattice³⁰, which allows generating solid lattice structures by an algorithm. Figure 2 presents the geometry achieved with has layer size of 0.2 mm and pore size of 483.379 μm.

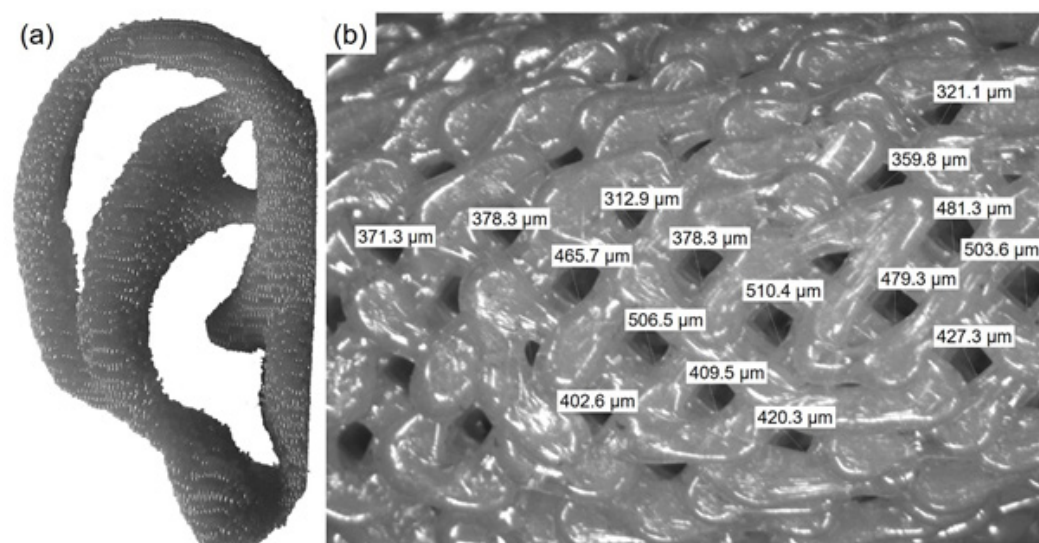


Figure 1 – Test scaffold printed with PLA using FDM fill pattern rectilinear, orientation lateral, layer size of 0.2 mm and pore size 487±36 μm, (a) complete and (b) zoom⁶.

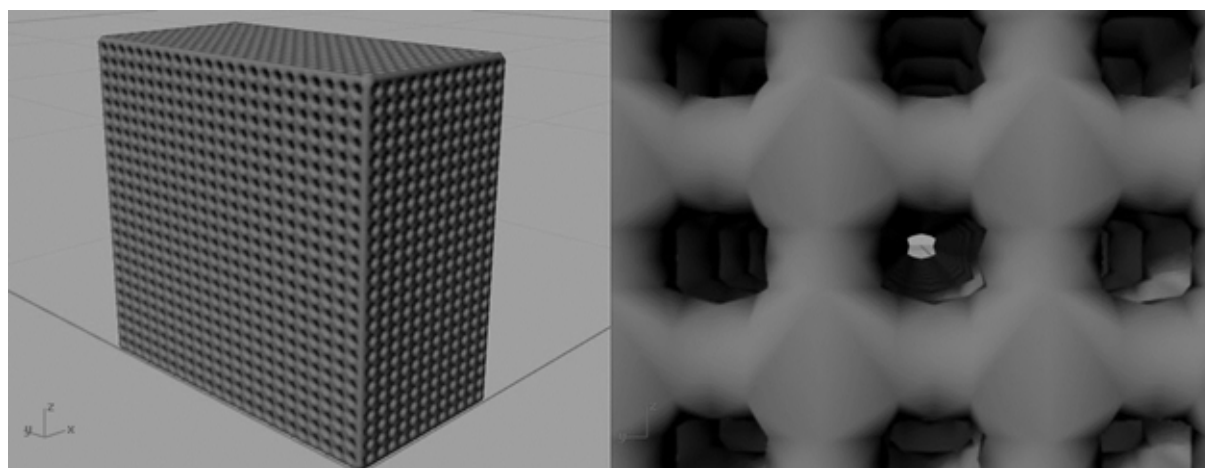


Figure 2 – Scaffold created to perform computational fluid dynamic tests (left) and detail of the fill pattern (right).

Flow simulation by lattice-Boltzmann method Bhatnagar–Gross–Krook scheme

The evolution of particle distribution functions $f_i(\vec{x}, t, \vec{V})$ is specified by the Boltzmann equation, which is expressed as a function of the collision operator Ω :³¹

$$\frac{\partial f}{\partial t} + \vec{V} \cdot \nabla f = \Omega \quad (1)$$

The collision operator describes the interactions of particles on micro scale. Equation (1) is discretized by the directional particle velocities (\vec{e}_i) and in space and time ($c = \Delta x / \Delta t$), to obtain the lattice Boltzmann equation with the Bhatnagar–Gross–Krook (BGK) collision operator considering the dimensionless relaxation time related to mass transfer (τ_m)³¹,

$$f_i(\vec{x} + \vec{e}_i \Delta t, t + \Delta t) - f_i(\vec{x}, t) = -\frac{1}{\tau_m} [f_i(\vec{x}, t) - f_i^{eq}(\vec{x}, t)] \quad (2)$$

The equilibrium distribution function^{31,32}

$$f_i^{eq}(\vec{x}, t) = \rho w_i \left[1 + \frac{\vec{e}_i \cdot \vec{V}}{c_s^2} + \frac{(\vec{e}_i \cdot \vec{V})^2}{2c_s^4} - \frac{(\vec{V})^2}{2c_s^2} \right] \quad (3)$$

Where density is ρ , the macroscopic velocity is \vec{V} and the pseudo sound speed c_s , which is defined as $c_s = \sqrt{1/3c}$

The particle distribution function for advection and diffusion (g_i^{eq}) of a scalar field of temperature T is expressed as in function of dimensionless relaxation time related to heat transfer (τ_s)³²

$$g_i(\vec{x} + \vec{e}_i \Delta t, t + \Delta t) - g_i(\vec{x}, t) = -\frac{1}{\tau_s} [g_i(\vec{x}, t) - g_i^{eq}(\vec{x}, t)] \quad (4)$$

The linear form of the equilibrium distribution function for this case is³²

$$g_i^{eq}(\vec{x}, t) = T \cdot w_i \left[1 + \frac{\vec{e}_i \cdot \vec{V}}{c_s^2} \right] \quad (5)$$

For three-dimensional lattices with nineteen discrete velocities (D3Q19), the weight factors are $w_0=0$, $w_i=1/18$ for $i=1-6$, $w_i=1/36$ for $i=7-18$.³¹ The macroscopic density, velocity and temperature are calculated in each node of the lattice when is consider mass, momentum, and energy conservation, respectively³².

$$\sum_{i=0}^i f_i = \rho \quad (6)$$

$$\sum_{i=0}^i f_i \vec{e}_i = \rho \vec{V} \quad (7)$$

$$\sum_{i=0}^i g_i = T \quad (8)$$

The kinematic viscosity (ν) and thermal diffusivity (α) are expressed as a function of lattice units, respectively:³²

$$\nu = c_s^2 (\tau_m - 0.5) \frac{\Delta x^2}{\Delta t} \quad (9)$$

$$\alpha = c_s^2 (\tau_s - 0.5) \frac{\Delta x^2}{\Delta t} \quad (10)$$

The relation between kinematic viscosity and thermal diffusivity is known as Prandtl number (Pr).

Fluid flow in porous media

The Darcy flow transport model describes the fluid flow through a porous media. For Reynolds numbers lower than 10 the permeability is estimated by the volumetric flow rate (Q) and the pressure drop through the porous media (ΔP):^{13,33}

$$k = \frac{\mu}{\Delta P} L \left(\frac{Q}{A} \right) \quad (11)$$

Where μ is the dynamic viscosity, L and A are the thickness of the sample in the direction of the flow and the surface area of the scaffold to flow, respectively.

The Reynolds number is calculated based in:

$$R = \frac{\rho u_0 D_h}{\mu} = \frac{u_0 D_h}{\nu} \quad (12)$$

Where ρ is the fluid density, ν is the kinematic viscosity, D_h is the hydraulic diameter, and knowing that the velocity is $u_0 = Q/A$.

Cioffi *et al.*⁸ present an analytical equation to link permeability with average shear stress,

$$\bar{\tau} = \frac{\mu \cdot u_0}{\sqrt{k}} \quad (13)$$

Simulation conditions

The flow conditions were set to model a perfusion bioreactor and the respective domain of the simulation is shown in Figure 3, which are used to force culture medium through the pores of three-dimensional scaffolds. Perfusion bioreactors improve cartilage-like matrix synthesis for chondrocytes and chondrocyte growth³⁴. The flow simulations through test scaffold shown in Figure 2 were carried out by Palabos²⁶ using D3Q19 lattice model and BGK scheme because of the Reynolds numbers in perfusion bioreactor are low. A duct of rectangular section with walls with periodic boundary condition (in order to reduce the computational cost to model wall without friction) due to the wall effect can be considered negligible¹⁶, scaffold geometry with bounce-back boundary condition for no-slip condition, inlet flow with constant and uniform velocity in the x -axis, and outlet flow condition with constant pressure. The dimensions of the lattice N_x , N_y and N_z are 443, 80 y 77, respectively, for a total of 2.72888 million of elements.

Table 2 presents the parameters employed in the simulations. The values of viscosity and density of the culture medium were taken from Ferroni *et al.*²⁰, and the Prandtl number was set equal to the water. It was selected a group Reynolds numbers of low value and using these the corresponding inlet velocity for each case is estimated. In order to achieve these Reynolds numbers in the simulations and so that the solutions accomplish a convergence, the inlet velocity, the kinematic viscosity, and the velocity in lattice units are placed to achieve a value of dimensionless relaxation time close but not equal to 0.5. The resultant dimensionless relaxation time for each simulation results equal to 0.503570457 and 0.500522803 for flow and heat transfer, respectively.

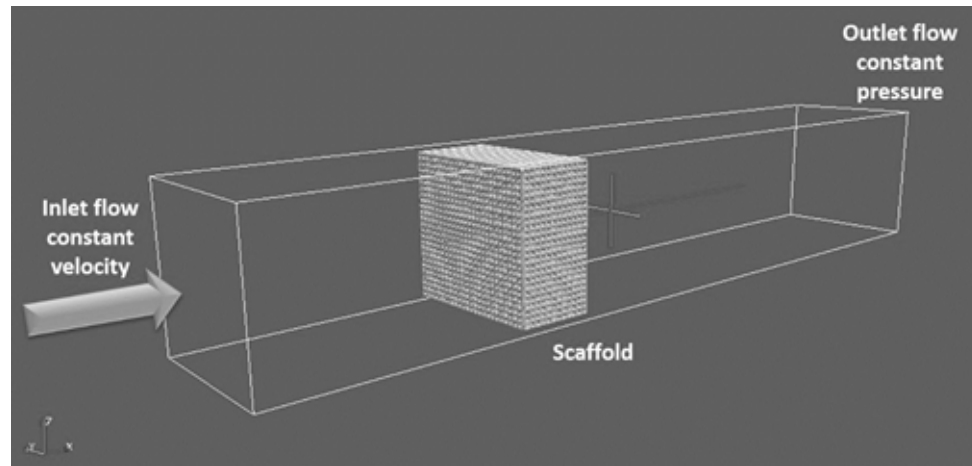


Figure 3 – Domain of the simulation.

D_h	hydraulic diameter of the scaffold	0.00437356112 m
μ	Viscosity of the culture medium	0.0012 g/(m·s)
ρ	Density of the culture medium	1029 kg/m ³
ν	Kinematic viscosity	1.17×10 ⁻⁶ m ² /s
Pr	Prandtl number	7

Table 2 – Values employed in the simulations.

Results and Discussion

The lattice Boltzmann method is highly parallelizable which allows using many cores of a central processing unit (CPU). In this case, using the entire cores of a desktop with a processor Intel® Core™ i5-7400 of RAM 8 GBytes each simulation achieved convergence for average energy lower than 10⁻⁶ of error at 8 h 15 min for isothermal cases (32292 iterations, 52.577 s of lattice time) and 20 h 21 min for flow and heat transfer cases (81480 iterations, 129.427 s of lattice time). During simulations, Palabos printed vti files every 2 s of lattice time which contain velocity, pressure and temperature field of the fluid flow in lattice units. Paraview was used

to obtain velocity, pressure, and shear stress in physical units. Figures 4 and 5 show the scaffold permeability and shear stress, respectively, as a function of Reynolds number. The shear stress ($\mu \times \nabla^2 V$) was calculated using the data obtained from each simulation. It is observed that at different Reynolds numbers the permeability values are close between them for $Re \leq 0.2$, and these are in the order of magnitude of bone and cartilage scaffolds compiled by Pennella et al. 13 Figure 5 shows that the shear stress values into the scaffold as a function of Reynolds number increase linearly described by Eq. (14),

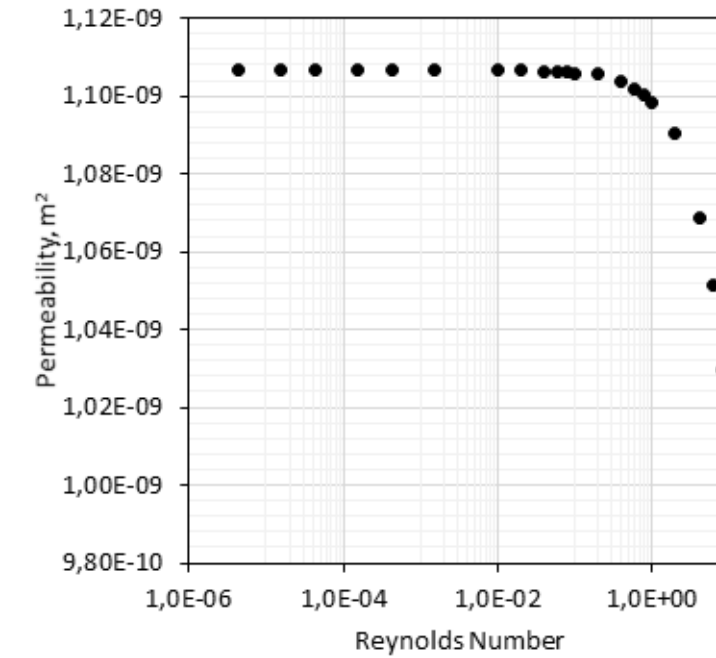


Figure 4 – Achieved scaffold permeability as a function of Reynolds number.

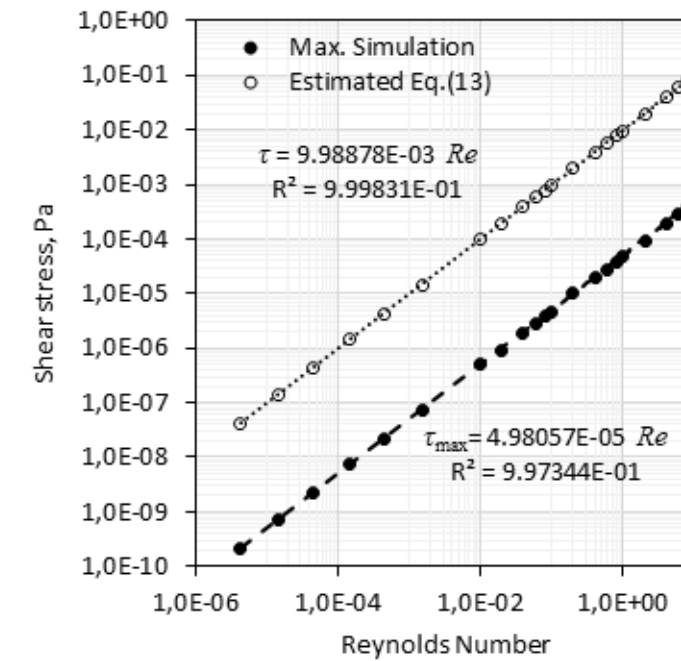


Figure 5 – Shear stress as a function of Reynolds number.

$$\tau_{\max} = 4.98057 \times 10^5 Re \quad (14)$$

which can be used to adjust the flow velocity or volumetric flow rate to a desired maximum shear stress. The values of average shear stress from Eq. (13) are higher than those ones obtained from simulation. Cioffi et al.⁸ reported a similar difference between the values calculated by numerical simulation and the estimated by Eq. (13). The values of shear stress obtained correspond to high percentage of cell viability according to values reported by Nair et al.²⁴ Figure 6 illustrates that the relation between the measured maximum shear stress and the permeability for the geometry presented herein achieves a linear function represented by Eq. (15). This relation only applies for this specific geometry in this range of permeability values.

$$\tau_{\max} = -5.06865 \times 10^6 k + 5.61111 \times 10^{-3} \quad (15)$$

The influence of the difference of the temperature between the culture medium and the scaffold in the permeability and maximum shear stress is evaluated varying the temperature of the scaffold wall from 20 to 40 degrees Celsius respect to the culture medium at 30 degrees Celsius (303.15

K). The maximum difference attained for permeability is 0.03871 percent and for shear stress is 0.03369 percent when the object wall is equal to 35 degrees Celsius. This indicate that the small variations in temperature that may occur in the bioreactor do not affect largely the conditions in the culture medium.

Figures 7 and 8 present pressure, velocity magnitude, and shear stress along (x-axis) in the middle and wide (z-axis) between the first two layers of the scaffold geometry, respectively, at $Re=4.374 \times 10^{-5}$. It is observed along x-axis that the velocity initially increases, and then slight falls of this when going through the scaffold, a characteristic pressure drop in flow through porous media, and that the shear stress is highest between the first two layers of the scaffold along x-axis direction. Figure 8 shows that the pressure varies between layers of the geometry in a regular way, however the velocity magnitude is larger in the center of the geometry in almost symmetrical distribution, and the shear stress present a non-regular distribution. Nevertheless, shear stress profiles in regular scaffolds obtained by Vossenberget al.16 and Hossain, Bergstrom, and Chen23 have regular distribution. This difference may be due in these two previous mentions works, flow field is simulated through small geometries of two and five layers along z-axis, respectively, and in the geometry present herein have twenty-four, representing a larger domain where the flow field could develop in other way.

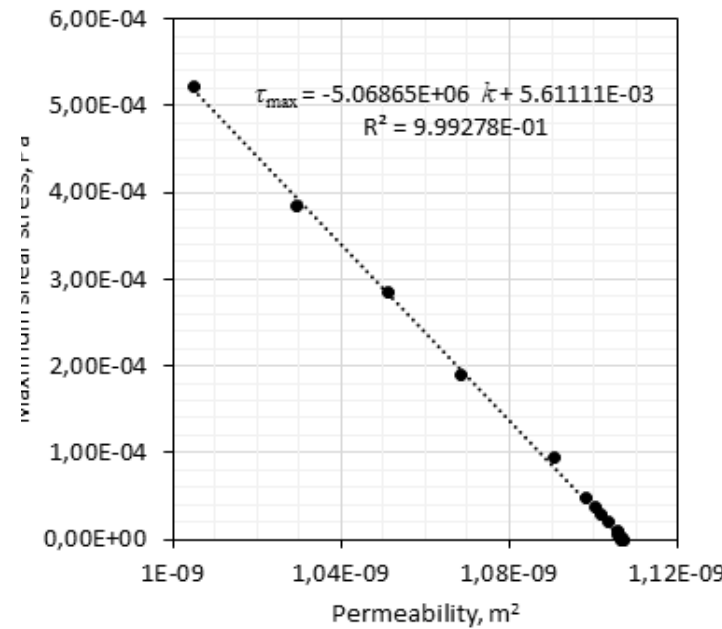


Figure 6 – Maximum shear stress as a function of scaffold permeability.

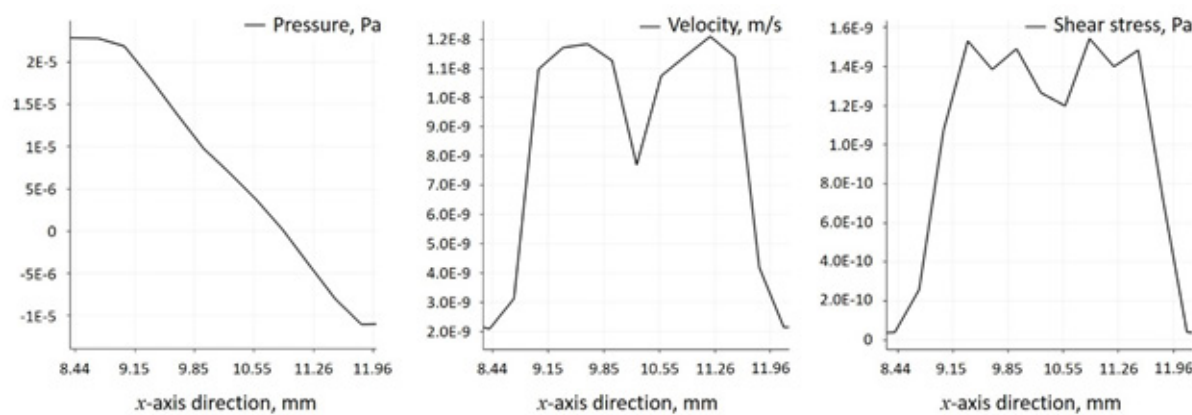


Figure 7 – Pressure, velocity magnitude, and shear stress in x-axis direction of the scaffold at Reynolds number equal to 4.374×10^{-5} .

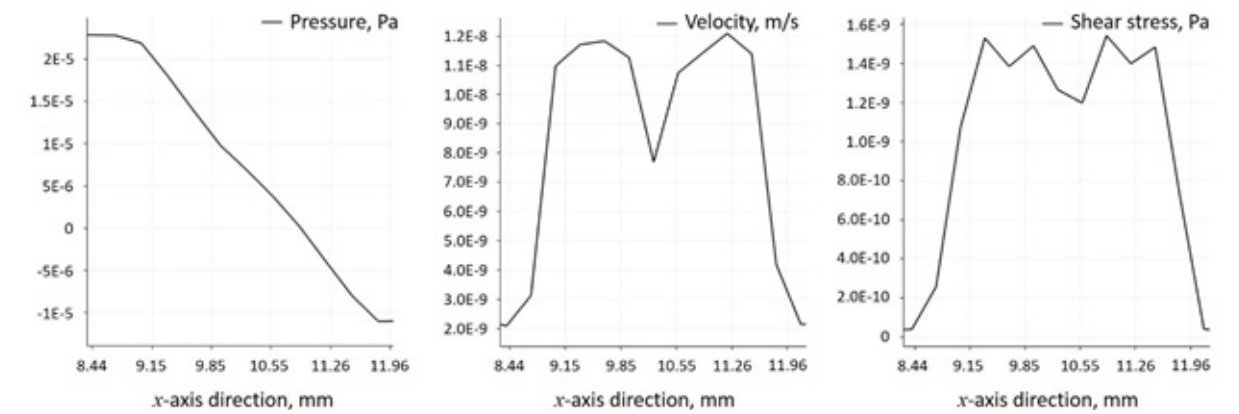


Figure 7 – Pressure, velocity magnitude, and shear stress in x-axis direction of the scaffold at Reynolds number equal to 4.374×10^{-5} .

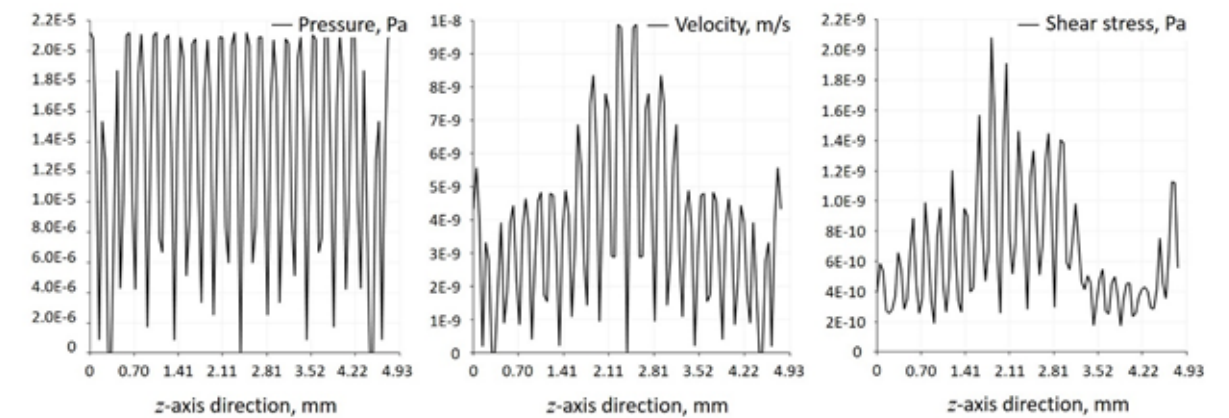


Figure 8 – Pressure, velocity magnitude, and shear stress in z-axis direction of the scaffold at Reynolds number equal to 4.374×10^{-5} .

Conclusions

The flow through a test piece based on the scaffold of the human auricular cartilage for microtia proposed for cell culture in a perfusion bioreactor was simulated using the Lattice Boltzmann method to evaluate the flow transport characteristics in a porous media. It was determined that the permeability of the scaffold is in the order of magnitude of scaffold used for cell culture, and the possible variations of temperature in the tissue chamber do not affect significantly permeability and shear stress values. Linear dependences between maximum shear stress and Reynolds number, and maximum shear stress and permeability, respectively, were found. The values of shear stress achieved correspond to high percentage of cell viability. Based on the results obtained, it can be concluded that the scaffolds for microtia treatment with the proposed filling pattern select is appropriate for cell culture in a perfusion bioreactor with characteristics similar to those described in this work.

Acknowledgements

Authors want to thank to Dean of Research and Development, Simon Bolivar University at Caracas, Venezuela for the financial support.

Conflict of interest statement
There is not conflict of interest.

References

- Brent B. What is microtia? Microtia-Atresia, <http://www.microtia.us.com/> (2011).
- Aase JM, Tegtmeier RE. Microtia in New Mexico: Evidence for multifactorial causation. *Birth Defects Orig Artic Ser* **13**: 113–6 (1977).

- Tanzer RC. Total Reconstruction of the External Ear. *Plast Reconstr Surg Transplant Bull* **23**: 1–15 (1959).
- Tanzer RC. Microtia—a Long-Term Follow-Up of 44 Reconstructed Auricles. *Plast Reconstr Surg* **61**: 161–166 (1978). <https://doi.org/10.1097/00006534-197802000-00001>.
- Brent B. Auricular Repair with Autogenous Rib Cartilage Grafts: Two Decades of Experience with 600 Cases. *Plast Reconstr Surg* **90**: 355–374 (1992).
- Berroterán MV. Implantes de Microtia Fabricados con Manufactura Aditiva Usando Polímeros Biocompatibles e Hidrogeles Moldeados. Master Thesis. Universidad Simón Bolívar (2015).
- Porter B, Zauel R, Stockman H, Guldberg, R, Fyhrie, D. 3-D computational modeling of media flow through scaffolds in a perfusion bioreactor. *J Biomech* **38**: 543–549 (2005). <https://doi.org/10.1016/j.jbiomech.2004.04.011>.
- Cioffi M, Boschetti F, Raimondi MT, Dubini, G. Modeling evaluation of the fluid-dynamic microenvironment in tissue-engineered constructs: A micro-CT based model. *Biotechnol Bioeng* **93**: 500–510 (2006). <https://doi.org/10.1002/bit.20740>.
- Cioffi M, Galbusera F, Raimondi MT, Dubini, G. Computational modelling of microfluidynamics in bioreactor-cultured cellular constructs. *J Biomech* **39**: S225 (2006). [https://doi.org/10.1016/S0021-9290\(06\)83831-5](https://doi.org/10.1016/S0021-9290(06)83831-5).

10. Zeiser T, Bashoor-Zadeh M, Darabi A, Baroud G. Pore-scale analysis of Newtonian flow in the explicit geometry of vertebral trabecular bones using lattice Boltzmann simulation. *Proc Inst Mech Eng Part H J Eng Med* **222**: 185–194 (2008). <https://doi.org/10.1243/09544119JEM261>.
11. Voronov R, VanGordon S, Sikavitsas VI, Papavassiliou, DV. Computational modeling of flow-induced shear stresses within 3D salt-leached porous scaffolds imaged via micro-CT. *J Biomech* **43**: 1279–1286 (2010). <https://doi.org/10.1016/j.jbiomech.2010.01.007>.
12. Pennella F, Cerino G, Massai D, Gallo D, Falvo D'Urso Labate G, Schiavi A, Deriu, MA, Audenino, A, and Morbiducci, UA. A Survey of Methods for the Evaluation of Tissue Engineering Scaffold Permeability. *Ann Biomed Eng* **41**: 2027–2041 (2013). <https://doi.org/10.1007/s10439-013-0815-5>.
13. Pennella F, Gentile P, Deriu MA, Gallo, D, Schiavi, A, Ciardelli, G, Lorenz, E, Hoekstra, AG, Audenino, A, and Morbiducci, U. A Virtual Test Bench to Study Transport Phenomena in 3D Porous Scaffolds Using Lattice Boltzmann Simulations. SBC2013–14489. In: *ASME 2013 Summer Bioengineering Conference*, Sunriver, Oregon, p. V01AT07A020 (2013). <https://doi.org/10.1115/SBC2013-14489>.
14. Alam TA, Pham QL, Sikavitsas VI, Papavassiliou D V., Shambaugh RL, Voronov RS. Image-based modeling: A novel tool for realistic simulations of artificial bone cultures. *Technology* **04**: 229–233 (2016). <https://doi.org/10.1142/S233954781620003X>.
15. Boschetti F, Raimondi MT, Migliavacca F, Dubini, G. Prediction of the micro-fluid dynamic environment imposed to three-dimensional engineered cell systems in bioreactors. *J Biomech* 2006; 39: 418–425.
16. Vossenbergh, P, Higuera, GA, van Straten, G, van Blitterswijk, CA, van Bortel, AJB. Darcian permeability constant as indicator for shear stresses in regular scaffold systems for tissue engineering. *Biomech Model Mechanobiol* **8**: 499–507 (2009). <https://doi.org/10.1007/s10237-009-0153-6>.
17. Ali D, Ozalp M, Blanquer S, Onel, S. Permeability and fluid flow-induced wall shear stress in bone scaffolds with TPMS and lattice architectures: A CFD analysis. *Eur J Mech - B/Fluids* **79**: 376–385 (2020). <https://doi.org/10.1016/j.euromechflu.2019.09.015>
18. Malvè M, Bergstrom DJ, Chen XB. Modeling the flow and mass transport in a mechanically stimulated parametric porous scaffold under fluid-structure interaction approach. *Int Commun Heat Mass Transf* **96**: 53–60 (2018). <https://doi.org/10.1016/j.icheatmass-transfer.2018.05.014>
19. Hossain MS, Chen XB, Bergstrom DJ. Fluid flow and mass transfer over circular strands using the lattice Boltzmann method. *Heat Mass Transf* **51**: 1493–1504 (2015). <https://doi.org/10.1007/s00231-015-1514-6>.
20. Ferroni M, Giusti S, Nascimento D, Silva A, Boschetti F, Ahluwalia A. Modeling the fluid-dynamics and oxygen consumption in a porous scaffold stimulated by cyclic squeeze pressure. *Med Eng Phys* **38**: 725–732 (2016). <https://doi.org/10.1016/j.medengphy.2016.04.016>.
21. Croughan MS, Wang DIC. Hydrodynamic Effects on Animal Cells in Microcarrier Bioreactors. *Biotechnology* **17**:213–49 (1991).
22. Liu J, Bi X, Chen T, Zhang, Q, Wang, SX, Chiu, JJ, Liu, GS, Zhang, Y, Bu, P, Jiang, F. Shear stress regulates endothelial cell autophagy via redox regulation and Sirt1 expression. *Cell Death Dis* **6**: e1827–e1827 (2015). <http://dx.doi.org/10.1038/cddis.2015.193>
23. Hossain MS, Bergstrom DJ, Chen XB. A mathematical model and computational framework for three-dimensional chondrocyte cell growth in a porous tissue scaffold placed inside a bi-directional flow perfusion bioreactor. *Biotechnol Bioeng* **112**: 2601–2610 (2015). <http://dx.doi.org/10.1016/j.btre.2014.12.002>.
24. Nair K, Gandhi M, Khalil S, Chang Yan, K, Marcolongo, M, Barbee, K. Characterization of cell viability during bioprinting processes. *Biotechnol J*; 4: 1168–1177 (2009). <https://doi.org/10.1002/biot.200900004>.
25. Schuerlein S, Schwarz T, Krzimirski S, Gätzner, S, Hoppensack, A, Schwedhelm, I, Schweinlin, M, Walles, H, Hansmann, J. A versatile modular bioreactor platform for Tissue Engineering. *Biotechnol J* **12**: 1600326 (2017). <https://dx.doi.org/10.1002%2Fbiot.201600326>.
26. FlowKit Ltd. *Palabos, CFD, complex physics*. <http://www.palabos.org/index.php> (2012). [accessed 16 October 2017].
27. Wu L, Zhang H, Zhang J, Ding, J. Fabrication of Three-Dimensional Porous Scaffolds of Complicated Shape for Tissue Engineering. I. Compression Molding Based on Flexible-Rigid Combined Mold. *Tissue Eng* **11**: 1105–1114 (2005). <https://doi.org/10.1089/ten.2005.11.1105>.
28. Sobral JM, Caridade SG, Sousa RA, Mano, J, Reis, R. Three-dimensional plotted scaffolds with controlled pore size gradients: Effect of scaffold geometry on mechanical performance and cell seeding efficiency. *Acta Biomater* **7**: 1009–1018 (2011). <https://doi.org/10.1016/j.actbio.2010.11.003>.
29. Robert McNeel & Associates. *Rhinoceros, modeling tool for designers*, Software Package, Ver. 5 SR14 64-bit (5.14.522.8390, 22/5/2017). Seattle, WA (2017).
30. Kurtz A. *Intralattice, Generative Lattice Design with Grasshopper*. McGill's Additive Design & Manufacturing Laboratory (ADML). <http://intralattice.com/> (2018) [accessed 26 October 2017].
31. Liu Z, Wu H. Pore-scale modeling of immiscible two-phase flow in complex porous media. *Appl Therm Eng* **93**: 1394–1402 (2016). <https://doi.org/10.1016/j.applthermaleng.2015.08.099>.
32. Parmigiani A. Lattice Boltzmann calculations of reactive multiphase flows in porous media. Doctoral Thesis. Université de Genève. (2011).
33. Bear J. *Dynamics of Fluids in Porous Media*. Dover, New York, pp 133 (1972).
34. Salehi-Nik N, Amoabediny G, Pouran B, Tabesh, H, Shokrgozar, MA, Haghighipour, N, Khatibi, N, Anisi, F, Mottaghy, K, Zandieh-Doulabi, B. Engineering Parameters in Bioreactor's Design: A Critical Aspect in Tissue Engineering. *Biomed Res Int* **2013**: 1–15 (2013). <http://dx.doi.org/10.1155/2013/762132>.



Fluid flow in a Porous Scaffold for Microtia by Lattice Boltzmann Method

Pedro J. Boschetti^{1*}; Orlando Pelliccioni^{2,3}; Mariángel Berroterán³; María V. Candal^{2,3}; Marcos A. Sabino⁴

*Corresponding author: E-mail address: pboschetti@usb.ve

Abstract: The birth deformity of ear, known as microtia, varies from a minimal deformed ear to the absence of auricular tissue or anotia. This malformation has been treated by reconstructing the external ear, mainly by autogenous rib cartilage in auricular repair. The fabrication of the ear framework is a prolonged reconstructive procedure and depends of the surgeon's skill. In order to avoid these inconveniences and reduce surgery time, it was proposed in a previous work to use implants made with biocompatible materials. One of these is a scaffold made by fused deposition modeling using PLA based in the three-dimensional geometry of the ear cartilage. The aim of this work is to evaluate the feasibility of this scaffold to perform cell culture in a perfusion biorreactor by estimating the flow transport characteristics in porous media using a scaffold with the porous geometry of the human auricular cartilage for microtia. Flow and heat transfer through the scaffold were simulated by the lattice Boltzmann method, and permeability and shear stress distribution were obtained at different Reynolds numbers. The permeability values of the scaffold achieved are in the order of magnitude of scaffolds used for cell culture. Linear dependencies between maximum shear stress and Reynolds number, and between maximum shear stress and permeability were obtained. The values of shear stress achieved correspond to high percentage of cell viability. The scaffolds for microtia treatment with the proposed filling pattern select is appropriate for cell culture in a perfusion bioreactor with characteristics similar to those described herein.

Keywords: Microtia treatment; Lattice Boltzmann method; Perfusion biorreactor; Scaffold; Shear stress in porous media.

Introduction

The birth deformity of ear is known as microtia, which varies from a minimal deformed ear, known as grade 1, to the absence of auricular tissue or anotia.¹ The more frequent cases of microtia are grade 3 and these look "like a little sausage-shaped Wrinkle of skin"¹. Microtia grade 2 looks like a miniature ear¹. This malformation occurs once in every 6,000 births, 2 only one side is involved in 90 percent of the cases, and 63.1 percent of the patients are males and the other 36.9 percent are females².

This malformation has been treated by reconstructing the external ear. In 1959, Tanzer made a successful reconstruction employing an autogenous rib cartilage as framework³. The use of autogenous rib cartilage in auricular repair has been used since that date and the results in a long term had reported^{4,5}. The fabrication of the ear framework is a prolonged reconstructive procedure and depends of the surgeon's skill. In order to avoid these inconveniences and reduce surgery time, Berroterán⁶ proposed to use implants made with biocompatible materials to treat microtia. One of these is a scaffold made by fused deposition modeling (FDM) using polylactic acid (PLA) based in the three-dimensional geometry of the ear cartilage.⁶ This must have the appropriate conditions to develop a cell culture.

The objective of the present research is to evaluate the feasibility of a scaffold proposed in a previous work to perform cell culture in a biorreactor by estimating the flow transport characteristics in porous media using a scaffold with the porous geometry of the human auricular cartilage for microtia. The micro-fluid dynamics through a scaffold is simulated by three-dimensional lattice Boltzmann method. The characteristic properties in porous media are the Darcy permeability and the shear stress distribution, because the feasibility of a specific scaffold to perform in vitro cell culture could be set knowing these characteristic properties.

One of the scopes of previous research works is to evaluate charac-

teristic properties of fluid flow in porous media of the employed scaffold by computational fluid dynamics. Some of these works simulated flow in a geometry of the employed scaffold obtained by microtomography,⁷⁻¹³ and when the geometry of the scaffold is built by three-dimensional printing, the model used in the simulations is draw using of the same parameters of the printing.¹⁴⁻¹⁶ For this application the flow field has been modeled by the finite volume method,^{8,9,14,17} the finite element method,^{15,16,18} and the lattice Boltzmann method^{7,8,10-13,19} with results similar to experimental data, however not precise to these. Pennella *et al.*¹³ explain some causes of the difference between the permeability values obtained experimentally and those calculated by computational fluid dynamic among which are the reconstructed scaffold volumes are in different orders of magnitude than the experimental samples and the resolution of the microtomography images used to reconstruct the three-dimensional models is not adequate. These previous publications differ in the way that they model the flow through the porous media and in the characteristic properties due to the specific objectives of each research. For example, Ferroni *et al.*²⁰ in addition to simulate flow through the porous scaffold, they also studied the oxygen consumption in this, and Alam *et al.*¹⁴ present a tool to simulate cell growth in bone tissue. Table 1 shows details about each referenced work.

The shear stress produced by the flow at the internal walls of the scaffold has been studied due to shear stress is an important regulator in cell function⁷. Croughan and Wang²¹ describe the shear stress effects on metabolism of living animal cells in bioreactors, and Liu, *et al.*²² demonstrated that shear stress induced by laminar flow can promote autophagy in vascular endothelial cells. According to its magnitude, shear stress could have a beneficial effect on cell growth²³, can damage cells²⁴ or prevents attachment of the cells to the scaffold^{15,16}. Computational fluid dynamics have been employed to obtain shear stress values in scaffolds concluding that shear stress is a function of the porous geometry and flow regime¹⁵,

¹ Departamento Tecnología Industrial, Universidad Simón Bolívar, Camurí Grande Valley, Naiguatá, 1160, Venezuela.

² Departamento de Mecánica, Universidad Simón Bolívar. AP 89000, Caracas, Venezuela.

³ Grupo de Biomecánica, Universidad Simón Bolívar. AP 89000, Caracas, Venezuela.

⁴ Grupo B5IDA, Departamento de Química, Universidad Simón Bolívar. AP 89000, Caracas, Venezuela.

Reference	Method	Details about method	Flow conditions	Porous geometry
Porter et al. (2005)7	Lattice Boltzmann method	Lattice Boltzmann method, BGK, D3Q15 lattice	$0.15 < Re < 0.9$, Darcy flow	Porous scaffolds imaged via micro-CT of human trabecular bone
Boschetti et al. (2006)15	Finite element method	FIDAP (Fluent Inc) for finite element method	Velocity=689, 338, 163, and 105 mm/s Density=1000 kg/m ³ Viscosity=8.2×10 ⁴ kg/(m·s) Re=3.97 and 5.37×10 ³	Microporous polymeric scaffold (Degrapol®) by micro-computed tomography
Cioffi et al. (2006a)8	Finite element method	Fluent for finite volume method	Velocity=0.000053 m/s, Density=1000 kg/m ³ , Viscosity=8.1×10 ⁴ Pa s, Re= 3.42×10 ⁴ , 3.71×10 ⁴ , and 3.70×10 ⁴	Microporous polymeric scaffold (Degrapol®) by micro-computed tomography
Cioffi et al. (2006b)8	Finite volume method and lattice Boltzmann method	Fluent for finite volume method and Lattice Boltzmann method	Volumetric flow rate=0.5 cm ³ /min through a 15 mm diameter scaffold	Microporous polymeric scaffold (Degrapol®) by micro-computed tomography
Zeiser et al. (2008)10 and a lattice Boltzmann method (LBM)	Lattice Boltzmann method	Lattice Boltzmann method, BGK, D3Q19 lattice	Velocity=1 mm/s Density=1200 kg/m ³ , Viscosity=500 to 2000 Pa s, Re=10 ⁻⁶ for vertebroplasty application Characteristic length of the trabecular bone=1 mm,	Pore-scale structure by segment X-ray microcomputed tomography of bone
Vossenberget al. (2009)16	Finite element method	COMSOL Multiphysics 3.3	Re=7.5×10 ⁻³	Printed regular scaffolds with fiber radius equal to 75 μm
Voronov et al. (2010)11	Lattice Boltzmann method	Lattice Boltzmann method, BGK, D3Q15 lattice	Velocity=0.0044 cm/s	Porous scaffolds imaged via micro-CT of a salt grain
Pennella et al. (2013)13	Lattice Boltzmann method	Palabos for lattice Boltzmann method, BGK, D3Q19 lattice,	Re≪1	Porous scaffolds imaged via micro-CT
Alam et al. (2016)14	lattice Boltzmann method	Lattice Boltzmann method, BGK, D3Q15 lattice	No show	Porous scaffolds imaged via micro-CT
Ferroni et al. (2016)20	Finite element method	Comsol Multiphysics 4.3b for two-dimensional and three-dimensional flow simulations	Density=1029 kg/m ³ , Viscosity=0.0012 kg/(m·s), Re=2×10 ⁵	Idealized geometry – printed scaffolds
Malvè et al (2018)18	Finite element method	Adina R&D	Density=1000 kg/m ³ , Viscosity=0.00001 kg/(m·s)	Idealized geometry – printed scaffolds
Ali et al. (2020)17	Finite volume method	Ansys Fluent software	Velocity=0.1 mm/s, Density=1000 kg/m ³ , Viscosity=0.0037 kg/(m·s)	Eight idealized geometries – printed scaffolds

Table 1 – Computational fluid dynamic methods, flow conditions, and porous geometry employed in each referenced work.

and more specific of the Darcy permeability coefficient¹⁶.

Generally, cell cultures are performed at constant temperature around 37 degrees Celsius, the initial conditions are at room temperature (around 21 degrees Celsius). Schuerlein *et al.*²⁵ report a variation of temperature in the medium in tissue chamber from initially 21 to 36 degrees Celsius within 60 min in a perfusion bioreactor. These temperature variations could change the flow properties in the scaffold and are studied herein.

The lattice Boltzmann method has been very useful to solve flow in porous media because of it avoids to create an intricate mesh in this media, required by other computational fluid dynamic methods, besides this method allows multi-physics applications like flow and heat transfer. In this case, the open access code Palabos²⁶, based in this method, is chosen to perform the simulations. This code is capable of modeling three-dimensional, unsteady, low Reynolds flow.

**Methodology
Geometry employed**

Berrotoran6 built six different samples of scaffolds with the geometry of the human auricular cartilage by fused deposition modeling (FDM) using a thread of polylactic acid (PLA) fibers. These samples differ in orientation (horizontal, vertical, and lateral), fill pattern (honeycomb, line, and rectilinear), layer thickness, and fill density. To print these scaffolds was used

FDM machine brand RepRapBCN®, Esun 3D filament PLA as building material (Esun 3D filament PVA as support material). Two of these scaffolds were selected and reported an average pore size between 200 and 500 μm, which is considered appropriate for the adequate cellular proliferation in the scaffold according to Wu *et al.*²⁷ and Sobral *et al.*²⁸ These two scaffolds were printed with orientation and fill pattern horizontal honeycomb and lateral rectilinear, layer size of 0.4 and 0.2 mm, respectively, and both with a fill density of 60%. The resultant average pore sizes are 471±19 and 487±36 μm, respectively.

Using the data of the scaffold printed with orientation lateral and fill pattern rectilinear, a digital geometry with the same orientation and fill pattern, layer size of 0.2 mm and pore size 487±36 μm was created in order to simulate fluid flow in a small sample of the complete scaffold geometry. Figure 1 presents photographs of this scaffold. The digital geometry of the test scaffold has twelve layers of depth, due to this is the maximum resultant number of layers depth of the printed scaffold of the human auricular cartilage at its thickest point. Its dimensions are height 4.925 mm, width 5.225 mm and length 2.675 mm. The geometry was drawn using the design program Rhinoceros²⁹ joint with the plugin Intralattice³⁰, which allows generating solid lattice structures by an algorithm. Figure 2 presents the geometry achieved with has layer size of 0.2 mm and pore size of 483.379μm.

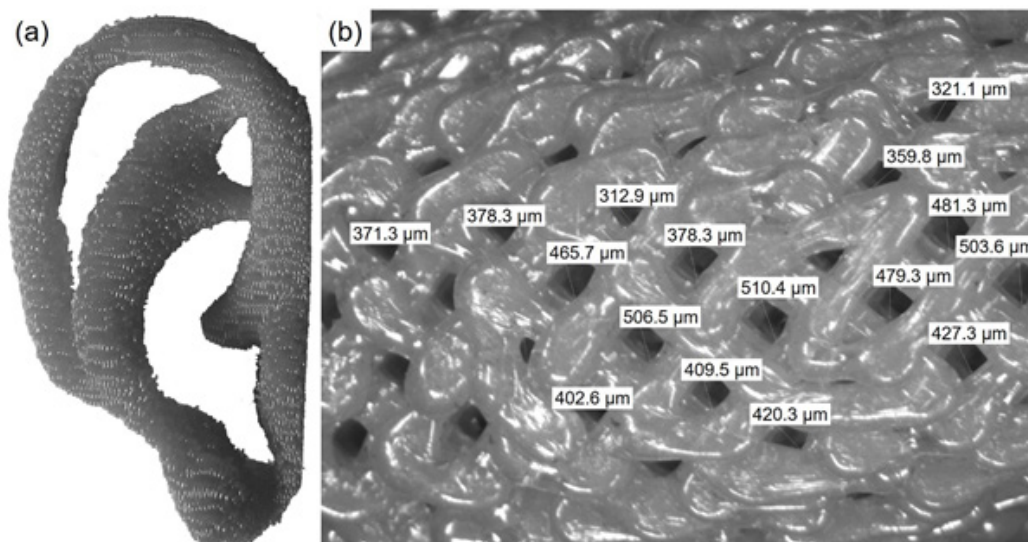


Figure 1 – Test scaffold printed with PLA using FDM fill pattern rectilinear, orientation lateral, layer size of 0.2 mm and pore size 487±36 μm, (a) complete and (b) zoom⁶.

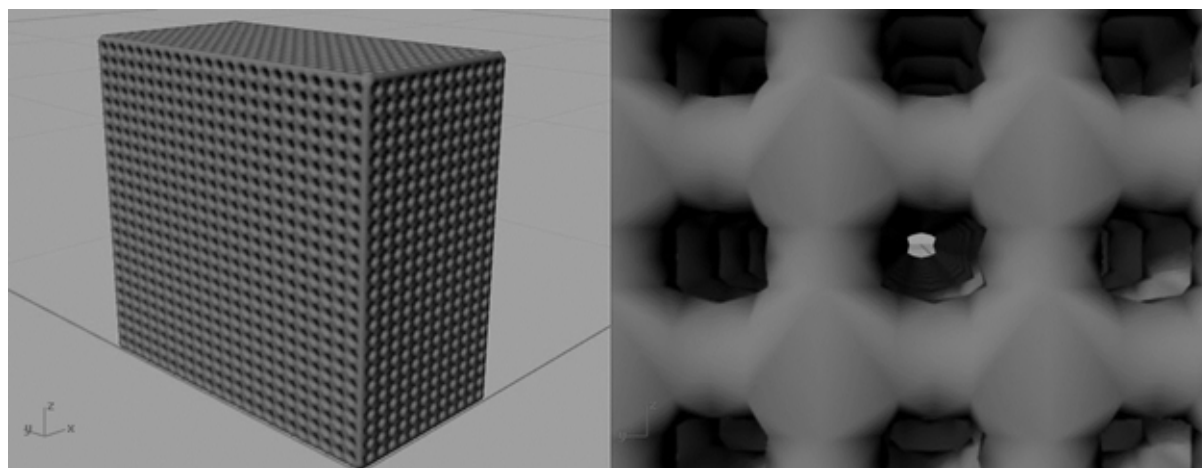


Figure 2 – Scaffold created to perform computational fluid dynamic tests (left) and detail of the fill pattern (right).

Flow simulation by lattice-Boltzmann method Bhatnagar-Gross-Krook scheme

The evolution of particle distribution functions $f_i(\vec{x}, t, \vec{V})$ is specified by the Boltzmann equation, which is expressed as a function of the collision operator Ω :³¹

$$\frac{\partial f}{\partial t} + \vec{V} \cdot \nabla f = \Omega \tag{1}$$

The collision operator describes the interactions of particles on micro scale. Equation (1) is discretized by the direction of particle velocities (\vec{e}_i) and in space and time ($c = \Delta x / \Delta t$), to obtain the lattice Boltzmann equation with the Bhatnagar-Gross-Krook (BGK) collision operator considering the dimensionless relaxation time related to mass transfer (τ_m)³¹,

$$f_i(\vec{x} + \vec{e}_i \Delta t, t + \Delta t) - f_i(\vec{x}, t) = -\frac{1}{\tau_m} [f_i(\vec{x}, t) - f_i^{eq}(\vec{x}, t)] \tag{2}$$

The equilibrium distribution function^{31,32}

$$f_i^{eq}(\vec{x}, t) = \rho w_i \left[1 + \frac{\vec{e}_i \cdot \vec{V}}{c_s^2} + \frac{(\vec{e}_i \cdot \vec{V})^2}{2c_s^4} - \frac{(\vec{V})^2}{2c_s^2} \right] \tag{3}$$

Where density is ρ , the macroscopic velocity is \vec{V} and the pseudo sound speed c_s , which is defined as $c_s = \sqrt{1/3c}$

The particle distribution function for advection and diffusion (g_i^{eq}) of a scalar field of temperature T is expressed as in function of dimensionless relaxation time related to heat transfer (τ_h)³²

$$g_i(\vec{x} + \vec{e}_i \Delta t, t + \Delta t) - g_i(\vec{x}, t) = -\frac{1}{\tau_h} [g_i(\vec{x}, t) - g_i^{eq}(\vec{x}, t)] \tag{4}$$

The linear form of the equilibrium distribution function for this case is³²

$$g_i^{eq}(\vec{x}, t) = T \cdot w_i \left[1 + \frac{\vec{e}_i \cdot \vec{V}}{c_s^2} \right] \tag{5}$$

For three-dimensional lattices with nineteen discrete velocities (D3Q19), the weight factors are $w_0=0$, $w_i=1/18$ for $i=1-6$, $w_i=1/36$ for $i=7-18$.³¹ The macroscopic density, velocity and temperature are calculated in each node of the lattice when is consider mass, momentum, and energy conservation, respectively³².

$$\sum_{i=0}^i f_i = \rho \tag{6}$$

$$\sum_{i=0}^i f_i \vec{e}_i = \rho \vec{V} \tag{7}$$

$$\sum_{i=0}^i g_i = T \tag{8}$$

The kinematic viscosity (μ) and thermal diffusivity (α) are expressed as a function of lattice units, respectively:³²

$$\nu = c_s^2 (\tau_m - 0.5) \frac{\Delta x^2}{\Delta t} \tag{9}$$

$$\alpha = c_s^2 (\tau_h - 0.5) \frac{\Delta x^2}{\Delta t} \tag{10}$$

The relation between kinematic viscosity and thermal diffusivity is

known as Prandtl number (Pr).

Fluid flow in porous media

The Darcy flow transport model describes the fluid flow through a porous media. For Reynolds numbers lower than 10 the permeability is estimated by the volumetric flow rate (Q) and the pressure drop through the porous media (ΔP):^{13,33}

$$k = \frac{\mu}{\Delta P} L \left(\frac{Q}{A} \right) \tag{11}$$

Where μ is the dynamic viscosity, L and A are the thickness of the sample in the direction of the flow and the surface area of the scaffold to flow, respectively.

The Reynolds number is calculated based in:

$$R = \frac{\rho u_0 D_h}{\mu} = \frac{u_0 D_h}{\nu} \tag{12}$$

Where ρ is the fluid density, ν is the kinematic viscosity, D_h is the hydraulic diameter, and knowing that the velocity is $u_0=Q/A$.

Cioffi *et al.*⁸ present an analytical equation to link permeability with average shear stress,

$$\bar{\tau} = \frac{\mu \cdot u_0}{\sqrt{k}} \tag{13}$$

Simulation conditions

The flow conditions were set to model a perfusion bioreactor and the respective domain of the simulation is shown in Figure 3, which are used to force culture medium through the pores of three-dimensional scaffolds. Perfusion bioreactors improve cartilage-like matrix synthesis for chondrocytes and chondrocyte growth³⁴. The flow simulations through test scaffold shown in Figure 2 were carried out by Palabos²⁶ using D3Q19 lattice model and BGK scheme because of the Reynolds numbers in perfusion bioreactor are low. A duct of rectangular section with walls with periodic boundary condition (in order to reduce the computational cost to model wall without friction) due to the wall effect can be considered negligible¹⁶, scaffold geometry with bounce-back boundary condition for no-slip condition, inlet flow with constant and uniform velocity in the x -axis, and outlet flow condition with constant pressure. The dimensions of the lattice N_x , N_y and N_z are 443, 80 y 77, respectively, for a total of 2.72888 million of elements.

Table 2 presents the parameters employed in the simulations. The values of viscosity and density of the culture medium were taken from Ferroni *et al.*²⁰, and the Prandtl number was set equal to the water. It was selected a group Reynolds numbers of low value and using these the corresponding inlet velocity for each case is estimated. In order to achieve these Reynolds numbers in the simulations and so that the solutions accomplish a convergence, the inlet velocity, the kinematic viscosity, and the velocity in lattice units are placed to achieve a value of dimensionless relaxation time close but not equal to 0.5. The resultant dimensionless relaxation time for each simulation results equal to 0.503570457 and 0.500522803 for flow and heat transfer, respectively.

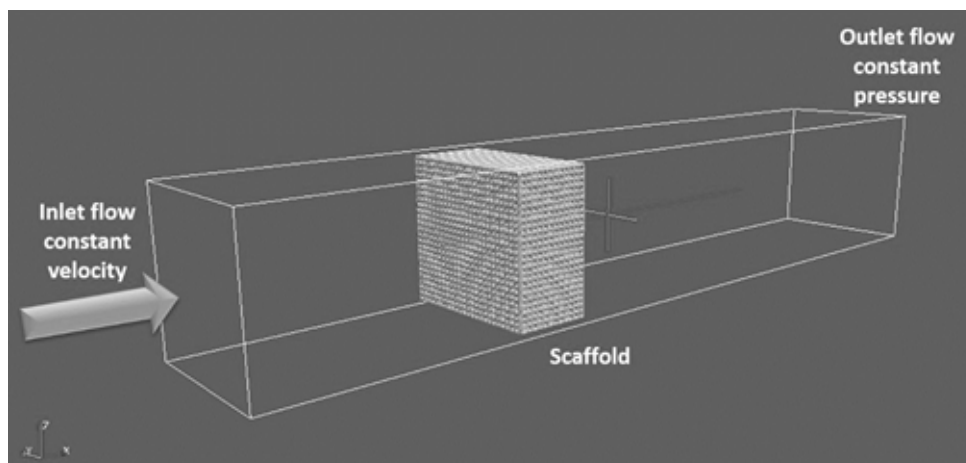


Figure 3 – Domain of the simulation.

Parameter	Description	Value
D_h	hydraulic diameter of the scaffold	0.00437356112 m
μ	Viscosity of the culture medium	0.0012 g/(m·s)
ρ	Density of the culture medium	1029 kg/m ³
ν	Kinematic viscosity	1.17×10 ⁻⁶ m ² /s
Pr	Prandtl number	7

Table 2 – Values employed in the simulations.

Results and Discussion

The lattice Boltzmann method is highly parallelizable which allows using many cores of a central processing unit (CPU). In this case, using the entire cores of a desktop with a processor Intel® Core™ i5–7400 of RAM 8 GBytes each simulation achieved convergence for average energy lower than 10⁻⁶ of error at 8 h 15 min for isothermal cases (32292 iterations, 52.577 s of lattice time) and 20 h 21 min for flow and heat transfer cases (81480 iterations, 129.427 s of lattice time). During simulations, Palabos printed vti files every 2 s of lattice time which contain velocity, pressure and temperature field of the fluid flow in lattice units. Paraview was used to obtain velocity, pressure, and shear stress in physical units.

Figures 4 and 5 show the scaffold permeability and shear stress, respectively, as a function of Reynolds number. The shear stress ($\mu \times \nabla \vec{V}$) was calculated using the data obtained from each simulation. It is observed that at different Reynolds numbers the permeability values are close between them for $Re \leq 0.2$, and these are in the order of magnitude of bone and cartilage scaffolds compiled by Pennella et al. 13 Figure 5 shows that the shear stress values into the scaffold as a function of Reynolds number increase linearly described by Eq. (14),

$$\tau_{max} = 4.98057 \times 10^5 Re \tag{14}$$

which can be used to adjust the flow velocity or volumetric flow rate to a desired maximum shear stress. The values of average shear stress

from Eq. (13) are higher than those ones obtained from simulation. Cioffi et al.⁸ reported a similar difference between the values calculated by numerical simulation and the estimated by Eq. (13). The values of shear stress obtained correspond to high percentage of cell viability according to values reported by Nair et al.²⁴ Figure 6 illustrates that the relation between the measured maximum shear stress and the permeability for the geometry presented herein achieves a linear function represented by Eq. (15). This relation only applies for this specific geometry in this range of permeability values.

$$\tau_{max} = -5.06865 \times 10^6 k + 5.61111 \times 10^{-3} \tag{15}$$

The influence of the difference of the temperature between the culture medium and the scaffold in the permeability and maximum shear stress is evaluated varying the temperature of the scaffold wall from 20 to 40 degrees Celsius respect to the culture medium at 30 degrees Celsius (303.15 K). The maximum difference attained for permeability is 0.03871 percent and for shear stress is 0.03369 percent when the object wall is equal to 35 degrees Celsius. This indicate that the small variations in temperature that may occur in the bioreactor do not affect largely the conditions in the culture medium.

Figures 7 and 8 present pressure, velocity magnitude, and shear stress along (x-axis) in the middle and wide (z-axis) between the first two layers

of the scaffold geometry, respectively, at $Re=4.374 \times 10^{-5}$. It is observed along x -axis that the velocity initially increases, and then slight falls of this when going through the scaffold, a characteristic pressure drop in flow through porous media, and that the shear stress is highest between the first two layers of the scaffold along x -axis direction. Figure 8 shows that the pressure varies between layers of the geometry in a regular way, however the velocity magnitude is larger in the center of the geometry in almost symmetrical distribution, and the shear stress present a non-regular distribution. Nevertheless, shear stress profiles in regular scaffolds

obtained by Vossenberget al.16 and Hossain, Bergstrom, and Chen23 have regular distribution. This difference may be due in these two previous mentions works, flow field is simulated through small geometries of two and five layers along z -axis, respectively, and in the geometry present herein have twenty-four, representing a larger domain where the flow field could develop in other way.

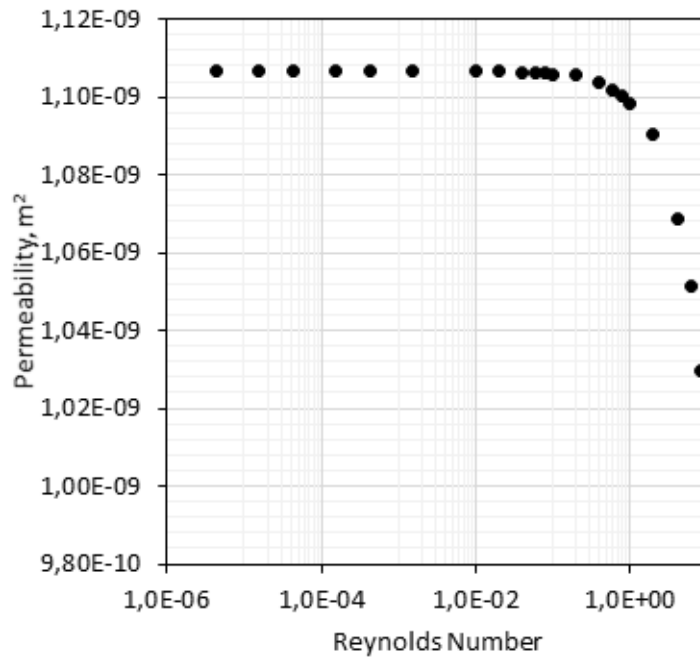


Figure 4 – Achieved scaffold permeability as a function of Reynolds number.

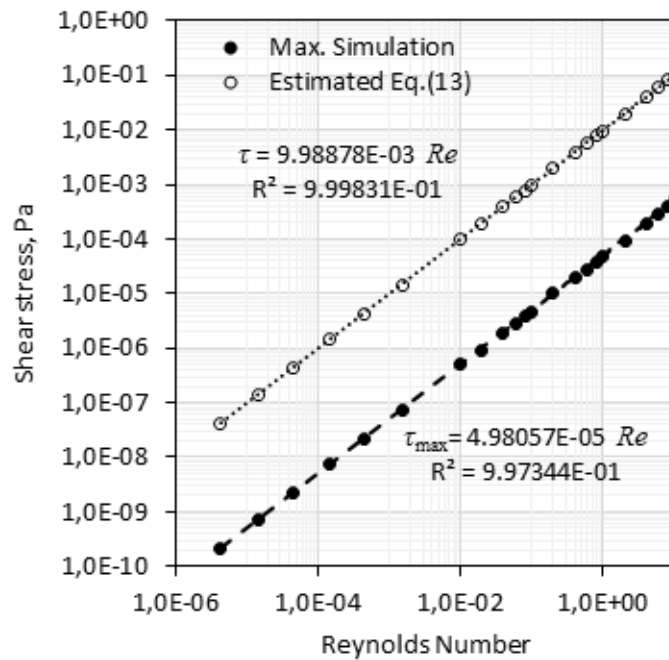


Figure 5 – Shear stress as a function of Reynolds number.

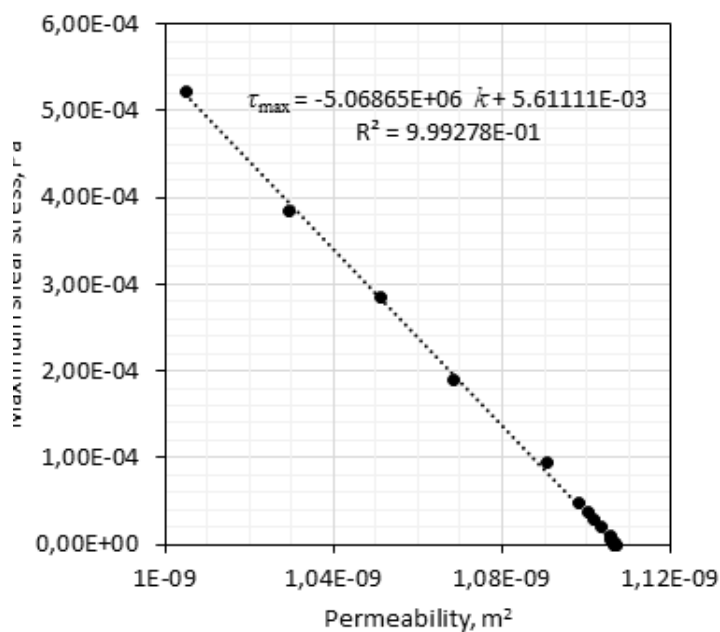


Figure 6 – Maximum shear stress as a function of scaffold permeability.

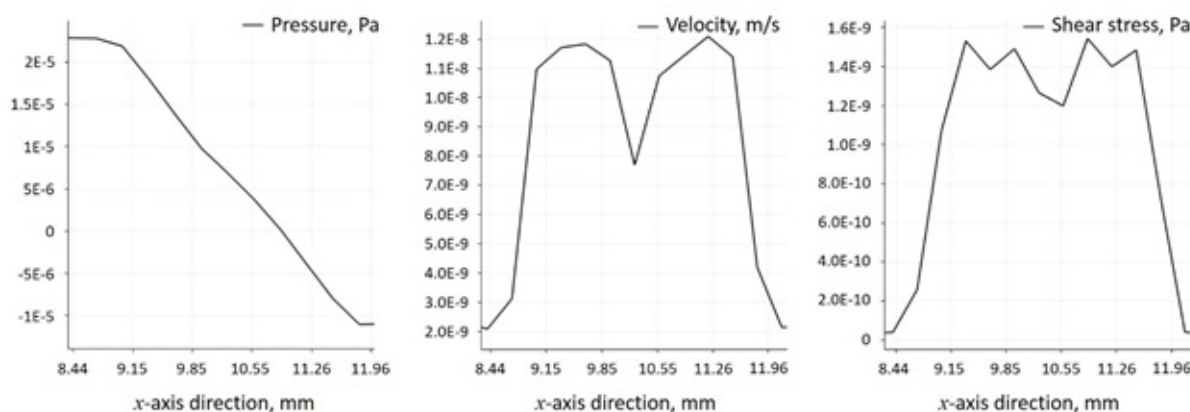


Figure 7 – Pressure, velocity magnitude, and shear stress in x-axis direction of the scaffold at Reynolds number equal to 4.374×10^{-5} .

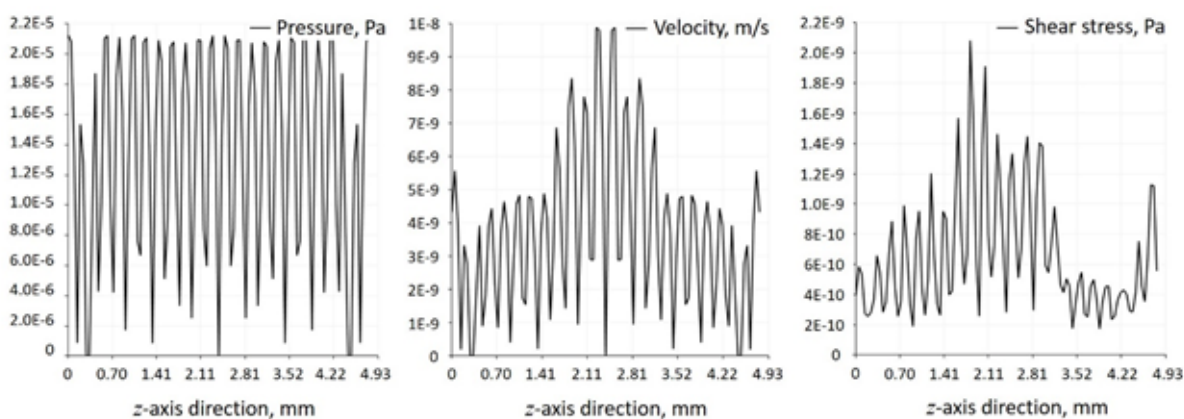


Figure 8 – Pressure, velocity magnitude, and shear stress in z-axis direction of the scaffold at Reynolds number equal to 4.374×10^{-5} .

Conclusions

The flow through a test piece based on the scaffold of the human auricular cartilage for microtia proposed for cell culture in a perfusion biorreactor was simulated using the Lattice Boltzmann method to evaluate the flow transport characteristics in a porous media. It was determined that the permeability of the scaffold is in the order of magnitude of scaffold used for cell culture, and the possible variations of temperature in the tissue chamber do not affect significantly permeability and shear stress values. Linear dependences between maximum shear stress and Reynolds number, and maximum shear stress and permeability, respectively, were found. The values of shear stress achieved correspond to high percentage of cell viability. Based on the results obtained, it can be concluded that the scaffolds for microtia treatment with the proposed filling pattern select is appropriate for cell culture in a perfusion bioreactor with characteristics similar to those described in this work.

Acknowledgements

Authors want to thank to Dean of Research and Development, Simon Bolívar University at Caracas, Venezuela for the financial support.

Conflict of interest statement

There is not conflict of interest.

References

- Brent B. What is microtia? Microtia-Atresia, <http://www.microtia.us.com/> (2011).
- Aase JM, Tegtmeier RE. Microtia in New Mexico: Evidence for multifactorial causation. *Birth Defects Orig Artic Ser* **13**: 113–6 (1977).
- Tanzer RC. Total Reconstruction of the External Ear. *Plast Reconstr Surg Transplant Bull* **23**: 1–15 (1959).
- Tanzer RC. Microtia—a Long-Term Follow-Up of 44 Reconstructed Auricles. *Plast Reconstr Surg* **61**: 161–166 (1978). <https://doi.org/10.1097/00006534-197802000-00001>.
- Brent B. Auricular Repair with Autogenous Rib Cartilage Grafts: Two Decades of Experience with 600 Cases. *Plast Reconstr Surg* **90**: 355–374 (1992).
- Berroterán MV. Implantes de Microtia Fabricados con Manufactura Aditiva Usando Polímeros Biocompatibles e Hidrogeles Moldeados. Master Thesis. Universidad Simón Bolívar (2015).
- Porter B, Zauel R, Stockman H, Guldberg, R, Fyhrie, D. 3-D computational modeling of media flow through scaffolds in a perfusion bioreactor. *J Biomech* **38**: 543–549 (2005). <https://doi.org/10.1016/j.jbiomech.2004.04.011>.
- Cioffi M, Boschetti F, Raimondi MT, Dubini, G. Modeling evaluation of the fluid-dynamic microenvironment in tissue-engineered constructs: A micro-CT based model. *Biotechnol Bioeng* **93**: 500–510 (2006). <https://doi.org/10.1002/bit.20740>.
- Cioffi M, Galbusera F, Raimondi MT, Dubini, G. Computational modelling of microfluidynamics in bioreactor-cultured cellular constructs. *J Biomech* **39**: S225 (2006). [https://doi.org/10.1016/S0021-9290\(06\)83831-5](https://doi.org/10.1016/S0021-9290(06)83831-5).
- Zeiser T, Bashoor-Zadeh M, Darabi A, Baroud G. Pore-scale analysis of Newtonian flow in the explicit geometry of vertebral trabecular bones using lattice Boltzmann simulation. *Proc Inst Mech Eng Part H J Eng Med* **222**: 185–194 (2008). <https://doi.org/10.1243/09544119JEM261>.
- Voronov R, VanGordon S, Sikavitsas VI, Papavassiliou, DV. Computational modeling of flow-induced shear stresses within 3D salt-leached porous scaffolds imaged via micro-CT. *J Biomech* **43**: 1279–1286 (2010). <https://doi.org/10.1016/j.jbiomech.2010.01.007>.
- Pennella F, Cerino G, Massai D, Gallo D, Falvo D'Urso Labate G, Schiavi A, Deriu, MA, Audenino, A, and Morbiducci, UA. A Survey of Methods for the Evaluation of Tissue Engineering Scaffold Permeability. *Ann Biomed Eng* **41**: 2027–2041 (2013). <https://doi.org/10.1007/s10439-013-0815-5>.
- Pennella F, Gentile P, Deriu MA, Gallo, D, Schiavi, A, Ciardelli, G, Lorenz, E, Hoekstra, AG, Audenino, A, and Morbiducci, U. A Virtual Test Bench to Study Transport Phenomena in 3D Porous Scaffolds Using Lattice Boltzmann Simulations. SBC2013–14489. In: *ASME 2013 Summer Bioengineering Conference*, Sunriver, Oregon, p. V01AT07A020 (2013). <https://doi.org/10.1115/SBC2013-14489>.
- Alam TA, Pham QL, Sikavitsas VI, Papavassiliou D V., Shambaugh RL, Voronov RS. Image-based modeling: A novel tool for realistic simulations of artificial bone cultures. *Technology* **04**: 229–233 (2016). <https://doi.org/10.1142/S233954781620003X>.
- Boschetti F, Raimondi MT, Migliavacca F, Dubini, G. Prediction of the micro-fluid dynamic environment imposed to three-dimensional engineered cell systems in bioreactors. *J Biomech* 2006; **39**: 418–425.
- Vossenbergh, P, Higuera, GA, van Straten, G, van Blitterswijk, CA, van Boxtel, AJB. Darcian permeability constant as indicator for shear stresses in regular scaffold systems for tissue engineering. *Biomech Model Mechanobiol* **8**: 499–507 (2009). <https://doi.org/10.1007/s10237-009-0153-6>.
- Ali D, Ozalp M, Blanquer SBG, Onel, S. Permeability and fluid flow-induced wall shear stress in bone scaffolds with TPMS and lattice architectures: A CFD analysis. *Eur J Mech – B/Fluids* **79**: 376–385 (2020). <https://doi.org/10.1016/j.euromechflu.2019.09.015>
- Malvè M, Bergstrom DJ, Chen XB. Modeling the flow and mass transport in a mechanically stimulated parametric porous scaffold under fluid-structure interaction approach. *Int Commun Heat Mass Transf* **96**: 53–60 (2018). <https://doi.org/10.1016/j.icheatmasstransfer.2018.05.014>
- Hossain MS, Chen XB, Bergstrom DJ. Fluid flow and mass transfer over circular strands using the lattice Boltzmann method. *Heat Mass Transf* **51**: 1493–1504 (2015). <https://doi.org/10.1007/s00231-015-1514-6>.
- Ferroni M, Giusti S, Nascimento D, Silva A, Boschetti F, Ahluwalia A. Modeling the fluid-dynamics and oxygen consumption in a porous scaffold stimulated by cyclic squeeze pressure. *Med Eng Phys* **38**: 725–732 (2016). <https://doi.org/10.1016/j.medengphy.2016.04.016>.
- Croughan MS, Wang DIC. Hydrodynamic Effects on Animal Cells in Microcarrier Bioreactors. *Biotechnology* **17**:213–49 (1991).
- Liu J, Bi X, Chen T, Zhang, Q, Wang, SX, Chiu, JJ, Liu, GS, Zhang, Y, Bu, P, Jiang, F. Shear stress regulates endothelial cell autophagy via redox regulation and Sirt1 expression. *Cell Death Dis* **6**: e1827–e1827 (2015). <http://dx.doi.org/10.1038/cddis.2015.193>

23. Hossain MS, Bergstrom DJ, Chen XB. A mathematical model and computational framework for three-dimensional chondrocyte cell growth in a porous tissue scaffold placed inside a bi-directional flow perfusion bioreactor. *Biotechnol Bioeng* **112**: 2601–2610 (2015). <http://dx.doi.org/10.1016/j.btre.2014.12.002>.
24. Nair K, Gandhi M, Khalil S, Chang Yan, K, Marcolongo, M, Barbee, K. Characterization of cell viability during bioprinting processes. *Biotechnol J*; 4: 1168–1177 (2009). <https://doi.org/10.1002/biot.200900004>.
25. Schuerlein S, Schwarz T, Krzimirski S, Gätzner, S, Hoppensack, A, Schwedhelm, I, Schweinlin, M, Walles, H, Hansmann, J. A versatile modular bioreactor platform for Tissue Engineering. *Biotechnol J* **12**: 1600326 (2017). <https://dx.doi.org/10.1002%2Fbiot.201600326>.
26. FlowKit Ltd. *Palabos, CFD, complex physics*. <http://www.palabos.org/index.php> (2012). [accessed 16 October 2017].
27. Wu L, Zhang H, Zhang J, Ding, J. Fabrication of Three-Dimensional Porous Scaffolds of Complicated Shape for Tissue Engineering. I. Compression Molding Based on Flexible-Rigid Combined Mold. *Tissue Eng* **11**: 1105–1114 (2005). <https://doi.org/10.1089/ten.2005.11.1105>.
28. Sobral JM, Caridade SG, Sousa RA, Mano, J, Reis, R. Three-dimensional plotted scaffolds with controlled pore size gradients: Effect of scaffold geometry on mechanical performance and cell seeding efficiency. *Acta Biomater* **7**: 1009–1018 (2011). <https://doi.org/10.1016/j.actbio.2010.11.003>.
29. Robert McNeel & Associates. *Rhinoceros, modeling tool for designers*, Software Package, Ver. 5 SR14 64-bit (5.14.522.8390, 22/5/2017). Seattle, WA (2017).
30. Kurtz A. *Intralattice, Generative Lattice Design with Grasshopper*. McGill's Additive Design & Manufacturing Laboratory (ADML). <http://intralattice.com/> (2018) [accessed 26 October 2017].
31. Liu Z, Wu H. Pore-scale modeling of immiscible two-phase flow in complex porous media. *Appl Therm Eng* **93**: 1394–1402 (2016). <https://doi.org/10.1016/j.applthermaleng.2015.08.099>.
32. Parmigiani A. Lattice Boltzmann calculations of reactive multiphase flows in porous media. Doctoral Thesis. Université de Genève. (2011).
33. Bear J. *Dynamics of Fluids in Porous Media*. Dover, New York, pp 133 (1972).
34. Salehi-Nik N, Amoabediny G, Pouran B, Tabesh, H, Shokrgozar, MA, Haghhighipour, N, Khatibi, N, Anisi, F, Mottaghy, K, Zandieh-Doulabi, B. Engineering Parameters in Bioreactor's Design: A Critical Aspect in Tissue Engineering. *Biomed Res Int* **2013**: 1–15 (2013). <http://dx.doi.org/10.1155/2013/762132>.

State of the art in the use of bioceramics to elaborate 3D structures using robocasting

Juliana Kelmy Macário Barboza Daguano^{1,2*}; Claudinei dos Santos³; Manuel Felipe Rodrigues Pais Alves⁴; Jorge Vicente Lopes da Silva²; Marina Trevelin Souza⁵; Maria Helena Figueira Vaz Fernandes⁶

*Corresponding author: E-mail address: juliana.daguano@ufabc.edu.br

Abstract: Robocasting, also known as Direct Ink Writing, is an Additive Manufacturing (AM) technique based on the direct extrusion of colloidal systems consisting of computer-controlled layer-by-layer deposition of a highly concentrated suspension (ceramic paste) through a nozzle into which this suspension is extruded. This paper presents an overview of the contributions and challenges in developing three-dimensional (3D) ceramic biomaterials by this printing method. State-of-art in different bioceramics as Alumina, Zirconia, Calcium Phosphates, Glass/Glass-ceramics, and composites is presented and discussed regarding their applications and biological behavior, in a survey comprising from the production of customized dental prosthesis to biofabricating 3D human tissues. Although robocasting represents a disruption in manufacturing porous structures, such as scaffolds for Tissue Engineering (TE), many drawbacks still remain to overcome and although widely disseminated this technique is far from allowing the obtention of dense parts. Thus, strategies for manufacturing densified bioceramics are presented aiming at expanding the possibilities of this AM technique. The advantages and disadvantages and also future perspectives of applying robocasting in bioceramic processing are also explored.

Keywords: Additive Manufacturing (AM); Direct Ink Writing (DIW); Robocasting; Bioceramics; Challenges; Perspectives.

Introduction

Technical Approaches – Additive Manufacturing and Robocasting

By definition, Biomaterials are nonviable materials, natural or synthetic, that are useful towards the repair or even replacement of damaged body parts via interacting with living systems. The interaction of the material with the host tissue can occur at different levels, from a minimum response (inert biomaterial), to an intimate interaction with the human cells, sometimes replacing a component of the body or even carrying out their functions (bioactive or resorbable biomaterials).¹ As soon as scientists and engineers understood that it was possible to modulate the biocompatibility of materials for biomedical applications, novel and advanced manufacturing techniques were explored. Those processes aimed to produce multicomponent structures otherwise difficult to obtain using conventional routes, reduce cost and also improve performance after implantation. Within this context, Additive Manufacturing (AM) arises as a solution.

Ceramic robocasting is a direct AM technology, also named as Direct Ink Writing (DIW), based on the Material Extrusion process. In 2000, Cesarano patented and developed the technique, that consists in a computer-controlled extrusion of a viscous ceramic suspension with a high solid loading through a small orifice creating filaments that are placed in a layer-by-layer deposition process.² Figure 1 shows a schematic diagram illustrating this technique for obtaining of inert ceramic based on $ZrO_2-Y_2O_3$ (Y-TZP).

This suspension (or colloidal system) must demonstrate a suitable rheological behavior, undergoing a transformation from a pseudoplastic to a dilatant behavior when extruded in air, and following a computer-aided design model to form the 3D structures.³ Unlike other AM techniques, as Stereolithography (SLA), Digital-Light-Processing (DLP), and Fused Deposition Material (FDM), that usually involve binder-rich contents (above 40% (v/v)) – which may lead to sudden outgassing and crack formation due to excessive shrinkage of the structure⁴ – in robocasting process, concentrated ceramic suspensions are prepared using solid loading close to 40% (v/v) and dispersants/binders less than 3% (v/v).

As ceramic robocasting is not a one-step AM process, the resultant green body needs to undergo a debinding process to burn off the organic additives and a subsequent sintering process to densify the structures.⁵ After drying, the materials fabricated by robocasting have a high green density (up to 60%), which allows almost complete densification upon sintering, achieving a sintered strut density near 95%.^{6,7,8} A recent study explored the rapid sintering of 3D-plotted tricalcium phosphate (TCP) scaffolds with the aim of getting the on-demand scaffold fabrication closer towards the clinical practice. The rapid and reactive pressure-less sintering of β -TCP scaffolds can be achieved merely during 10 min by applying fast heating rates in the order of 100 °C/min.⁹

Robocasting appears as a new tool to process bioceramics since this is a notoriously difficult material to be processed. Firstly, due to its inherent high melting point. Ceramics usually have complex phase diagrams, which indicate that after melting new phases can form as well as unexpected

¹Universidade Federal do ABC, Grupo de Pesquisa em Biomateriais (UFABC-GPBiomat), Alameda da Universidade, s/n, Anchieta, São Bernardo do Campo (SP), Brazil.

²Centro de Tecnologia da Informação – Renato Archer, Núcleo de Tecnologias Tridimensionais (CTI-NT3D), Dom Pedro I Highway (SP-65), Km 143,6 – Amaraís – Techno Park, Campinas (SP), Brazil.

³Universidade do Estado do Rio de Janeiro, Faculdade de Tecnologia de Resende (UERJ-FAT), Rodovia Presidente Dutra, km 298, Polo Industrial, Resende (RJ), Brazil.

⁴Universidade de São Paulo, Escola de Engenharia de Lorena (USP-EEL-DEMAR), Pólo Urbo-Industrial, Gleba AI-6, s/n, Lorena (SP), Brazil.

⁵Universidade Federal de São Carlos, Laboratório de Materiais Vítreos (UFSCar-LaMaV), Rodovia Washington Luís, km 235, São Carlos (SP), Brazil.

⁶University of Aveiro, Aveiro Institute of Materials (CICECO-UA), Campus Universitário de Santiago, 3810-193 Aveiro, Portugal.

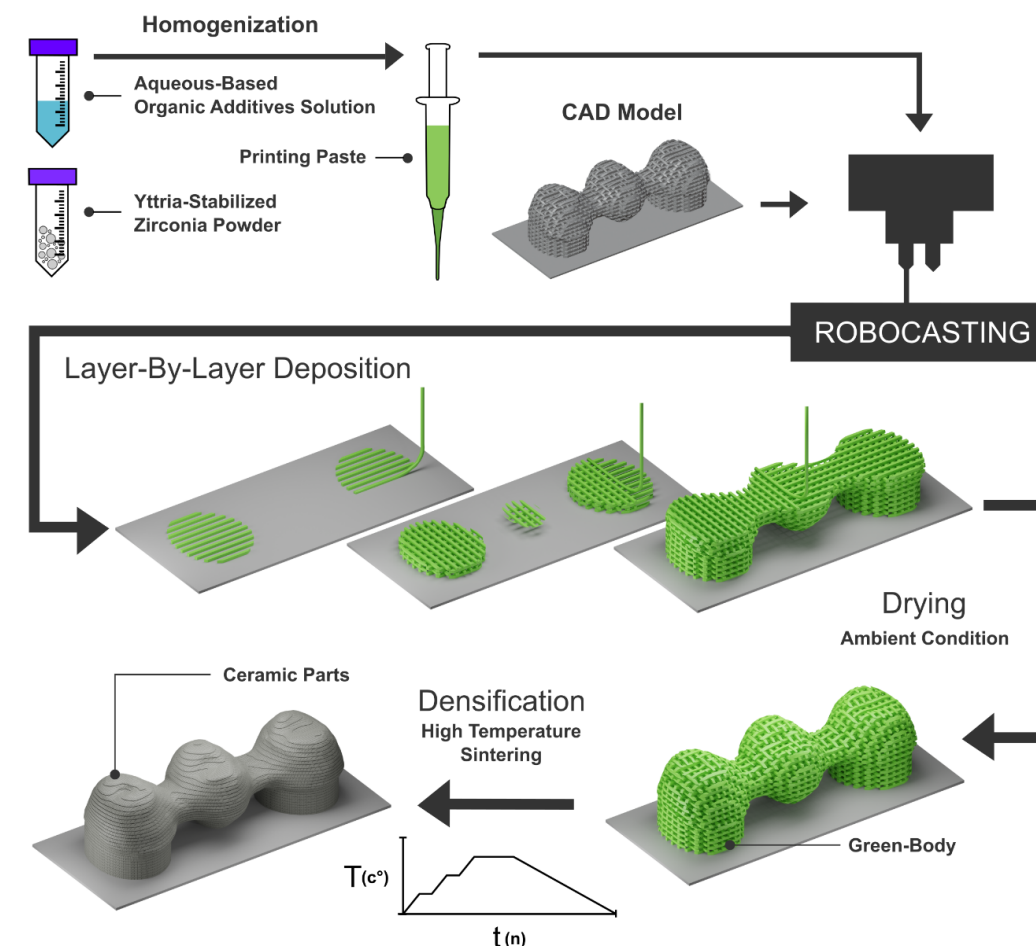


Figure 1 – Example of development steps of robocasted Y-TZP parts.

changes in their properties, even the biocompatibility. Secondly, the high-temperature processing of ceramics can cause uncontrolled porosity and cracks.¹⁰ When it comes to porous materials for Tissue Engineering, interconnected pores are desirable to promote cellular growth and implant fixation, although they can decrease the mechanical properties of the final parts.^{11,12,13} Hence, a balance between mechanical properties and biological behavior should be found for different applications.¹⁴ An advantage of almost all ceramic systems is that ceramic powders are commercially available with a wide range of characteristics. Therefore, the possibility of using the robocasting technique, regarding the manufacture of porous or dense ceramic structures with complex morphology is particularly attractive when compared with the slurry-based methods, especially to produce biomedical devices that are aimed to meet the peculiarities of each patient.^{15,16}

In this article, we aim to review the most recent contributions and challenges on porous and dense bioceramic structures obtained by the robocasting technique as well as the latest trends on 4D printing materials for biomedical applications. Some current challenges and possible solutions regarding the ideal system for the fabrication of dense robocast ceramic parts with optimal properties will be discussed with the perspective of the potential popularization and viability of this technique.

Main Challenges in Robocasting

The manufacture of dense parts by robocasting encounters severe reservations mainly because the applications of dense bioceramics are associated with the need of adequate mechanical strength and reliability for long use periods. Also, it should be considered the requirement of an

appropriate biological response, independently of the particular application (dental prostheses or implants, intraoral pins, orthopedic).

Technologies that use of a large amount of volatile content such as robocasting, as ~60% of the extruded paste is composed of water and polymeric binder, debinding is a potentially problematic step when dense monolithic components are intended.

An efficient strategy to circumvent the limitation to robocasting dense parts is based on the knowledge from developing similar bioceramics, obtained by techniques that use ceramic masses such as injection molding or gelcasting.^{17,18,19,20} These conventional molding methods are used for the manufacture of near-net-shape ceramics with highly complex final geometries. A major challenge is the controlling of the spatial distribution of the pores, and in the case of dense biomaterials, the control and minimization of pores and the overall porosity.

After the removal of the liquid phase or plasticizers, which is notably a very complex stage, considerably high relative densities can be achieved, depending, among other factors, mainly on the sinterability of the studied ceramic material. Currently, most ceramic suspensions or pastes used as feedstock for AM are based on significant amounts (40 to 60% v/v) of organic binders.^{21,22} The efficient removal of the remaining organics requires experimental skills and acquired knowledge of the process, but many limitations still exist when it comes to monolithic structures that present a large wall thicknesses or large volumes. Thus, plasticizers should be adequately chosen because their evaporation rate is crucial for the process and it can be adapted to the specific needs of the particular AM method.

In recent years, this technique has been employed to form green parts of different ceramic structures such as alumina (Al_2O_3),^{23,24} silicon carbide

(SiC),^{17,25} silicon nitride (Si_3N_4),^{7,26} Yttrium-stabilized zirconia ($\text{ZrO}_2/\text{Y}_2\text{O}_3$),⁸ and some bioactive glasses.^{27,28,29} Most of the reported works include rheological studies that allow the formulation of the ideal compositions of ceramic masses and their respective optimized suspensions aiming at particular porosity and mechanical performance of the sintered parts.

Another challenge is related to mechanical properties of robocasted bioceramics. Essentially, ceramics are fragile. In this sense, a strategy proposed to ripen mechanical properties of robocast bioceramic scaffolds could be to combine the ceramic with a polymeric material. The fabrication of hybrid polymer/ceramic porous scaffolds with core/shell struts thus, appears as an interesting possibility. This strategy provides enhanced toughness without affecting, in principle, the bioactivity of the scaffold surfaces or the interconnected porosity required for bone tissue regeneration.³⁰ Another possibility is creating 3D Printing Bioinspired ceramic composites, using the biomimetic concept. A classic example is nacre, which boasts a combination of high stiffness, strength, and fracture

toughness. Various microstructural features contribute to the toughness of nacre, including mineral bridges, nano-asperities, and waviness of the constituent platelets. In this sense, it would be possible to replicate natural structures and build highly mineralized materials that retain strength while enhancing toughness.³¹

Bioceramics for 3D printing using the Robocasting technique

Due to their unique properties, bioceramics play a privileged role within the diversity of available biomaterials.^{32,33,34} The bioceramics market is expected to rise around 7% during the forecast period of 2019 – 2024.³⁵ This is a motivation for a fast progress in bioceramic robocasting technology, and to keep up with the growth of the market.

For a better understanding of the state-of-art of robocasting, the literature review will be divided into two sections, (i) porous bioceramics and (ii) fully dense monolithic bioceramics, as schematically distinguished in Figure 2.

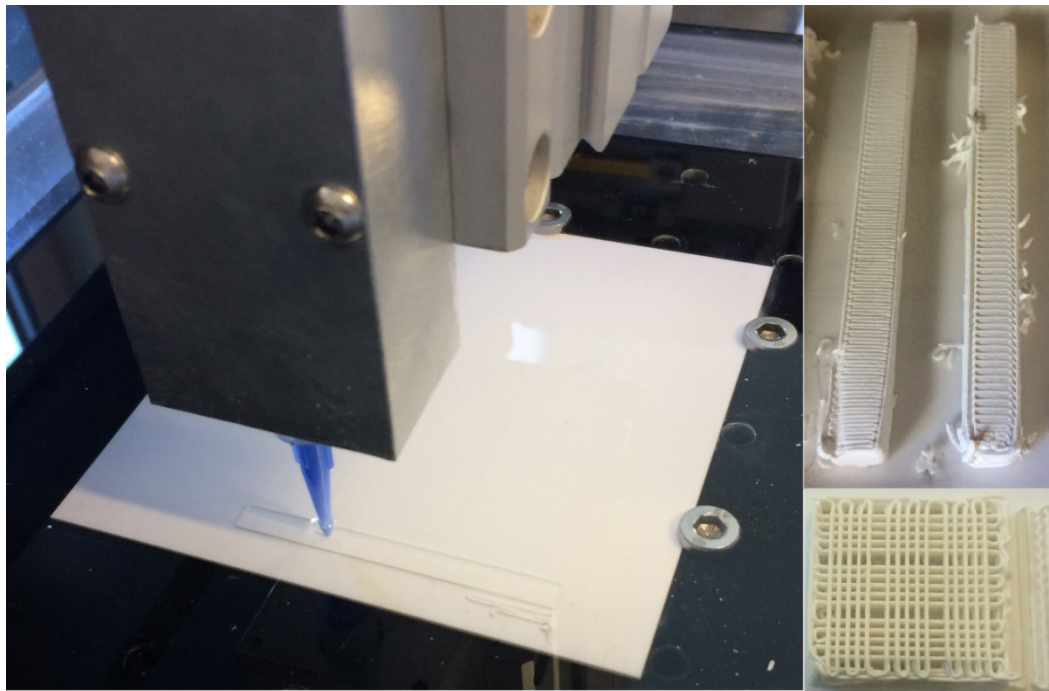


Figure 2 – Bioceramics fabricated by robocasting: (top right hand corner) fully dense monolithic parts, (bottom right hand corner) porous structures.

Porous Bioceramics

TE is a multidisciplinary research field that began in 1980's and combines engineering and life sciences in order to develop new methods for tissue replacement with improved functionality.³⁶ A prime step in TE is the development of complex 3D shapes with tailored external geometries, pore volume fractions, pore sizes and controlled interconnectivity. The 3D scaffolds are mainly designed to be a temporary implant, acting as a template for new cells growth while continuously and steadily degrading during/after the healing process, so that the seeded cells can grow and proliferate to regenerate into a new tissue.^{37,38,39}

Currently, most of the studies have used 3D printing as a tool to make scaffolds for TE. Therefore, the microstructure features, i.e., interconnected porosity, pore size distribution, and filament aspects, are crucial factors to assure mechanical properties similar to those of the tissue and appropriate biocompatibility.⁴⁰

Some aspects of bioceramic ink parameters, such as ink chemistry, processing additive (dispersant, binder, gelation agent), solids loading, powder reactivity, ceramic particle size, and distribution, must be understood since they have a significant effect on the printing quality. Besides, there is a strong correlation between particle size distribution and the force needed to extrude ceramic loaded inks, such that a wide particle distribution allows the formulation of higher particle loaded inks. Nommeots-Nomm et al. described how wide distributions allow for intimate packing of the particles within the ink, resulting in denser filaments post sintering. Also, they suggested that Pluronic F-127, a water soluble block co-polymer surfactant with thermally reversing rheological behaviour, consisting of poly(ethylene oxide)-poly(propylene oxide)-poly(ethylene oxide) tri-blocks (PEO-PPO-PEO), can be used as a universal binder.⁴¹ Eqtseadi et al. have suggested a simple recipe for robocasting 3D scaffolds. They reported that aqueous suspensions containing 45% (v/v) of 45S5 Bioglass were successfully prepared using 1 %wt carboxymethyl cellulose (CMC-250MW) as additive, tuning the rheological properties of the inks to meet the stringent requirements of robocasting. Another information is that an incomplete surface allowing bridging flocculation to occur is the key to obtain highly performing inks.⁴² Recently, Koski et al. proposed a natural polymer binder system in ceramic composite scaffolds, through the utilization of naturally sourced gelatinized starch with hydroxyapatite (HA), in order to obtain green parts without the need of crosslinking or post processing.⁴³

Scaffolds produced by robocasting generally possess better mechanical properties compared to those produced by indirect AM technologies, because they usually exhibit a cubic geometry with orthogonal pores, whereas scaffolds produced by other techniques mostly present a cylindrical geometry with orthogonal or radial pores. The difference in strength can reach one order of magnitude. Scaffold struts produced by robocasting can be almost dense after sintering thus improving their mechanical properties.^{44,45}

Marques et al. reported the development of 3D porous calcium phosphate scaffolds by robocasting from biphasic ($\text{HA}/\beta\text{-TCP} \approx 1.5$) powders, undoped and co-doped with Sr and Ag, where the ceramic slurry content was around 50% (v/v). After sintering at 1100 °C, scaffolds with different pore sizes and rod average diameter of 410 μm were obtained. The compressive strength was comparable to or even higher than that of cancellous bone. Sr and Ag enhanced the mechanical strength of scaffolds, conferred good antimicrobial activity against *Staphylococcus aureus* and *Escherichia coli*, and did not induce any cytotoxic effects on human MG-63 cells. Furthermore, the co-doped powder was more effective in inducing pre-osteoblastic proliferation.⁴⁶

To meet the requirements of a 3D scaffold, *in vitro* and *in vivo* tests are key steps for the development of new suitable biomaterials. In the following tables, we present a concise review on the *in vitro* and *in vivo* assays performed with robocasted bioceramics and biocomposite scaffolds and their outcomes and relevance to the field. There is a vast literature exploring the mechanical behavior of 3D bioactive glass scaffolds manu-

factured by the robocasting technique, but the literature regarding the interaction of cells with bioceramic scaffolds obtained by this processing method is fairly scarce. Generally, researchers focus on constructing hybrid materials and biocomposites aiming the optimization of the process. Some interesting studies on cell viability and proliferation when in contact with robocast bioceramics and biocomposites are presented in Table 1.

Regarding *in vivo* tests, up to this date, the five most relevant studies using bioglasses robocast scaffolds were conducted by Liu et al. in 2013,^{30,47} Deliormanli et al. in 2014,⁴⁸ Rahaman et al. in 2015,⁴⁹ and Lin et al. in 2016.⁵⁰ As to other bioceramics several studies are reported and the most important outcomes are presented in Table 2.

Authors	Material Tested	Scaffold Characteristic	Porosity	In Vitro Test	Cell Line	Time	Outcomes	Ref
Chung-Hun et al.	Sol-gel bioactive glass (70SiO ₂ - 25CaO - 5P ₂ O ₅) and PCL	Degradable macro-channeled scaffolds	Pore size of 500 x 500 μm	MTT assays in static and dynamic conditions	hASCs	Up to 28 days	Cells were viable and grew actively on the scaffold assisted by the perfusion culturing (dynamic condition). Osteogenic development of hASCs was upregulated by perfusion culturing	51
Gao et al.	Gelatin + sol-gel bioactive glass (70SiO ₂ - 25CaO - 5P ₂ O ₅ mol-%)	Cubic shaped scaffolds and a grid-like microstructure	~ 30%	Cell viability and ALP activity	MC3T3-E1	Up to 21 days	Scaffolds supported cell proliferation, ALP activity, and mineralization	52
Richard et al.	β-TCP, β-TMCP, and BCMP	Inter-rod spacing of ~460 μm	β-TCP= 32% β-TCMP=45% BCMP=48%	MTT assay, ALP, Osteocalcin, TGF- 1, and Collagen	MC3T3-E1	7, 14 and 21 days	No toxicity for this cell line. Calcium nodule formation and bone markers activity suggested that the materials would induce bone formation in vivo.	53
Won et al.	Fibronectin+ nanobioactive glass (85 SiO ₂ - 15CaO %wt) and PCL	Bioactive nanocomposite scaffolds	Pore size of 0.5 mm x 0.5 mm	Cell adhesion and proliferation	rMSCs	14 days	Scaffolds significantly improved cells responses, including initial anchorage and subsequent cell proliferation	54
Varanasi et al.	PCL and PLA-hydroxyapatite (70 wt-%)	2D films and 3D porous scaffolds	~76%	MTT assay	M3T3-E1	7 days	No deleterious influence of the polymer degradation products on the cells and HA acted as a support for osteoblast cytoskeletal attachment, promoting their proliferation	55
Andrade et al.	β-TCP nd gelatin	Flexible bioceramic scaffolds with pore size of ~200 μm	45%	Cell proliferation in static and dynamic conditions	MC3T3-E1	3, 7, 13 and 21 days	Both culture systems fostered cell proliferation up to day 21, however, the dynamic methodology (oscillatory flow variation) achieved a higher cell proliferation	56
Martínez-Vázquez et al.	Hydroxyapatite (HA)	Prepared by drying at room temperature or the freeze-drying method	71-77%	Cell Viability	MC3T3	1, 3, 7, and 12 days	Freeze-dried scaffolds presented a significantly increase in initial cell count and cell proliferation rate when compared to the conventional evaporation method	57
Fiocco et al.	Silica-bonded calcite	Two spacing between rods: 300 μm and 350 μm	56%-64%	Cell adhesion and distribution	ST-2 cells	1, 3, 7 and 14 days	Cells showed high metabolic activities and expressed typical osteoplastic phenotype. Mineral deposit after cell cultivation was observed and all the scaffolds stimulated cell adhesion and proliferation	58
Stanciuc et al.	Zirconia-toughened alumina (ZTA)	Robocasting of 2D pieces and 3D-ZTA scaffolds	30-50%	Cell viability, ALP activity, gene expression and mineralization	human primary osteoblasts (hOb)	10, 20 and 30 days	2D-ZTA presented a higher ALP activity and an increased hOb cells proliferation than the 3D-ZTA scaffolds. RUNX2 was upregulated on all samples after 10 days.	59
Ben-Arfa et al.	Sol-gel glass composition (64.4SiO ₂ -4.9Na ₂ O-21.53CaO - 9.09 P ₂ O ₅ ,% wt.)	Different pore sizes = 300, 400 and 500 μm; with dimensions of 3 x 3 x 4 m	~47%	MTT assays according to ISO 10993-5 standard	MG63 osteoblasts	7 days	Within the pore size range tested, pore size did not exert any significant influence on cell viability, presenting no cytotoxicity towards the osteoblasts	60

Table 1 – In vitro studies with robocast scaffolds from different materials.

Authors	Material Tested	Characteristics	Porosity	In Vivo Test	Animal Model	Time	Outcomes	Ref
Liu et al.	Bioactive glass 13-93	Scaffolds BMP2 loaded and/or pretreated in phosphate solution	50%	Histomorpho-metric analysis	Calvarial defects of Ø4.6 mm in rats	6 weeks	BMP-2 pre-conditioned scaffolds significantly enhanced the capacity to support new bone formation	59
Liu et al.	Bioactive glass 13-93	6 x 6 x 6 mm scaffolds, pore width of 300 µm	47%	Mechanical properties during in vitro and in vivo tests	Subcutaneous model in rats	Up to 12 weeks	In vivo reduction in mechanical properties was greater than in vitro due to greater glass dissolution and faster conversion of the glass into HCA	30
Deliormanli et al.	Bioactive glass 13-93B	Scaffolds with different pore sizes =300, 600 and 900 µm	45-60%	Histological exploring tissue growth and blood vessel infiltration	Subcutaneous model in rats	4 weeks	All scaffolds were infiltrated with fibrous tissue and blood vessels. No difference was found in the formation of the fibrous tissue for the different pore sizes.	60
Rahaman et al.	Bioactive glass 13-93	Scaffolds with or without BMP2 and pretreatment in phosphate solution	50%	Histological, histomorpho-metric analysis and SEM	Calvarial defects of Ø 4.6 mm in rats	6, 12 and 24 weeks	Bone regeneration increased with implantation time, and pretreating and BMP2 loading significantly enhanced the bone formation rate (for all studied times).	61
Lin et al.	Bioactive glass 13-93	Scaffolds with or without BMP2 loading	47%	Histological, SEM, and Histomorpho-metric analysis	Calvarial defects of Ø 4.6 mm in rats	6, 12 and 24 weeks	BMP2 scaffolds significantly enhanced bone regeneration and their pores were almost completely infiltrated with lamellar bone within 12 weeks. BMP2 scaffolds also had a significantly higher number of blood vessels at 6 and 12 weeks.	62
Simon et al.	Hydroxyapatite (HA)	Scaffolds with different rod sizes and porosities (different macro-pores channels)	Different pore channels. From 250 to 750 µm ²	Micro-CT scans, histological and SEM analysis	Calvarial defects of Ø 11 mm in rabbits	8 and 16 weeks	Bone ingrowth at 8 and 16 weeks were comparable for all samples. Bone attached directly to HA rods indicating osteoconduction.	61
Dellinger et al.	Hydroxyapatite (HA)	Scaffolds with and without BMP-2 loading	Pores of 100-700 µm	Histological analysis	Metacarpal and metatarsal bones defects of Ø 6 mm in goats	4 and 8 weeks	BMP-2 loaded scaffolds presented a significantly greater bone formation at both experimental times. The cells used the scaffolds as a template since the lamellar bone was aligned near the scaffolds' rod junctions.	62
Luo et al.	Ca ₇ Si ₂ P ₂ O ₁₆	Hollow-struts-packed (HSP) bioceramic scaffolds	Up to 85%	Micro-CT and histological analysis	Critical femoral bone defects of Ø8 x 10 mm in rabbits	4 and 8 weeks	HSP scaffolds possessed a superior bone-forming ability and micro-CT analysis showed that the new bone started to grow in the macropores and also into the hollow channels of the scaffolds.	63
Lin et al.	Collagen and hydroxyapatite (CHA)	Biomimetic 3D scaffolds via a low-temperature process 3 rod widths: 300, 600 and 900 µm	72-83%	micro-CT and histological analysis	Ø 5 mm defects in the femur (condyle) of rabbits	2, 4, 8, or 12 weeks	CHA scaffolds facilitated new bone growth, as the biomaterial was resorbed or incorporated into the newly formed bone. CHA promoted better defect repair compared to the nonprinted CHA scaffolds.	64
Shao et al.	Magnesium-doped Wollastonite/TCP	CSi-Mg10 (10 mol% of Mg in CSi), CSi-Mg10/TCP15 (15-wt% TCP content) and pure β-TCP.	52-60%	Micro-CT, histological and mechanical tests	Calvarial defects of Ø 8 mm in rabbits	4, 8 and 12 weeks	CSi-Mg10/TCP15 scaffolds displayed higher osteogenic capability when compared to CSi-Mg10 and β-TCP after 8 weeks. After 8 and 12, CSi-Mg10/TCP15 presented an increase in their mechanical properties, possibly due to the new bone tissue ingrowth into the scaffolds	65

Table 2 – In vivo studies with robocast scaffolds from different materials.

Fully dense monolithic bioceramics

When developing dense bioceramics by robocasting several parameters should be examined in a sequential step process that should be used to plan new studies. Based on information regarding the materials and the processing parameters, it is possible to create a robocasting suspension development strategy. This is shown in Figure 3.

Figure 3 shows the level of complexity associated with the development of new ceramic inks. It necessarily involves a technical study aimed at understanding the effects of solid fractions (particle quantities, sizes,

and morphology) on the ink. At the same time, it is crucial to understand the interaction of the ceramic material with the fluid selected for the ink manufacture, i.e., which additives can be used to achieve a stable and printable suspension. Finally, it is of major importance the definition of the printing strategy and for the robocasting processing parameters to be optimized.

The following sections detail the relevant parameters to guide future developments on high densification of bioceramics.

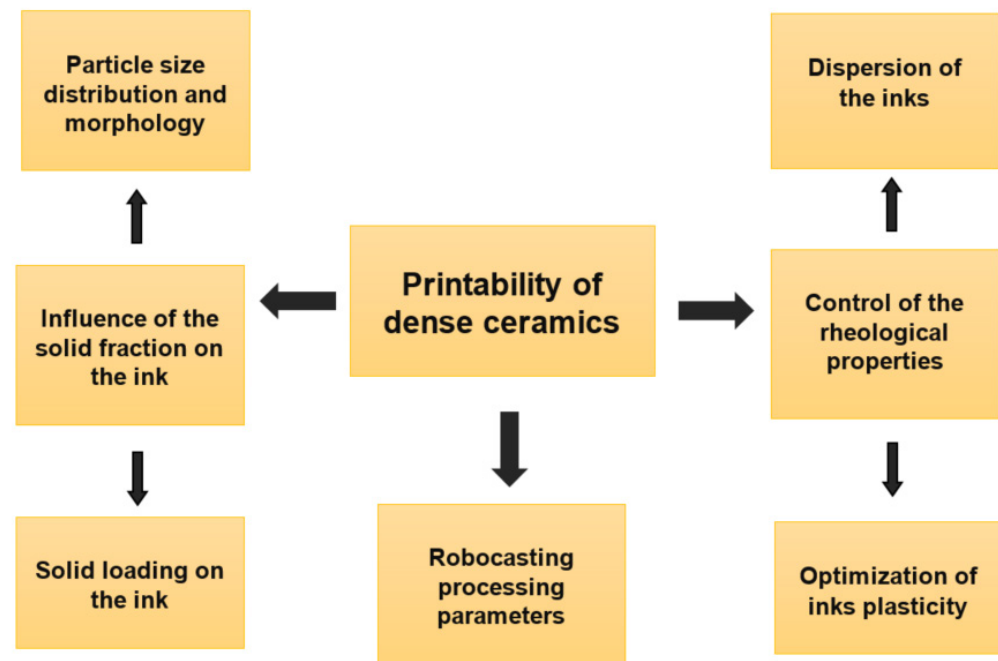


Figure 3 – Robocasting suspension development strategy.

Morphology and Particle size distribution

There is a consensus in the literature on the need for highly refined starting powders with broad particle size distribution to maximize green body compactability and sinterability.^{66,67,68} In parallel, some authors state that solid loads with bimodal distributions induce a reduction of the ink's viscosity when compared to suspensions manufactured with monomodal distribution, for the same volume of suspended solids.^{69,70,71}

Olhero and Ferreira fabricated three starter powder systems with variations in mean particle size for the preparation of trimodal suspensions. The authors found that the viscosity of the suspensions increased as the percentage of fine powders increased and, contrary to common sense, the powders with a high concentration of coarse solids showed a decrease in viscosity. This fact is due to the rheological behavior of the powders against the shear stress.⁷²

Particle morphology, on the other hand, affects the rheology of suspensions secondarily, due to the dispersed solids content and particle size distribution, being much more impactful in colloidal suspensions. Besides, suspensions based on high aspect ratio particles, or heterogeneous morphologies, are more susceptible to shear flow than those based on spherical particles.

Nutz et al. studied the rheology of two groups of graphite particles with different morphology, size, and surface area. The authors concluded that suspensions made with spherical particles had a significantly lower viscosity than those made with particles of anisotropic morphology.⁷³ Regarding the shear flow mechanism, this phenomenon is explained by the resistance promoted by the viscous suspension to the rotation of the elongated particles against the ease of spherical particles, which offer

low rotational resistance.^{74,75}

Figure 4 shows volumetric defects promoted by the concentric alignment of particles with high aspect ratio.

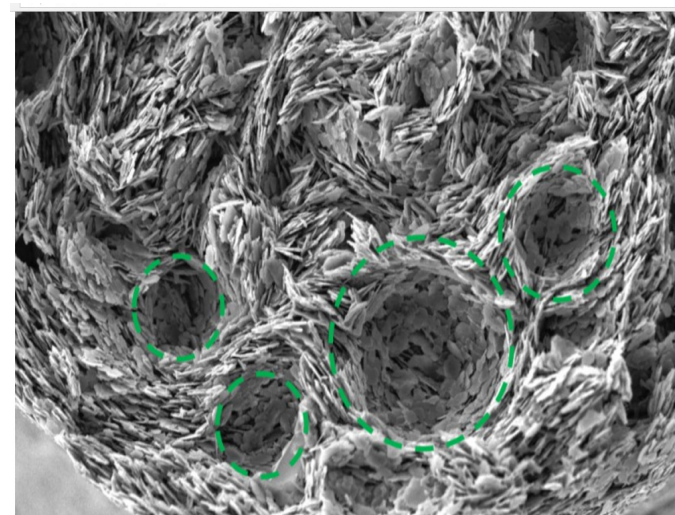


Figure 4 – Cross section of dried platelet paste, with the location of several bubbles marked. Reproduced with permission.⁷⁶

Mass solids content

Some authors reported that, whenever possible, the ideal solids content of inks for use in robocasting should be in the range of 40 to 45%

and never below 30% (v/v), this would grant a dimensional and geometric predictability after sintering.^{77,78} Table 3 presents some shrinkage results for different materials and additives as a function of the volume of suspended solids.

Materials	Additives used	Solid loading (v/v)	Linear shrinkage	Ref.
3Y-TZP	PEG-DA, DEG and Diphenyl (2,4,6- trimethylbenzoyl) phosphine oxide	37,5%	~28%	
3Y-TZP	PVA (MW 31000), PEG (MW 400), C ₆ H ₈ O ₆ and C ₆ H ₈ O ₇	38%	33%	8
Si ₃ N ₄	H-PEI, L-PEI and HPMC	~35%	~28%	7
Si ₃ N ₄	Darvan 821A, nitric acid and ammonium hydroxide	52%	16%	
Al ₂ O ₃	Dolapix CA, magnesium chloride and Alginate acid	45%	~26%	
Al ₂ O ₃	Darvan C-N, Bermocoll E and a polyethylene-imine solution	56%	~17%	
Al ₂ O ₃	Dolapix CE 64, PEG 400 and methocellulose	55%	15-19%	

Table 3 – Linear shrinkage as a function of solid loading for some bioceramic inks.

Moreover, the literature reiterates that suspensions with high saturation, greater than 50% (v/v) produce parts with high densification rates and low shrinkage and warp. Nevertheless, the stabilization of suspensions with large volumes of solids requires a thorough rheological analysis, mainly due to the need of controlling the shear stresses during the extrusion process.^{79,80,81} In general, the increase in mass viscosity with increasing volume of suspended solids can be directly attributed to the fact that a higher volumetric fraction of suspended ceramic particles further restricts the media flow.⁸²

Rheological stabilization of suspensions

Controlling the rheological properties of the filament is essential to prevent sag and part deformation after filament extrusion, especially when geometry includes complex shapes and bridged structures such as in scaffolds. An adequate behavior can be achieved in some ways, such as by controlled flocculation of the ceramic suspension to form a gel (e.g., change in pH, solvent ionic strength, the addition of polyelectrolytes) or by using gelling additives such as a reverse thermal gel.

The literature highlights three mechanisms of solids stabilization in a suspension: electrostatic stabilization, arising from the presence of electric charges on the surface of the particles which counterbalances the attraction promoted by the van der Waals forces; steric stabilization, where the adsorption of polymers on the surface of the suspended material promotes the mechanical immobilization of the particles; and electrosteric stabilization, a combination of electrostatic and steric stabilization, where polyelectrolytes are adsorbed on the surface of the particles and ions from the dissociation of the polyelectrolytes promote an adjacent electrostatic barrier.^{83,84,85} The mechanisms are demonstrated in Figure 5.

For the study of the stability of suspensions, a handy tool is the Zeta potential measurement, as it describes the potential difference between the dispersion medium and the stationary layer of boundary fluid at the

surface of the dispersed particles. In other words, the technique makes it possible to assess the variation of a repulsive or attractive tendency among the solid particles as a function of the pH change in suspension and can be used to predict and control suspension stability. From this knowledge, the interaction forces can be adjusted accordingly, from a highly dispersed state in which repulsion forces dominate to a weakly flocculated or even strongly aggregated state by which attractive forces are predominant. In the case of aqueous suspensions with high solids concentration, it is common to use polyelectrolytes containing ionizable functional groups, such as amine (-NH₂) or carboxylic (-COOH), for electrostatic stabilization, in addition to pH control.^{89,90,91}

Some authors support ideal rheological parameters to ensure mass printability, such as viscosity between 10 and 100 Pa.s, elastic modulus between 10⁵ and 10⁶ Pa and yield stress between 10⁻² and 10⁻³ Pa. For successive printing, concentrated ceramic suspension for robocasting has to possess suitable viscoelastic properties, as described by the Herschel-Bulkley model, shear-thinning flow behavior, and possessing relatively high modulus (G') with τ_y > 200 Pa to allow structural self-support and fabrication of high aspect ratio structures (Figure 6).⁶

For this optimization, appropriate rheological modifiers, such as flocculating/binder agents, should be added to the already stabilized, i.e., deflocculated, suspensions.^{18,79,86} In the usual approach to obtain the ideal parameters, reported in the literature, it is proposed the use of a deflocculating agent/charge binder, as opposed to the one used for the dispersion of the particles.^{5,87,88} This addition intends to control flocculation by promoting a reduction of the adsorbed layer. This procedure improves a bonding effect among the particles and should be accompanied by the addition of a rheological modifier, usually a long-chain polymer, aimed at stabilizing mass plasticity (steric stabilization). Table 4 summarizes these parameters.

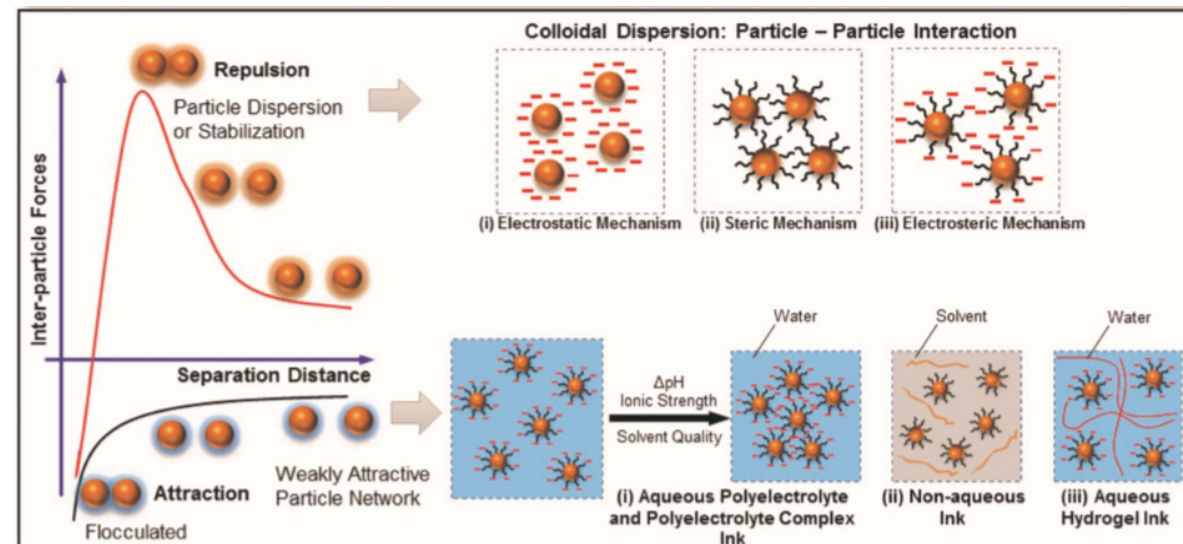


Figure 5 – Representation of mechanisms to improve the particle dispersion. Reproduced with permission. © Copyright 2018, John Wiley and Sons.

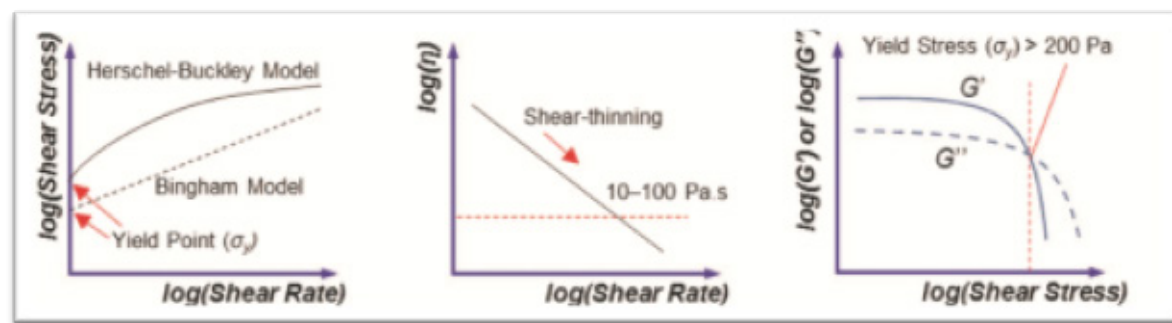


Figure 6 – Rheological behaviors required for ceramic robocasting. Reproduced with permission. © Copyright 2018, John Wiley and Sons.

Finally, some equations are presented as support for the controlling of parameters and print design. The ideal volumetric flow rate (Q) to fill the path taken by the print nozzle, ensuring the maintenance of the predicted specimen dimensions is essential for defining the robocasting parameters. Several authors suggest Equation (1) to specify this parameter:

$$Q = (\pi r^3 / 4) \cdot \dot{\gamma} \quad (1)$$

where: Q = ideal volumetric flow rate (μm³/s), r = radius of extrusion nozzle (μm) and (γ̇) = shear rate (s⁻¹).

Since suspensions used in robocasting must have a dispersed solids fraction higher than 30% (v/v), they eventually exhibit shear-thinning flow behavior. Thus, several authors claim that the Herschel-Bulkley model, Equation (2), satisfactorily describes the degree in which the ink presents a shear-thinning or shear-thickening behavior.

$$\sigma = \sigma_y^{D_{yn}} + K\dot{\gamma}^n \quad (2)$$

where: σ = shear stress (Pa), σ_y(D_yn) = dynamic yield stress (Pa), K = viscosity parameter (Pa.sⁿ), γ̇ = shear rate (s⁻¹) and n = shear exponent, for n < 1 the fluid is shear-thinning, whereas for n > 1 the fluid is shear-thickening.

Smay et al. proposed another strong feature for determining printing strategy and extrusion parameters. The authors described an approach to predict the maximum span by which a structure can be constructed in green without experiencing deformation, as depicted in Equation (3).

$$G' \geq 1.4 \cdot \rho \cdot S^2 D \quad (3)$$

where: G' = shear modulus, ρ = specific weight of the ink, S = relation between the span length and the layer height and D = nozzle diameter.

Another challenge experienced during the printing process is the collapse of free walls, mostly associated with the rheological properties of the ink. Figure 7 exemplifies a case in which the poor stability of the ink leads to a completely collapse of the structure.

In turn, M'Barki et al. proposed an equation to define the maximum

printable height (h_max) of a free wall, without the risk that it will collapse due to gravitational action, Equation (4).

$$h_{max} = \frac{\sigma_y^{D_{yn}}}{\rho g} \quad (4)$$

where: σ_y^{D_{yn}} is the dynamics yield stress (Pa), ρ is the specific weight of the ink and g is the gravitational contribution (9.81 m/s²)

Future Perspectives

An urging trend in robocasting is 4D printing. The conception that “time” can be incorporated into the conventional concept of 3D printing as the 4th dimension is commonly known as 4D printing. This novel model of printing can potentially benefit many different areas in biomedical applications, such as tissue regeneration, medical device fabrication, and drug delivery.

A perceived possibility to conduct a 4D printing is to combine different materials during processing. Multi-material printing, i.e. polymer and ceramics, could prevent the secondary shaping after printing from the polymeric materials. In most of the reported AM techniques, the form of the as-printed green body usually dictates the final shape of the sintered structure, while post-printing secondary shaping of the green body obtained from the AM process is minimal. However, a deep understanding on how external stimuli such as temperature, moisture, light, magnetic field, electric field, pH, ionic concentration or chemical compounds can affect the characteristics of the printed materials is yet to be established.

Another possibility in the AM field is the obtention of smart materials. Some interesting features could be achieved using this type of materials such as controlled swelling, predicted shape alterations, functionalities change and self-assembly. Self-shaping geometries, like as bending, twisting or combinations of these two basic movements, can be implemented by programming the material's microstructure to undergo local anisotropic shrinkage during heat treatment, as presented in Figure 8. This functional design may be achieved by magnetically aligning functionalized ceramic platelets in a liquid ceramic suspension, subsequently consolidated through an established enzyme-catalysed reaction, and finally achieved deliberate control over shape change during the sintering step.

Regarding the robocasting process, geopolymeric slurries could be



Figure 7 – Experimental buckling response of the free wall, the three stages of failure: buckling initiation, buckling development and full collapse. Reproduced with permission.

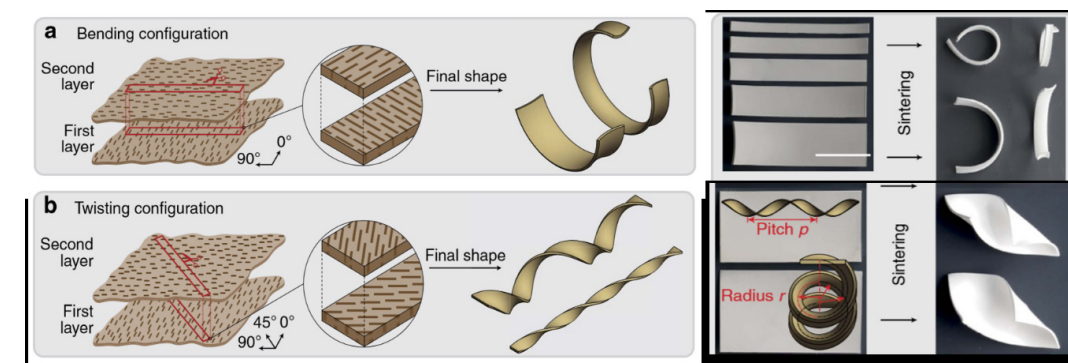


Figure 8 – Illustration of the proposed self-shaping mechanism: (a) bending and (b) twisting configuration, based on bottom-up shaping method of ceramic suspensions. Reproduced with permission.

Materials	Additives used			Solid loading (v/v)	Average grain size (d ₅₀)	Relative density	Ref
	Dispersants	Flocculant / binder	Rheological modifier				
SiC	Darvan 670, PEG 10.000 and NH ₄ Ac			44%	0.7 m	~95%	89
Al ₂ O ₃		Pluronic F-127		39%	0.3 m	~97%	17
Al ₂ O ₃	Darvan C, psyllium and Glycerol			49%	0.4 m	~98%	85
Al ₂ O ₃	Darvan 821A		PVP	55%	0.6 m	92%	86
3Y-TZP	Dolapix CE 64/ NH ₄ OH			50%	0.04 m	~99%	87
3Y-TZP	C ₆ H ₈ O ₆ / C ₆ H ₈ O ₇	PVA (MW 31000)	PEG (MW 400)	38%	~0.4 m	94%	8
Si ₃ N ₄	H-PEI/L-PEI		HPMC	52%	0.77 m	~99%	7
Si ₃ N ₄	H-PEI/L-PEI	Darvan-821	HPMC	44%	0.5 m	97%	27

Table 4 – Relationship between additives used, suspended solids loading, average particle size, and relative density of the final part.

good candidates as smart materials for 4D printing provided their reaction over time could be effectively controlled.⁹⁶ However, within bioceramic content, the evidence on works reported in 4D systems does not show specific cases that support these advances.

In the last decades, a discussion on how to relate AM and TE brought up another printing concept, a new bottom-up printing system. This emerging technology, also called bioprinting, relies on the possibility of assembling building blocks (cells) that can mimic the healthy structure into larger tissue constructs. Bottom-up TE means to pattern the individual components of one tissue according to a predefined organization that guides the maturation of the construct towards a functional histo-architecture, owing in part to the promotion of cellular self-sorting and self-assembly capabilities and morphogenetic mechanisms.⁹⁷ However, for this process cells are a mandatory component of a bioink. So, obtaining a formulation that includes biologically active elements or molecules and also the biomaterials is a challenge that is still to be faced. To the best of our knowledge, up to this date, no study has been dedicated to the development of a functional bioink to be processed by robocasting. Up to now, robocasting technology has been mostly employed in the fabrication of a wide range of technical and functional scaffolds with complex morphologies. In order to push the progress of this processing method the combination of fundamental knowledge across different fields will allow the fabrication of unique and exciting architectures beyond simple robocasting technique.⁵

As presented in this review, the key factor towards multi-material printing and other AM future technologies relies on multidisciplinary research to face all the imposed challenges. Developing new ink formulations for robocasting bioprinting as well as designing smart materials will certainly expand the range of clinical applications for these materials and demonstrate the potential of AM in the biomedical field.

Acknowledgement

J Daguano and J Silva would like to thank the São Paulo Research Foundation – FAPESP, grant number 2019/11950–6. C Santos would like to thank the FAPERJ (E–26–201.476/2014) and CNPq (308684/2013–3 and 3311119/2017–4) for financial support. M Souza is grateful to the São Paulo Research Foundation – Fapesp, grant number 2013/00793–6. Also, J. Daguano is grateful to O Amorim for providing graphical art help.

MHV Fernandes acknowledges the project CICECO–Aveiro Institute of Materials, UIDB/50011/2020 & UIDP/50011/2020, financed by national funds through the Portuguese Foundation for Science and Technology/MCTES

References

- Salerno A, Netti PA, Introduction to biomedical foams, in *Biomedical Foams for Tissue Engineering Applications*, ed by Netti PA. Woodhead Publishing, pp 3–39 (2014).
- Cesarano J, Calvert PD, and Inventor: Sandia Corporation, Assignee, Freeforming Objects with Low-Binder Slurry. US Patent 6027326 A (2000).
- Lewis JA, Smay JE, Stuecker J, Cesarano J, Direct ink writing of three dimensional ceramic structures. *J Am Ceram Soc* 89: 3599(2006).
- Johansson E, Lidström O, Johansson J, Lyckfeldt O, Adolfsson E, Influence of resin composition on the defect formation in alumina manufactured by stereolithography. *Mater* 10: 138 (2017).
- Peng E, Zhang D, Ding J, Ceramic Robocasting: Recent Achievements, Potential, and Future Developments. *Adv Mater* 30 (47): 1802404(1–14) (2018).
- Stuecker JN, Cesarano J, Hirschfeld DA, Control of the Viscous Behavior of Highly Concentrated Mullite Suspensions for Robocasting. *J Mater Process Technol* 142 [2] 318–25 (2003).
- Zhao S, Xiao W, Rahaman MN, O'Brien D, Seitz-Sampson JW, Sonny Bal B, Robocasting of silicon nitride with controllable shape and architecture for biomedical applications. *Int J Appl Ceram Technol* 14(2): 117–127 (2017).
- Barry III AR, Shepherd RF, Hanson JN, Nuzzo RG, Wiltzius P, Lewis JA, Direct Write Assembly of 3D Hydrogel Scaffolds for Guided Cell Growth. *Adv Mater* 21: 2407–2410 (2009).
- Casas-Luna M, Tan H, Tkachenko S, Salamon D, Montufar EB, Enhancement of mechanical properties of 3D-plotted tricalcium phosphate scaffolds by rapid sintering. *J Eur Ceram Soc* 39: 4366–4374 (2019).
- Bose S, Ke D, Sahasrabudhe H, Bandyopadhyay A, Additive manufacturing of biomaterials. *Prog Mater Sci* 93: 45–111 (2018).
- Leong KF, Cheah CM, Chua CK. Solid freeform fabrication of three-dimensional scaffolds for engineering replacement tissues and organs. *Biomater* 24:2363–78 (2003).
- Murphy SV, Atala A. 3D bioprinting of tissues and organs. *Nat Biotechnol* 32:773–85 (2014).
- Fielding G, Bose S. SiO₂ and ZnO dopants in three-dimensionally printed tricalcium phosphate bone tissue engineering scaffolds enhance osteogenesis and angiogenesis in vivo. *Acta Biomater* 9:9137–48 (2013).
- Woodfield TBF, Malda J, de Wijn J, Péters F, Riesle J, van Blitterswijk CA. Design of porous scaffolds for cartilage tissue engineering using a three-dimensional fiber-deposition technique. *Biomater* 25:4149–61 (2004).
- Eqtesadi S, Motealleh A, Perera FH, Miranda P, Pajares A, Wendelbo R, Guiberteau F, Ortiz AL, Fabricating geometrically-complex B₄C ceramic components by robocasting and pressureless spark plasma sintering. *Scr Mater* 145: 14–18 (2018).
- Feilden E, Blanca EGT, Giuliani F, Saiz E, Vandepierre L, Robocasting of structural ceramic parts with hydrogel inks. *J Eur Ceram Soc* 36: 2525–2533 (2016).
- Quackenbush CL, French K, Neil JT, Fabrication of sinterable silicon nitride by injection molding. *Ceram Eng Sci Proc* 3:(1–2) Chapter 3 (1982).
- Millan AJ, Nieto MI, Moreno R, Aqueous injection moulding of silicon nitride. *J Eur Ceram Soc* 20:2661–2666 (2000).
- Albano MP, Garrido LB, Processing of concentrated aqueous silicon nitride slips by slip casting. *J Am Ceram Soc* 81:837–844 (1998).
- Wan T, Yao T, Hu H, Xia Y, Zuo K, Zheng Y, Fabrication of porous Si₃N₄ ceramics through a novel gelcasting method. *Mater Lett* 133:190–192 (2014).
- Griffith ML, Halloran JW, Freeform Fabrication of Ceramics via Stereolithography. *J Am Ceram Soc* 79(10): 2601–8 (1996).
- Homa J, Schwentenwein M, A Novel Additive Manufacturing Technology for High-Performance Ceramics, in *Advanced Processing and Manufacturing Technologies for Nanostructured and Multifunctional Materials*. Ceramic Engineering and Science Proceedings, ed by Ohji T, Singh M, Mathur S. John Wiley & Sons, Inc., Hoboken, NJ, pp. 33–40 (2014).
- Cesarano J III, Segalman R, Calvert P, Robocasting provides mold-less fabrication from slurry deposition. *Ceram Ind* 148:94–102 (1998).
- Lewis JA, Smay JE, Stuecker J, Cesarano J III, Direct ink writing of three-dimensional ceramic structures. *J Am Ceram Soc* 89:3599–3609 (2006).
- Cai K, Román-Manso B, Smay JE, et al, Geometrically complex silicon carbide structures fabricated by robocasting. *J Am Ceram Soc* 95:2660–2666 (2012).
- He GP, Hirschfeld DA, Cesarano J III, Stuecker JN, Robocasting and mechanical testing of aqueous silicon nitride slurries, Technical Report, Sandia National Laboratory, SAND2000–1493C (2000).
- Fu Q, Saiz E, Tomsia AP, Direct ink writing of highly porous and strong glass scaffolds for load-bearing bone defects repair and regeneration. *Acta Biomater* 7:3547–3554 (2011).
- Liu X, Rahaman MN, Hilmas GE, Bal BS, Mechanical properties of bioactive glass (13–93) scaffolds fabricated by robotic deposition for structural bone repair. *Acta Biomater* 9(6):7025–7034 (2013).
- Xiao W, Zaeem MA, Bal BS, Rahaman MN, Creation of bioactive glass (13–93) scaffolds for structural bone repair using a combined finite element modeling and rapid prototyping approach. *Mater Sci Eng C* 68:651–662 (2016).
- Paredes C, Martínez-Vázquez FJ, Pajares A, Miranda P, Novel strategy for toughening robocast bioceramic scaffolds using polymeric cores. *Ceram Int* 45:19572–19576 (2019).
- Gu GX, Libonati F, Wettermark SD, Buehler MJ, Printing nature: Unraveling the role of nacre's mineral bridges. *J Mech Behav Biomed Mater* 76: 135–144 (2017).
- Soon G, Pingguan-Murphy B, Lai KW, Akbar SA, Review of zirconia-based bioceramic: Surface modification and cellular response. *Ceram Int* 42(11): 12543–12555 (2016).
- Baino F, Novajra G, Vitale-Brovarene C. Bioceramics and Scaffolds: A Winning Combination for Tissue Engineering. *Front Bioeng Biotechnol* 3:202 (2015).
- Hongshi Ma, Chun Feng, Jiang Chang, Chengtie Wu, 3D-printed bioceramic scaffolds: From bone tissue engineering to tumor therapy. *Acta Biomater* 79: 37–59 (2018).
- Mordor Intelligence, Bioceramics Market – Growth, Trends, And Forecast (2019 – 2024). <https://www.mordorintelligence.com/industry-reports/bioceramics-market> [accessed 9 September 2019].
- Cengiz IF, Pitikakis M, Cesario L, Parascandolo P, Vosilla L, Viano G, et al., Building the basis for patient-specific meniscal scaffolds: from human knee MRI to fabrication of 3D printed scaffolds. *Bio-print* 1: 1–10 (2016). doi:10.1016/j.bprint.2016.05.001
- Do AV, Khorsand B, Geary SM, Salem AK, 3D printing of scaffolds for tissue regeneration applications. *Adv Healthc Mat* 4: 1742–1762. (2015). doi: 10.1002/adhm.201500168
- Duarte Campos DF, Blaeser A, Buellesbach K, Sen KS, Xun W, Tillmann W, et al., Bioprinting organotypic hydrogels with improved mesenchymal stem cell remodeling and mineralization properties for bone tissue engineering. *Adv Healthc Mater* 5: 1336–1345 (2016). doi: 10.1002/adhm.201501033
- Jang J, Park HJ, Kim SW, Kim H, Park JY, Na SJ, et al., 3D printed complex tissue construct using stem cell-laden decellularized extracellular matrix bioinks for cardiac repair. *Biomater* 112: 264–274 (2017). doi:10.1016/j.biomaterials.2016.10.026
- Hwa LC, Rajoo S, Noor AM, Ahmad N, Uday MB, Recent advances in 3D printing of porous ceramics: A review. *Curr Opin Sol State Mater Sci* 21: 323–347 (2017).
- Nommeots-Nomm A, Lee PD, Jones JR. Direct ink writing of highly bioactive glasses. *J Eur Ceram Soc* 38: 837–844 (2018).
- Eqtesadi S, Motealleh A, Miranda P, Lemos A, Rebelo A, Ferreira JMF. A simple recipe for direct writing complex 45S5 Bioglass 3D scaffolds. *Mater Letters* 93: 68–71 (2013).
- Koski C, Onuike B, Bandyopadhyay A, Bose S. Starch-hydroxyapatite composite bone scaffold fabrication utilizing a slurry extrusion-based solid freeform fabricator. *Addit Manuf* 24: 47–59 (2018).
- Miranda P, Pajares A, Saiz E, Tomsia AP, Guiberteau F, Fracture Modes Under Uniaxial Compression in Hydroxyapatite Scaffolds Fabricated by Robocasting. *J Biomed Mater Res A* 83A(3): 646–55 (2007).
- Dellinger JG, Cesarano J, Jamison RD, Robotic Deposition of Model Hydroxyapatite Scaffolds with Multiple Architectures and Multi-scale Porosity for Bone Tissue Engineering. *J Biomed Mater Res A*, 82A(2): 383–94 (2007).
- Marques CF, Perera FH, Marote A, Ferreira S, Vieira SI, Olhero S, Miranda P, Ferreira JMF, Biphasic calcium phosphate scaffolds fabricated by direct write assembly: Mechanical, anti-microbial and osteoblastic properties. *J Eur Ceram Soc* 37(1):359–368 (2017).
- Chung-Hun OH, Seok-Jung Hong, IJ, Hye-Sun Y, Seung-Hwan J, Hae-Won K, Development of Robotic Dispensed Bioactive Scaffolds and Human Adipose-Derived Stem Cell Culturing for Bone Tissue Engineering. *Tissue Eng Part C* 16(4): 561–71 (2010). doi: 10.1089=ten.tec.2009.0274
- Gao C, Rahaman MN, Gao Q, Teramoto A, Abe K, Robotic deposition and in vitro characterization of 3D gelatin-bioactive glass hybrid scaffolds for biomedical applications. *J Biomed Mater Res A* 101(7): 2027–37 (2013). doi: 10.1002/jbm.a.34496.
- Richard RC, Sader MS, Dai J, Thir RMSM, Soares GDA, Beta-type calcium phosphates with and without magnesium: From hydrolysis of brushite powder to robocasting of periodic scaffolds. *J Biomed Mater Res A* 102A: 3685–3692 (2014). doi: 10.1002/jbm.a.35040
- Won JE, Mateos-Timoneda MA, Castano O, Planell JA, Seo SJ, Lee EJ, Han CM, Kim HW, Fibronectin immobilization on to robotic-dispensed nanobioactive glass/polycaprolactone scaffolds for bone tissue engineering. *Biotechnol Lett* 37(4): 935–42 (2015). doi: 10.1007/s10529-014-1745-5.
- Varanasi VG, Russias J, E, Loomer PM, Tomsia AP. Novel PLA-

- and PCL–HA Porous 3D Scaffolds Prepared by Robocasting Facilitate MC3T3–E1 Subclone 4 Cellular Attachment and Growth. In: *Biomaterials Science: Processing, Properties, and Applications V: Ceramic Transactions, Volume 254*. (2015). <https://doi.org/10.1002/9781119190134.ch16>.
52. Andrade S, Abdalla A, Montufar E, Corté L, Vanegas P. Fabrication of 3D Bioactive Ceramic Scaffolds by Robocasting. In: Braidot A., Hadad A. (eds) VI Latin American Congress on Biomedical Engineering CLAIB 2014, Paraná, Argentina 29, 30 & 31 October 2014. IFMBE Proceedings, vol 49. Springer, Cham, (2015).
 53. Martínez Vázquez F, Pajares A, Miranda P, Effect of the drying process on the compressive strength and cell proliferation of hydroxyapatite derived scaffolds. *Int J Appl Ceram Technol* 14:1101–1106 (2017). <https://doi.org/10.1111/ijac.12755>.
 54. Fiocco L, Elsayed H, Badocco D, Pastore P, Bellucci D, Cannillo V, Detsch R, Boccaccini AR, Bernardo E, Direct ink writing of silica-bonded calcite scaffolds from preceramic polymers and fillers. *Biofabric* 9: 025012 (2017). <https://doi.org/10.1088/1758-5090/aa6c37>.
 55. Stanciu AM, Sprecher CM, Adrien J, Roiban LI, Alini M, Gremillard L, Peroglio M, Robocast zirconia-toughened alumina scaffolds: Processing, structural characterisation and interaction with human primary osteoblasts. *J Eur Ceram Soc* 38: 845–853 (2018). <http://dx.doi.org/10.1016/j.jeurceramsoc.2017.08.031>.
 56. Ben-Arfa BAE, Neto AS, Palamá IE, Salvado IMM, Pullar RC, Ferreira JMF, Robocasting of ceramic glass scaffolds: Sol-gel glass, new horizons. *J Eur Ceram Soc* 39: 1625–1634 (2019). <https://doi.org/10.1016/j.jeurceramsoc.2018.11.019>.
 57. Liu X, Rahaman MN, Liu Y, Bal BS, Bonewald LF, Enhanced bone regeneration in rat calvarial defects implanted with surface-modified and BMP-loaded bioactive glass (13–93) scaffolds. *Acta Biomater* 9(7): 7506–7517 (2013). doi: 10.1016/j.actbio.2013.03.039.
 58. Deliormanli AM, Liu X, Rahaman MN. Evaluation of borate bioactive glass scaffolds with different pore sizes in a rat subcutaneous implantation model. *J Biomater Appl* 28(5): 643–653, 2014.
 59. Rahaman MN, Lin Y, Xiao W, Liu X, Bal B. Evaluation of Long-Term Bone Regeneration in Rat Calvarial Defects Implanted With Strong Porous Bioactive Glass (13–93) Scaffolds. In book: *Biomaterials Science: Processing, Properties, and Applications V. 1*, John Wiley & Sons, Ins. New Jersey (2015). DOI: 10.1002/9781119190134.ch9.
 60. Lin Y, Xiao W, Liu X, Bal BS, Bonewald LF, Rahaman MN, Long-term bone regeneration, mineralization and angiogenesis in rat calvarial defects implanted with strong porous bioactive glass (13–93) scaffolds. *J Non-Cryst Sol* 432: 120–129 (2016). <http://dx.doi.org/10.1016/j.jnoncrsol.2015.04.008>.
 61. Simon JL, Michna S, Lewis JA, Rekow ED, Thompson VP, Smay JE, Yampolsky A, Parsons JR, Ricci JL, In vivo bone response to 3D periodic hydroxyapatite scaffolds assembled by direct ink writing. *J Biomed Mater Res A*, 83(3): 747–58 (2007). <https://doi.org/10.1002/jbm.a.31329>.
 62. Dellinger JG, Eurell JAC, Jamison RD, Bone response to 3D periodic hydroxyapatite scaffolds with and without tailored microporosity to deliver bone morphogenetic protein 2. *J Biomed Mater Res A* 76(2): 366–76 (2006). DOI: 10.1002/jbm.a.30523.
 63. Luo Y, Zhai D, Huan Z, Zhu H, Xia L, Chang J, Wu C. Three-Dimensional Printing of Hollow-Struts-Packed Bioceramic Scaffolds for Bone Regeneration. *ACS Appl. Mater. Interfaces* 7: 24377–24383 (2015). doi: 10.1021/acsami.5b08911.
 64. Lin KF, He S, Song Y, Wang CM, Gao Y, Li JQ, Tang P, Wang Z, Bi L, Pei GX, Low-Temperature Additive Manufacturing of Biomimic Three-Dimensional Hydroxyapatite/Collagen Scaffolds for Bone Regeneration. *ACS Appl Mater Interfaces* 8(11): 6905–6916 (2016). <https://doi.org/10.1021/acsami.6b00815>.
 65. Shao H, Liu A, Ke X, Sun M, HE Y, Yang X, Fu J, Zhang L, Yang G, Liu Y, Xu S, Gou Z, 3D Robocasting Magnesium-doped Wollastonite/TCP Bioceramics Scaffolds with Improved Bone Regeneration Capacity in Critical Sized Calvarial Defects. *J Mater Chem B* 5(16): 2941–2951 (2017). doi: 10.1039/C7TB00217C.
 66. Zheng J, Carlson WB, Reed JS, Dependence of compaction efficiency in dry pressing on the particle size distribution. *J Am Ceram Soc* 78(9): 2527–2533 (1995).
 67. Konakawa Y, Ishizaki K, The particle size distribution for the highest relative density in a compacted body. *Powder Technol* 63: 241–246 (1990).
 68. Zheng J, Carlson WB, Reed JS, The packing density of binary powder mixtures. *J Eur Ceram Soc* 15: 479–483 (1995).
 69. Ferreira JMF, Diz HMM, Effect of the amount of deflocculant and powder size distribution on the green properties of silicon carbide bodies obtained by slip casting. *J Hard Mater* 3: 17–27 (1992).
 70. Taruta S, Takusagawa N, Okada K, Otsuka N, Slip casting of alumina powder mixtures with bimodal size distribution. *J Ceram Soc Japan* 104: 47–50 (1996).
 71. William JH, Zukoski CF, The rheology of bimodal mixtures of colloidal particles with long-range, soft repulsions. *J Colloid Interface Sci* 210: 343–351 (1999).
 72. Olhero S, Ferreira JM, Influence of particle size distribution on rheology and particle packing of silica-based suspensions. *Powder Technol* 139(1): 69–75 (2004). doi:10.1016/j.powtec.2003.10.004
 73. Nutz M, Furdin G, Medjahdi G, Maréché GF, Moreau M, Rheological properties of coal tar pitches containing micronic graphite powders. *Carbon* 35: 1023–1029 (1997).
 74. Yuan J, Murray HH, The importance of crystal morphology on the viscosity of concentrated suspensions of kaolins. *Appl Clay Sci* 12: 209–219 (1997).
 75. Joseph R, McGregor WJ, Martyn MT, Tanner KE, Coates PD, Effect of hydroxyapatite morphology/surface area on the rheology and processability of hydroxyapatite filled polyethylene composites. *Biomater* 23(21): 4295–4302 (2002). doi:10.1016/s0142-9612(02)00192-8
 76. Feilden E, Ferraro C, Zhang Q, García-Tuñón E, D'Elia E, Giuliani F, Vandepierre L, Saiz E. 3D Printing Bioinspired Ceramic Composites. *Sci Rep* 7: 13759 (2017). <https://doi.org/10.1038/s41598-017-14236-9>
 77. Miranda P, Saiz E, Gryn K, Tomsia AP, Sintering and robocasting of tricalcium phosphate scaffolds for orthopaedic applications. *Acta Biomater* 2(4): 457–466 (2006). doi:10.1016/j.actbio.2006.02.004
 78. Eqtesadi S, Motealleh A, Miranda P, Pajares A, Lemos A, Ferreira, JMF, Robocasting of 45S5 bioactive glass scaffolds for bone tissue engineering. *J Eur Ceram Soc* 34(1): 107–118 (2014). doi:10.1016/j.jeurceramsoc.2013.08.003
 79. Zhang D, Peng E, Borayek R, Ding J. Controllable Ceramic Green-Body Configuration for Complex Ceramic Architectures with Fine Features. *Adv Funct Mater* 1807082 (2019). doi:10.1002/adfm.201807082
 80. He G, Hirschfeld DA, Cesarano J (n.d.), Processing and Mechanical Properties of Silicon Nitride Formed by Robocasting Aqueous Slurries, in *Ceramic Engineering and Science Proceedings*, 607–614 (2000). doi:10.1002/9780470294635.ch72
 81. Glymond D, Vandepierre LJ, Robocasting of MgO-doped alumina using alginic acid slurries. *J Am Ceram Soc* 101(8): 3309–3316 (2018). doi:10.1111/jace.15509
 82. Schlordt T, Schwanke S, Keppner F, Fey T, Travitzky N, Greil P, Robocasting of alumina hollow filament lattice structures. *J Eur Ceram Soc* 33(15–16): 3243–3248 (2013). doi:10.1016/j.jeurceramsoc.2013.06.001
 83. Powell J, Assabumrungrat S, Blackburn S, Design of ceramic paste formulations for co-extrusion, *Powder Technol* 245:21–27 (2013).
 84. Bourret J, El Younsi I, Bienia M, Smith A, Geffroy PM, Marie J, Ono Y, Chartier T, Pateloup V, Micro extrusion of innovative alumina pastes based on aqueous solvent and eco-friendly binder. *J Eur Ceram Soc* 38(7): 2802–2807 (2018).
 85. Faes M, Valkenaers H, Vogeler F, Vleugels J, Ferraris E, Extrusion-based 3D Printing of Ceramic Components, in *Procedia CIRP* 28: 76–81 (2015).
 86. Li W, Ghazanfari A, McMillen D, Leu MC, Hilmas GE, Watts J, Characterization of zirconia specimens fabricated by ceramic on-demand extrusion. *Ceram Int* 44(11): 12245–12252 (2018).
 87. Azzolini A, Sglavo VM, Downs JÁ, Novel method for the identification of the maximum solid loading suitable for optimal extrusion of ceramic pastes. *J Adv Ceram* 3(1): 7–16 (2014).
 88. Franks GV, Tallon C, Studart AR, Sesso ML, Leo S, Colloidal processing: enabling complex shaped ceramics with unique multiscale structures. *J Am Ceram Soc* 100(2): 458–490 (2017). doi:10.1111/jace.14705
 89. Ben-Arfa BAE, Neto AS, Miranda Salvad IM, Pullar RC, Ferreira JMF, Robocasting: Prediction of ink printability in solgel bioactive glass. *J Am Ceram Soc* 102(4): 1608–1218 (2018). doi:10.1111/jace.16092
 90. Stickel JJ, Powell RL, Fluid mechanics and rheology of dense suspensions. *Annu Rev Fluid Mech* 37: 129–149 (2005). doi: 10.1146/annurev.fluid.36.050802.122132
 91. Schlordt T, Greil P, Robocasting of Alumina Lattice Truss Structures. *J Ceram Sci Technol* 3(2): 81–8 (2012).
 92. Smay JE, Cesarano J, Lewis JA, Colloidal Inks for Directed Assembly of 3-D Periodic Structures. *Langmuir*, 18(14), 5429–5437 (2002). doi:10.1021/la0257135
 93. Lewis JA, Colloidal Processing of Ceramics. *J Am Ceram Soc* 83(10): 2341–2359 (2004). doi:10.1111/j.1151-2916.2000.tb01560.x
 94. Wahl L, Lorenz M, Biggemann J, Travitzky N, Robocasting of reaction bonded silicon carbide structures, *J Eur Ceram Soc* 39(15): 4520–4526 (2019).
 95. M'Barki A, Bocquet L, Stevenson A, Linking Rheology and Printability for Dense and Strong Ceramics by Direct Ink Writing. *Scientific Reports* 7:6017 (2017).
 96. Wolfs, R.J.M., Suiker, A.S.J. Structural failure during extrusion-based 3D printing processes. *Int J Adv Manuf Technol* 104, 565–584 (2019). <https://doi.org/10.1007/s00170-019-03844-6franks>
 97. Lui YS, Sow WT, Tan LP, Wu Y, Lai Y, Li H, 4D Printing and Stimuli-responsive Materials in Biomedical Applications. *Acta Biomater* 92: 19–36 (2019).
 98. Gao B, Yang Q, Zhao X, Jin G, Ma Y, Xu F, 4D Bioprinting for Biomedical Applications. *Trends Biotechnol* 34(9): 746–756 (2016).
 99. Liu G, Zhao Y, Wu G, Lu J, Origami and 4D printing of elastomer-derived ceramic structures. *Sci Adv* 4: eaat0641 (2018).
 100. Tamay DG, Dursun Usal T, Alagoz AS, Yucel D, Hasirci N and Hasirci V, 3D and 4D Printing of Polymers for Tissue Engineering Applications. *Front Bioeng Biotechnol* 7:164 (2019). doi: 10.3389/fbioe.2019.00164
 101. Bargardi, F., Le Ferrand, H., Libanori, R. et al. Bio-inspired self-shaping ceramics. *Nat Commun* 7: 13912 (2016). <https://doi.org/10.1038/ncomms13912>
 102. Franchina G, Scanferla P, Zeffiro L, Elsayed H, Baliello A, Giacomello G, Pasetto M, Colombo P, Direct ink writing of geopolymeric inks. *J Eur Ceram Soc* 37: 2481–2489 (2017).